



Assessment and Insights into Renewable Energy

Confidential Report prepared for MBIE

September 2022

THIS REPORT AND THE INFORMATION CONTAINED HEREIN IS
CONFIDENTIAL, AND MAY BE SUBJECT TO LEGAL PRIVILEGE.

Prepared by:

Ben Liley, Christian Zammit, Richard Turner, Jim Griffiths, Stephen Stuart

For any information regarding this report please contact:

James Griffiths

Hydrologist

Hydrological Processes

+64-3-343 7858

james.griffiths@niwa.co.nz

National Institute of Water & Atmospheric Research Ltd

PO Box 8602

Riccarton

Christchurch 8011




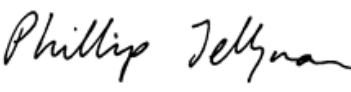
Phone +64 3 348 8987

NIWA CLIENT REPORT No: 2022012CH

Report date: September 2022

NIWA Project: ENR21502

Revision	Description	Date
Version 1.0	Final Report	8 February 2022
Version 2.0	Final Report with bias corrected inflow	2 September 2022
Version 2.1	Updated Figures 41 and 4.2	2 September 2022

Quality Assurance Statement		
 	Reviewed by:	Andrew Tait Ashley Broadbent
	Formatting checked by:	Nic McNeil
	Approved for release by:	Phillip Jellyman

© All rights reserved. This publication may not be reproduced or copied in any form without the permission of the copyright owner(s). Such permission is only to be given in accordance with the terms of the client's contract with NIWA. This copyright extends to all forms of copying and any storage of material in any kind of information retrieval system.

Whilst NIWA has used all reasonable endeavours to ensure that the information contained in this document is accurate, NIWA does not give any express or implied warranty as to the completeness of the information contained herein, or that it will be suitable for any purpose(s) other than those specifically contemplated during the Project or agreed by NIWA and the Client.

Contents

- Executive summary 7**

- 1 Introduction 10**
 - 1.1 Background 10
 - 1.2 Scope..... 10
 - 1.3 Units..... 11

- 2 Defining the ‘dry year’ problem..... 12**

- 3 Methods..... 14**
 - 3.1 Climate models 15
 - 3.2 River flow and hydro-electric lake inflow model – TopNet 17
 - 3.3 Measuring a climate change effect..... 19
 - 3.4 Multi-model averaging: mean versus median 19

- 4 Hydroelectric Generation 20**
 - 4.1 Observed dataset for climate change..... 20
 - 4.2 Hydrological bias correction 23
 - 4.3 Climate change analysis..... 28

- 5 Wind Energy 33**
 - 5.1 Climate change scenario 35

- 6 Solar Energy..... 44**
 - 6.1 Historical solar flux 47
 - 6.2 Climate change scenario 48

- 7 Combined Hydro, Wind, and Solar 52**
 - 7.1 Monthly generation 52
 - 7.2 Weekly generation – hydro-wind correlations..... 60
 - 7.3 Possible further analyses with present datasets 62
 - 7.4 Possible refinements and new datasets 63

- 8 Concluding remarks 65**
 - 8.1 Is a dry year characterised by historical inflow variation still appropriate?..... 65
 - 8.2 Does reliance on renewable generation sources exacerbate the dry year problem?
..... 65

8.3	Do future correlations between hydro inflows and wind flows, for example, mean the required battery solution needs to be larger or smaller?	66
9	References.....	67
Appendix A	Wind farms considered in this report.....	70
Appendix B	Hydrological bias correction for each hydro system considered	72
Appendix C	Monthly correlations for each period and RCP	82

Tables

Table 3-1:	Descriptions of the Representative Concentration Pathways (RCPs).	16
Table 4-1:	Modified HMD dataset supporting climate change investigation.	20
Table 4-2:	Range of TopNet parameter multipliers used during calibration process.	23
Table 5-1:	Temporal aggregation periods used in this study along with key comments.	33
Table 6-1:	CMIP5 model solar means relative to overall mean.	50
Table 6-2:	CMIP5 model solar mean changes from 2000 to 2050.	50
Table 6-3:	CMIP5 model solar trends per decade relative to model mean.	51
Table 6-4:	CMIP5 model solar annual cycle amplitudes relative to overall mean.	51
Table 7-1:	Correlations between residual variation in hindcast monthly generation.	59
Table 7-2:	Correlation of monthly South Island hydro generation with North Island wind.	60
Table 7-3:	Correlation of residuals for South Island hydro with North Island wind.	60
Table A-1:	Wind farms used in this report; name, region (see Figure 5-1), island, number of turbines, turbine capacity, total capacity, start year, status, and operator.	70

Figures

Figure 2-1:	Seasonality of NZ hydroelectric generation, years 1972–2016.	12
Figure 2-2:	Total seasonal flow into NZ hydroelectric catchments, 1972–2016.	13
Figure 3-1:	Schematic showing analysis approach used in the current report.	14
Figure 3-2:	CMIP5 climate models (2006–2120), the historical simulations.	17
Figure 4-1:	Annual average hydropower generation frequency analysis for the North Island (left panel) and the South Island (right panel).	21
Figure 4-2:	Seasonal average hydropower potential generation frequency analysis for summer (top) and winter (bottom) seasons for the North (left panels) and South (right) Islands.	22
Figure 4-3:	Validation of the water balance. The left panel shows annual mean discharge (QMean), while the right panel shows 7-day mean annual low flow (Q7DMALF).	25
Figure 4-4:	Daily hydrograph, cumulated hydrograph and flow duration curves (top) daily average inflows, precipitation, evapotranspiration and snow area (bottom) for Hawea inflows over the period 1985–2006.	26
Figure 4-5:	Comparison of simulated annual-average generation between HMD-gen dataset and hindcast bias-corrected CMIP5-driven for 1985–2006. North	

	Island (top panel) and South Island (bottom panel) plots show: HMD-gen dataset (red circle); CMIP5 median island-wide actual generation (red line); TopNet flows driven by HadGEM-ES (magenta), CESM1-CAM5 (black), GFDL-CM3 (grey), GISS-E2-R (gold), BCC-CSM1.1 (blue), and NorESM1-M (dark green).	27
Figure 4-6:	North Island 20-year centred 5 th percentile annual mean hydropower generation threshold (MW) for each RCP.	29
Figure 4-7:	South Island 20-year centred 5 th percentile annual mean hydropower generation threshold (MW) for each RCP.	30
Figure 4-8:	20-year median annual mean daily hydropower generation capacity distribution curves across North Island hydropower schemes for different time periods.	31
Figure 4-9:	20-year median annual mean daily hydropower generation capacity distribution curve across South Island hydropower schemes for different time periods.	32
Figure 5-1:	Maps showing location of wind farms for which generation scenarios were calculated in this study.	33
Figure 5-2:	Recent (2018–2020) seasonal cycle in wind generation for each island.	34
Figure 5-3:	Hindcast seasonal cycle in wind generation for each island from CMIP5 models.	35
Figure 5-4:	Scaled Hadley Centre GCM projections for 2031–2060 for the percentage of months exceeding specified generation (kWh) for the North Island.	36
Figure 5-5:	Scaled Hadley Centre GCM projections for 2031–2060 for the percentage of months exceeding specified generation (kWh) for the South Island.	37
Figure 5-6:	Scaled GIS GCM projections for 2031–2060 for the percentage of months exceeding specified generation (kWh) for the North (upper panel) and South (lower) Islands.	38
Figure 5-7:	Scaled BCC GCM projections for 2031–2060 for the percentage of months exceeding specified generation (kWh) for Region A.	39
Figure 5-8:	Per cent changes (2031 to 2060 vs 1981–2005) in wind generation for each RCP scenario grouped by the six CMIP5 models.	40
Figure 5-9:	Per cent changes (2031 to 2060 vs 1981–2005) for in monthly variance of generation for each RCP scenario grouped by the six CMIP5 models.	41
Figure 5-10:	Relative changes (1981–2005 to 2031–2060) in North Island seasonal wind generation for each CMIP5 model as grouped by RCP.	41
Figure 5-11:	Relative changes (1981–2005 to 2031–2060) in South Island seasonal wind generation for each CMIP5 model as grouped by RCP.	42
Figure 5-12:	The minimum, average and maximum per cent change from 1981–2005 to future wind generation due to climatic changes in wind over the 6 CMIP5 GCMs.	42
Figure 5-13:	The minimum, average and maximum percent change from 1981–2005 to future wind generation due to climatic changes in wind over the 6 CMIP5 GCMs.	43
Figure 6-1:	Annual average global horizontal irradiance for Aotearoa-New Zealand compared with its antipodes.	44
Figure 6-2:	Climate zones for NZ.	46
Figure 6-3:	Historical solar generation for 10 GWp of PV systems distributed in proportion to population.	47

Figure 6-4:	Histograms of potential generation for 10 GWp distributed PV in NZ, annually and by season.	48
Figure 6-5:	Daily and monthly mean PV generation for NorESM1-M model, RCP 8.5, assuming 10 GWp.	49
Figure 6-6:	Relative monthly residuals from mean annual cycle for BCC-CSM1.1, RCP 2.6.50	
Figure 7-1:	Projected monthly hydro, wind, and solar generation for North and South Islands with six GCMs for hindcast and future RCP 4.5.	52
Figure 7-2:	Correlations of hindcast monthly hydro, wind, and solar generation by island for the six CMIP5 models.	54
Figure 7-3:	Correlation of projected 2051–2070 monthly North and South Island hydro, wind, and solar generation for RCP 6.0 in the six CMIP5 models.	55
Figure 7-4:	Seasonality of hydro, wind, and solar generation for North and South Islands in hindcast monthly totals.	56
Figure 7-5:	Seasonality of hydro, wind, and solar generation for the North and South Islands in 2031-2050 RCP 4.5 monthly totals.	57
Figure 7-6:	Seasonality of hydro, wind, and solar generation for the North and South Islands in 2051-2070 RCP 6.0 monthly totals.	58
Figure 7-7:	Seasonality of North Island wind and South Island hydro from hindcast to future projections for the four RCPS.	58
Figure 7-8:	Comparison of various CMIP5 hydro - wind correlations by island for four RCP's plus hindcast vs a previous climate station-based correlation analysis.	61
Figure 7-9:	Change in hydro - wind correlation by island for each CMIP5 model and RCP scenario.	62
Figure 7-10:	Average change in hydro-wind correlations from hindcast to 2051–2070 for each RCP scenario.	63

Executive summary

With the shift to 100% renewable energy in Aotearoa-New Zealand, there is increasing interest in the changing capacity and variability of NZ's wind, solar and hydro-power generation. This report looks at the present and possible future changes in such capacity with particular focus on the implications for long-term energy generation security.

With hydro-electricity (hydro) historically providing around 55% of NZ electricity, there have in the past been several periods of shortage of supply during so-called 'dry years'. Dry years occur when low autumn inflows result in low levels in hydro lakes in the critical winter months period. Fossil-fuel thermal generation (that provides approximately 20% of NZ power) has traditionally increased during such situations to cover the shortfall in hydro generation. However, in the future, alternative sources of power will be needed as NZ moves away from fossil fuels to new wind and solar power in accordance with the Zero Carbon Act (NZ Government 2019). As a consequence, the Ministry of Business, Innovation and Employment's 'NZ Battery' project seeks to assess the potential of using pumped hydro-electric storage as a method to store generated power for when demand is the greatest.

However, a number of questions arise from the prospect of using only renewable energy sources to cope with the natural variation of hydro inflows, particularly under the scenario of future climate change. For example:

- Will the definition of a 'dry year' as characterised by historical inflow variation continue to be appropriate?
- Will a reliance on renewable energy generation exacerbate the dry year problem?
- Will future correlations between different renewable energy sources (hydro inflows and wind for example) mean that the proposed NZ Battery solution needs to be larger or smaller than is currently envisaged?

To address the above questions, this report describes the energy generation capacity of observed and modelled historic river inflow, solar and wind data. The future energy generation capacity is then assessed using future climate scenario data. The correlations between river inflows, solar and wind energy potential are then determined for a historic period (1986–2005) and repeated for the future scenarios.

To characterise past climate and evaluate the potential of the three alternative types of generation we used the following sources of historical information:

- **Hydro:** The Hydrological Modelling Dataset (HMD) of historical stream and river flows into hydro lakes, from the Electricity Authority (EA).
- **Wind:** Reanalysis of data from a very high-resolution NZ Convective Scale (weather) Model (NZCSM), together with wind generation data for 2018–2020 from the EA.
- **Solar:** Pyranometer (solar radiation) data from the NIWA Climate Database, collated and quality-controlled into time series for 18 climate zones to represent NZ climates.

The analysis of hydro, wind, and solar generation in future climate scenarios made use of six General Circulation Models (GCMs) that, amongst the 41 in the Intergovernmental Panel on Climate Change (IPCC) AR5 model archive, were found in a previous NIWA study (MfE 2018) to represent NZ climates

well under past and expected climate change. The models had been run for the four Representative Concentration Pathways (RCPs) of IPCC AR5 assessments from 2021 to 2070, and for past greenhouse gas concentrations from 1981 to 2005 (from which we call the two decades 1986–2005 the ‘hindcast’). The climate model ensemble was coupled with NIWA’s TopNet hydrological model to simulate natural inflows at HMD dataset locations under past and future conditions. The scenario analysis was conducted in three stages:

- For each type of generation (hydro, wind, solar), the hindcasted generation potential was compared with historical data and bias-corrected if needed.
- Patterns of change from past to future climate scenarios were described in terms of their effects on potential power generation.
- The current and future correlations between the potential for hydro, wind and solar energy generation were assessed, and the implications for pumped hydro storage considered.

The findings for hydro, wind, and solar electricity generation were as follows:

Hydroelectricity:

- HMD modelled South Island hydro generation capacity is more than three times that of North Island.
- Inflows to hydro lakes were generally lower during the hindcast period (1986–2005) than earlier and later time periods.
- North Island summer hydroelectricity generation has been stable over the period from 1972–2017, while the South Island summer generation decreased after 1984.
- North Island winter flows diminished over the hindcast period, while South Island winter flows increased.

Future outlook for hydroelectricity:

- North Island annual hydro generation at lowest 5% may decrease by an ensemble average up to 10%.
- South Island annual hydro generation at lowest 5% is projected to increase by an average of about 16%.
- Variability in the lowest 5% of South Island annual generation doubles from the hindcast period to 2051–2070 under the warmest radiation forcing scenarios (RCP 6.0 and RCP 8.5).

Wind power:

- Installed wind capacity is about 1 GWp. There are consents for another 2 GWp, with another nearly 2 GWp proposed. We considered all of these, plus 5 GWp of hypothetical offshore generation for a future total of 10 GWp.
- Of the existing 1 GWp, 90% is in the North Island, and that proportion would be the same for the total 10 GWp.

- The overall pattern of wind generation for NZ is lower in autumn and higher in spring, similar to that of hydroelectricity. Both the seasonality and year-to-year variability of wind is relatively less than for hydro.

Future outlook for wind power:

- All GCM models and RCPs show a modest (5–10%) increase in spring generation, stronger in the South Island.
- Small (<5%) decreases in summer and autumn are predicted in most models, while winter generation has a comparably small increase.
- Future changes for given total wind capacity are very much less than the uncertainty in how much of that capacity will be built through future wind farm construction.

Solar energy:

- Solar power accounts for less than 0.3% of NZ generation at present, but it is expected to reach 2% within the next two years and continue to grow.
- Solar generation is two to four times higher in summer than in winter, so it will add relatively little to winter hydro and wind generation.
- Countering the previous point, abundant solar generation in summer would mean that hydro storage could be maximised going into autumn.
- Solar photovoltaic generation is expected to be widely distributed, probably in approximate proportion to population and associated demand, and the resulting solar power will vary much less year-to-year than either hydro or wind power.

Future outlook for solar energy:

- The Coupled Model Intercomparison Project 5 (CMIP5) models in hindcast mode closely match the distribution of measured daily solar radiation when both are applied to the putative future distribution of solar panels. This gives us confidence that the future projections of solar generation are representative.
- All models and RCPs show small and inconsistent changes in solar generation from hindcast amounts.

Linear correlations of the expected power output of the three forms of generation were explored at monthly and weekly time scales, and between islands, in both hindcast and future projections. Most important for national power generation was a moderate positive correlation ($R \sim 0.5$) between the two largest future renewable supplies, South Island hydro and North Island wind. It applies to both total generation and year-to-year differences from mean seasonality, indicating that dry months are also somewhat less windy.

The correlations vary between models, and between hindcast and future scenarios for four different RCPs, but there is no clear expectation that future correlations will differ from present, either with time or with climate scenario.

1 Introduction

1.1 Background

The purpose of the New Zealand Battery Project is to investigate options to resolve Aotearoa-New Zealand's 'dry year' risk problem in a highly renewable electricity system. The dry year problem arises from situations where the natural variability of hydro inflows means there is insufficient hydro generation to support demand in particularly dry (low rainfall or inflow) years. In this situation increasing thermal generation is called on to make up for the hydro deficit. Traditionally the dry year risk is assessed against the spread of historical inflows. This distribution is tacitly assumed to hold for future inflows (under the assumption of climate stationarity).

In the future however, as Aotearoa-New Zealand moves to 100% renewables, we will not be able to resort to fossil-fuel generation to support hydro generation in dry years. Renewable generation sources could provide a solution, but they come with intermittency issues that will potentially impact the operation and sizing of a solution based around pumped hydro-storage. Additionally, the prospect of changes (non-stationarity) to the potential utility of renewable sources of generation arising from climate change impacts need to be assessed.

The Ministry for Business and Employment (MBIE) expects significant increases in wind and/or solar generation to 2030 and beyond, with only modest increases in geothermal and hydro. This is primarily to replace the fossil-fuel generation and meet demand growth from electrification. MBIE suspect that with regard to the injection of intermittent energy into our electricity system, the current 'dry year' risk will be replaced by 'dry/calm/cloudy periods' risk.

A number of questions therefore arise from the prospect of 100% renewable electricity generation to cope with hydro inflow variation including:

- Is a dry year characterised by historical inflow variation still appropriate?
- Does reliance on renewable generation sources exacerbate the dry year problem?
- Do future correlations between hydro inflows and wind flows, for example, mean the required battery solution needs to be larger or smaller?

1.2 Scope

To address the above questions, this report presents analyses of historic river inflow, solar and wind data (observed and modelled) in relation to their renewable energy generation capabilities and variability. In addition, future generation and variability are assessed using General Circulation Models (GCMs) future climate scenario data.

The extent of correlation between river inflows, solar and wind energy potential is established for GCM-driven datasets for the hindcast period (1986–2005); i.e., six potential correlations. This analysis is then repeated for future scenarios.

The analysis is used to address the following aspects:

- Assessment of the present practice of assuming historical inflow variation is a good representation of future inflow distribution.
- Assessment of applicability of method of producing synthetic wind flow sequences.

- Insights into likely climate change impacts on future inflow variability.
- Insights into likely climate change impacts on future regional and seasonal wind flows and future wind flow variability.
- Insights into future climate change impacts on solar insolation variability, both regionally and seasonally.
- Insights into impacts of future correlations between hydro inflows, wind flows and insolation both intra-year and inter-year.

1.3 Units

SI units and their associated abbreviations used within this report to quantify power include gigawatts (GW), terawatts (TW), and megawatts (MW). The subscript 'p' is used to indicate system capacity or, in effect, peak power (e.g., MWp). Watt-hours (Wh), and MWh or GWh, are used as a measure of energy production over time; 1 kilowatt-hour (kWh) is equal to 1kW of power sustained for 1 hour.

2 Defining the ‘dry year’ problem

Hydroelectric and geothermal generation differ intrinsically from most other renewable energy sources in that they are stored, rather than just instantaneously available. The ‘dry year’ problem refers to a problem of energy storage levels, often over months and between seasons. That introduces the complication that it depends on patterns of usage over time and, for hydroelectricity generation, the timing of precipitation, catchment drainage, and river flows.

Wind and solar are the cheapest sources of additional generation, but any plan for their integration into the NZ grid assumes some system for short-term storage (hours to days) that can be turned on or off quickly. At present wind generation contributes about 5% part of the country’s electrical energy, and solar less than 0.3%, and at these low levels hydroelectric generation can buffer their variability. As the availability of both sources rise to rival hydroelectricity in their share of NZ electricity supply, wind and solar generation will need to be matched by other energy storage such as batteries. Here we assume such capacity is available, so that wind and solar power can be compared on the same time scales as hydroelectricity.

Figure 2-1 shows the seasonality of hydroelectric generation in the North and South Islands of NZ. Within each season, the data are in order of year from 1972 to 2016, and the lines show linear trends fitted to the values over that period. There is a marked downward trend in autumn (defined as Apr-May-Jun here) and an upward trend in winter (Jul-Aug-Sep) for total generation, arising from the dominant South Island generation. The trend there can be attributed to more of the precipitation falling as rain rather than snow, and to earlier melt, with climate warming over recent decades.

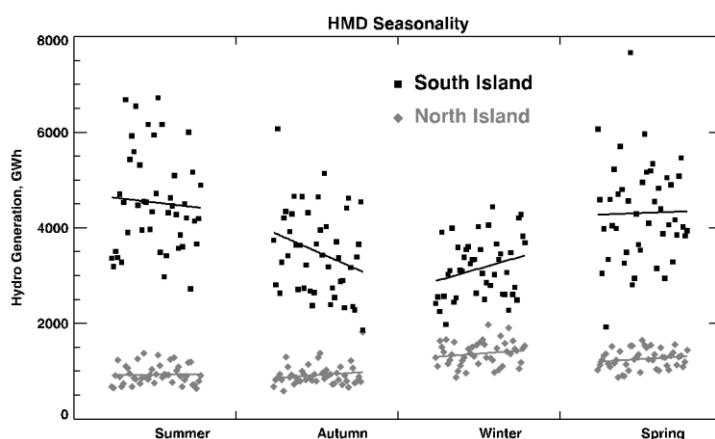


Figure 2-1: Seasonality of NZ hydroelectric generation, years 1972–2016. Data are from the NZ Hydrological Modelling Dataset (HMD) described in Section 4.1, with totals of all river flows in current hydroelectric schemes. For each season and island, the trend over the 45-year period is shown.

The other characteristics to note are that South Island generation is lowest in winter because in those hydro catchments much of the precipitation falls as snow. North Island generation is low in summer and autumn, mostly because of greater evaporation, and 30–50% higher in winter and spring. The total for NZ is dominated by the much larger South Island component, which can be lowest in autumn particularly in recent years.

The preponderance of low flows in autumn is clear in Figure 2-2, which shows the same data as Figure 2-1 but now as total NZ generation, coloured by season. As suggested by the previous figure, the lowest flows were often in winter before 1985, but since then the annual minima have been in autumn.

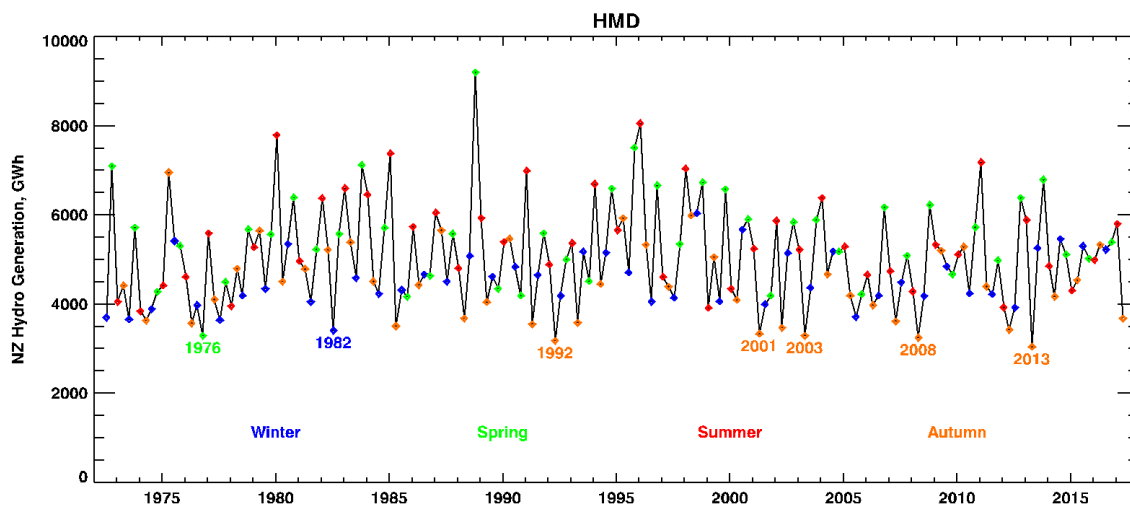


Figure 2-2: Total seasonal flow into NZ hydroelectric catchments, 1972–2016. Data are from the NZ HMD dataset, with the seven lowest seasonal flows highlighted. All recent lowest flows have been in autumn.

The low flow years shown in Figure 2-2 coincide with those in a report from the NZ Electricity Authority (2018c, p35) discussing the problem of ‘dry winters’:

Although conservation campaigns have not been needed for some time, there have been instances when a campaign has been necessary. For example, the public was asked to conserve electricity in 1992, 2001, 2003 and 2008, when hydro-lakes had sustained periods of low inflows. In 1992, the dry year necessitated some areas in the South Island having mandatory water heating cuts leaving many people with cold water. The South Island was worse affected than the North Island as a result of limitations in transmission of power from the North Island across the HVDC¹. No conservation campaigns have been required since 2008, despite dry periods in 2012, 2013 and 2017.

The relation between minimum flows in autumn and ‘dry winters’ is the obvious effect of cumulative low flow resulting in low lake storage just as low temperatures increase demand for heating.

For a future NZ with much more wind and solar generation, this seasonal difference is likely to be exacerbated. As described below in Section 5, wind speeds are also generally lower in autumn. They are highest in spring, though the relative amplitude of the seasonal variation is less pronounced for NZ as a whole. Solar energy has the largest seasonal cycle, as illustrated and discussed in Section 6.1.

As NZ progresses toward net zero greenhouse gas emissions by 2050, electricity generation will need to nearly double (MBIE 2019). In round figures, that means an increase from about 5 GW average production now (43 TWh/year) to at least 8 GW in 2050, all from renewables. Including replacement of the 1 GW presently produced from fossil fuels, that means an extra 4 GW from renewable generation.

Recent Electricity Authority figures of proposed and mostly consented new generation (Electricity Authority 2019) include renewable capacity comprising 506 MWp of hydro, 2433 MWp of wind, 317 MWp of geothermal, and 200 MWp of marine (on Kaipara Harbour). There was no mention of solar at that time, but there are few constraints on where it can be deployed in NZ. As described in Section 6, we assume a notional 10 GWp of solar capacity, providing on average 1.6 GW. As in Table A-1, the wind analysis allows for up to four times the above figure, with much of the extra offshore.

¹ High-voltage direct current.

3 Methods

The datasets used in this report are of two types: historical data from climate and hydrological records and analysis, and climate model projections in both hindcast and forecast mode. The historical data are used, as in the previous section, to frame the problem, and also to provide ‘ground truth’ for the hindcast model analyses against which future projections are assessed.

For traceability in our exploration of future scenarios, it is necessary to compare within models so that each future scenario is assessed relative to the hindcast with the same model. In its turn, that hindcast is referenced against the historical data, but a close match is neither necessary nor expected, as described below. Rather, we anticipate just that any future changes in generation patterns will be of the same kind and relative scale as the models project.

The historical climate datasets are specific to the type of generation, so they are described within those sections of this report. Here we describe the climate models and their integration with hydrological models driven by climate change projections.

The data used in the analysis include climate change projections for New Zealand (Ministry for the Environment 2018). For solar and wind generation capacity these projections are used directly; for hydroelectric generation the climate change projections are coupled with the national hydrological surface water model, TopNet (Clark et al. 2008), for inflow and river runoff.

The data analysed are weekly, monthly and annual aggregates of daily time-series of generation capacity from solar, wind, and hydrological sources. Each data set is the end result of sequential climate and/or hydrological modelling for combinations selected from under six GCMs and four Representative Concentration Pathways (RCPs), from 1971 up to 2070, resulting in a 24-member ensemble of simulations (i.e., six GCMs × four RCPs).

The methodological design to determine future trends and confidence in these projections is illustrated in Figure 3-1 below.

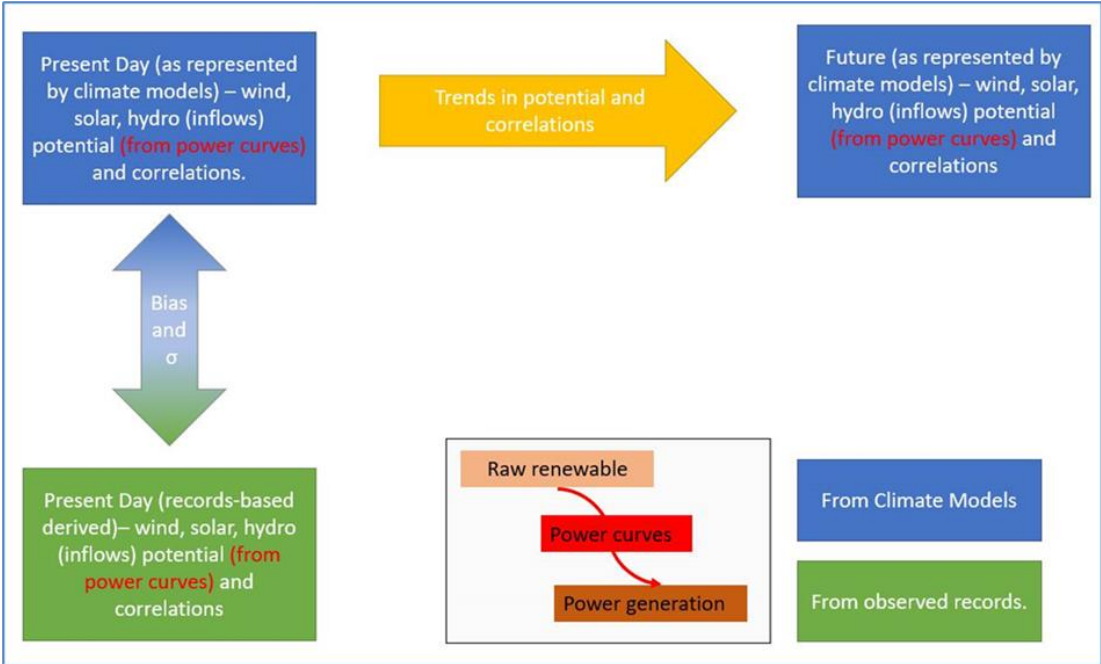


Figure 3-1: Schematic showing analysis approach used in the current report.

3.1 Climate models

As part of the fifth Intergovernmental Panel on Climate Change (IPCC) assessment report (AR5) (IPCC 2014), NIWA assessed up to 41 GCMs from the AR5 model archive (referred hereafter as Coupled Model Intercomparison Project version 5 (CMIP5) for their suitability for the New Zealand region. Validation of those GCMs was carried out through comparison with large-scale climatic and circulation characteristics across 62 metrics (Ministry for the Environment 2018). This analysis provided a performance-based ranking relative to New Zealand's historical climate. Six GCMs were chosen as being better at representing climatic dynamics around New Zealand and for spanning a useful range of climate change sensitivities to CO₂ projections. The six CMIP5 models selected were:

- HadGEM2-ES (Jones et al. 2011).
- CESM1-CAM5 (Meehl et al. 2013).
- NorESM1-M (Bentsen et al. 2013).
- GFDL-CM3 (Griffies et al. 2011).
- GISS-E2-R (Schmidt et al. 2014).
- BCC-CSM1.1 (Wu et al. 2014).

The GCMs were driven by four scenarios (i.e., RCPs) of future concentrations of greenhouse gases and aerosols, as well as by natural processes including solar irradiance and historical emissions. The GCM driven runs were otherwise free-running in that they are not constrained by historical climate observations. GCM outputs (i.e., boundary condition and Sea Surface Temperatures) were then used to drive a Regional Climate Model (RCM) to refine the variables to a more useful spatial scale for the country. The output of the regional climate modelling became the input for the hydrological modelling analysed here after rudimentary bias correction. Further details on the validation and the GCM and RCM modelling can be found in Sood (2014) and Ministry for the Environment (2018).

The downscaled climate data used here run from 1971 to 2100. From 2006 onward, as per IPCC recommendations, each GCM is in turn driven by four RCPs that encapsulate alternative scenarios of radiative forcing and reflect alternative trajectories of global societal behaviour with regard to greenhouse gas emissions and other activities. The range of RCPs used can help shed light on the utility of climate change mitigation. Descriptions and trajectories of the four RCPs are provided in Table 3-1 and Figure 3-2. By mid-century, the temperature trajectory of RCP2.6 is the least increase and RCP8.5 the greatest, with RCP4.5 and RCP6.0 producing intermediate warming. While RCP6.0 ends the century with more forcing than RCP4.5, early and mid-century it is RCP4.5 that has higher greenhouse gas concentrations and a stronger radiative forcing; this is somewhat reflected by the mid-century temperature change ranges for the New Zealand seven-station network (Table 3-1). RCP6.0 overtakes RCP4.5 after the middle of the century.

It is important to note that the climatic and hydrological effects of the RCPs are not simply a linear or monotonic progression from the lowest to highest RCP. Furthermore, the spatial patterns of climatic change across New Zealand vary across combinations of RCP-RCMs simulations.

Table 3-1: Descriptions of the Representative Concentration Pathways (RCPs). Temperature changes are the GCM mean (°C) and, in brackets, the likely ranges (Source MfE 2018).

Representative Concentration Pathway	Description	Seven-station temperature change (Ministry for the Environment 2016)		Global surface temperature change for 2081–2100 (IPCC 2014, Table 2.1)
		2031–2050	2081–2100	
RCP2.6	The least change in radiative forcing considered, by the end of the century, with +2.6 W/m ² by 2100 relative to pre-industrial levels.	0.7 (0.2–1.3)	0.7 (0.1–1.4)	1.0 (0.3–1.7)
RCP4.5	Low-to-moderate change in radiative forcing by the end of the century, with +4.5 W/m ² by 2100 relative to pre-industrial levels	0.8 (0.4–1.3)	1.4 (0.7–2.2)	1.8 (1.1–2.6)
RCP6.0	Moderate-to-high change in radiative forcing by the end of the century, with +6.0 W/m ² by 2100 relative to pre-industrial levels.	0.8 (0.3–1.1)	1.8 (1.0–2.8)	2.2 (1.4–3.1)
RCP8.5	The largest change in radiative forcing considered, by the end of the century, with +8.5 W/m ² by 2100 relative to pre-industrial levels.	1.0 (0.5–1.7)	3.0 (2.0–4.6)	3.7 (2.6–4.8)

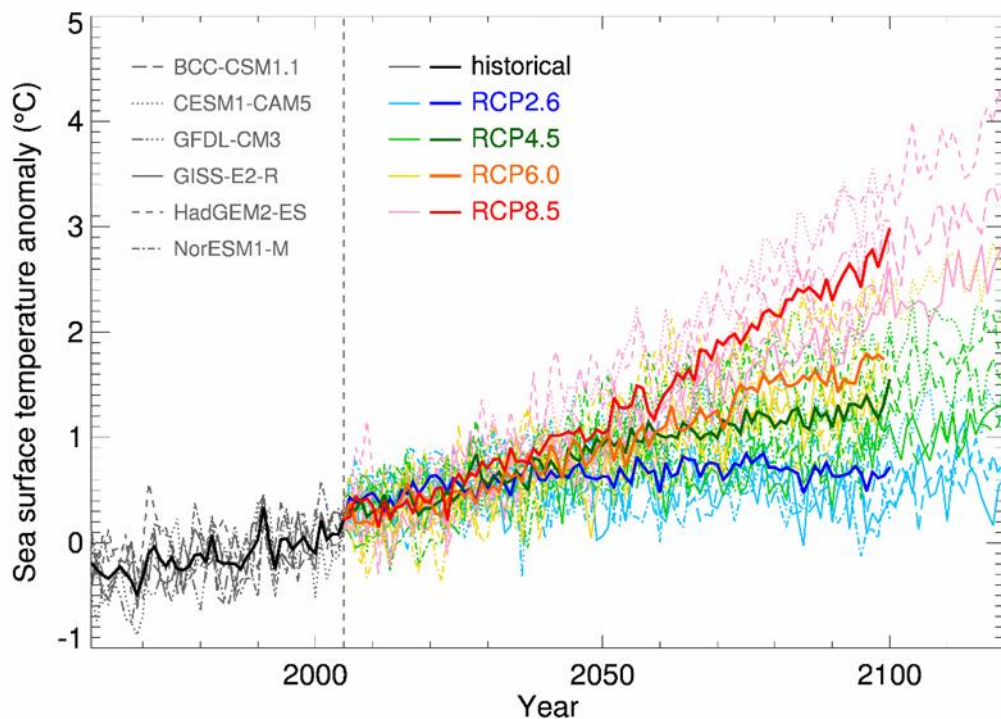


Figure 3-2: CMIP5 climate models (2006–2120), the historical simulations. Bias-adjusted sea surface temperature (SST), averaged over the RCM domain, for 6 (1960–2005), and four future simulations (RCPs 2.6, 4.5, 6.0 and 8.5), relative to 1986–2005. Individual models are shown by thin dotted or dashed or solid lines (shown in grey in the inset legend), and the 6-model ensemble-average by thicker solid lines, all of which are coloured according to the RCP pathway.

3.2 River flow and hydro-electric lake inflow model – TopNet

The catchment hydrological model used in this study is NIWA’s TopNet model (Clark et al. 2008), which is routinely used for surface water hydrological modelling applications in New Zealand. It is a spatially semi-distributed, time-stepping model of water balance. It is driven by time-series of precipitation and temperature, and additional weather elements where available. TopNet simulates water storage in the snowpack, plant canopy, rooting zone, shallow subsurface, lakes and rivers. It produces time-series of modelled river flow (without consideration of water abstraction, impoundments or discharges) throughout the modelled river network, as well as evapotranspiration (derived from weather/climate input information). TopNet does not adjust river flows for effects of irrigation, water take and redistribution through hydro-electric canals. TopNet has two major components, namely a basin module and a flow routing module.

The model combines TOPMODEL hydrological model concepts (Beven et al. 1995) with a kinematic wave channel routing algorithm (Goring 1994) and a simple temperature-based empirical snow model (Clark et al. 2008). TopNet can be applied across a range of temporal and spatial scales over large watersheds using smaller sub-basins as model elements (Ibbitt and Woods 2002; Bandaragoda et al. 2004). Considerable effort has been made during the development of TopNet to ensure that the model has a strong physical basis and that the dominant rainfall-runoff dynamics are adequately represented in the model. TopNet model equations and information requirements are provided by Clark et al. (2008) and McMillan et al. (2013). The version of the model used in this project does not consider water transfers from river to river or water storage, nor does it model aquifer water balances.

For the development of the national version of TopNet used in this study, spatial information in TopNet was provided by national datasets as follows:

- Catchment topography based on a national 30 m Digital Elevation Model (DEM).
- Physiographical data based on the Land Cover Database version three (LCDB3) and Land Resource Inventory (Newsome et al. 2000).
- Soil data based on the Fundamental Soil Layer information (Newsome et al. 2000).
- Hydrological properties (based on the River Environment Classification version two (REC2) (Snelder and Biggs 2010)²).

The method for deriving TopNet's parameters based on GIS data sources in New Zealand is given in Table 1 of Clark et al. (2008). Due to the paucity of some spatial information at national/regional scales, some soil parameters are set uniformly across New Zealand.

TopNet is currently configured to use LCDB3, which is based on satellite imagery from 2008, rather than the latest version, which is based on 2016 imagery. There are differences in land cover between the two dates, and these may have hydrological consequences, although they are likely to be small in comparison with changes up to 2070. During the course of the simulations from 1971 to 2070, however, land use is kept constant. The purpose of this is to isolate the effects of changing climate on the hydrological response; incorporating land use change scenarios would confound interpretation of the results.

Hydrological simulations are based on the REC2 network aggregated up to Strahler³ catchment order three (approximate average catchment area of 7 km²) used within previous national and regional scale assessments; residual coastal catchments of smaller stream orders that are not subsumed into larger catchments remain included. Large surface water bodies such as lakes, hydroelectric reservoirs and wetlands (characterised by surface area larger than 1 ha) are represented in the hydrological model as natural draining features. The simulation results comprise hourly time-series of various hydrological variables for each computational sub-catchment, and for each of the six GCMs and four RCPs considered. To manage the volume of output data, only river flow information was preserved; all the other state variables and fluxes can be regenerated on demand.

Because of TopNet assumptions, soil and land use characteristics within each computational sub-catchment are homogenised. Essentially this means that the soil characteristics and physical properties of different land uses, such as pasture and forest, will be spatially averaged, and the hydrological model outputs will be an approximation of conditions across land uses.

To carry out the simulations required for this study, TopNet was run continuously from 1971 to 2070, with the spin-up year 1971 excluded from the analysis. The climate inputs were stochastically disaggregated from daily to hourly time steps and the hydrological model was run in a "uncalibrated mode" before a simple bias correction of the hindcast hydrological simulation (see section 3.3) is performed using HMD dataset as historical observation. The GCM-specific bias correction (described in section 4.2) is then applied to future simulations time period (2006-2070). As the GCM simulations are "free-running" (based only on initial conditions, not updated with observations), comparisons

² Due to time constraints associated with this project, it is not possible to assess the effect of using the Digital River Network 3 on the potential impacts of climate change.

³ Strahler order describes river size based on tributary hierarchy. Headwater streams with no tributaries are order 1; 2nd order streams develop at the confluence of two 1st order tributaries; stream order increases by 1 where two tributaries of the same order converge.

between present and future hydrological conditions can be made directly (as each GCM is characterised by specific physical assumptions and parameterisations).

3.3 Measuring a climate change effect

To measure the effect of climate change on the chosen variable, simulated data from the baseline period from mid-1985 to mid-2006 (20 years) are compared to three future time periods: 2030–2049 (mid-century, referred as 2040s). 2040–2059 (referred as 2050s) and 2050–2069 (referred as 2060s). The magnitude of the effect is determined by the difference between the climate/hydrological characteristics or thresholds calculated over the baseline and future periods.

Results of this analysis are presented as follows:

- Absolute and relative change in potential hydrological generation capacity and their ranges across the six GCMs (see Section 4).
- Absolute and relative change in solar generation capacity and their ranges across the six GCMs (see Section 5).
- Absolute and relative change in wind generation capacity and their ranges across the six GCMs (see Section 6).

3.4 Multi-model averaging: mean versus median

One of the important elements of climate change projections is the use of multiple GCMs. Each GCM is in essence a plausible representation of the climate system as far as a particular research group is concerned. Using a suite of different GCMs allows us to compensate somewhat for uncertainties in climate science; the central tendency or ‘multi-model average’ of the suite of GCM results may be considered the most plausible climate change outcome. In statistics, however, there is no single definition of ‘average’ – it depends on how one defines the “centre”. The most commonly used measure of average is the ‘mean’, calculated as the sum of a series of numbers divided by the number of numbers. The ‘median’ is another kind of average and describes the middle-most number (i.e., half of the numbers are above the median and half are below the median). Lastly, the ‘mode’ is the value that occurs most often. Each type of average has its place depending on the nature of the data and the insights being sought from the data.

In climate science multi-model averages have more often been represented as means, and this has been the case for the key studies in New Zealand (e.g., Ministry for the Environment 2018), but multi-model medians have also been used internationally (e.g., IPCC 2014). The mean is reasonable if the distribution of a dataset is normal (or Gaussian), but for hydrological variables (particularly for discharge) normal distributions may not be a good approximation. Furthermore, the median gives a truer indication of the central tendency when decisions are to be made based on likelihood (i.e., 50 per cent chance that the results will be greater than the median and 50 per cent chance they will be lower) as it is less affected by outliers, which is more appropriate when averaging across alternative representations of reality and aligns better with the IPCC’s use of likelihood percentages. As a result, multi-model averages of hydropower generation capability will be represented in this report as medians.

4 Hydroelectric Generation

4.1 Observed dataset for climate change

Observed total hydropower generation capacity is provided by the HMD, referred to as the Power Archive, which is updated on an annual basis at the request of the Electricity Authority. This dataset provides harmonised daily run-of-river hydrological flows and hydropower inflows at 35 locations since 1 January 1932 (Electricity Authority 2018a,b). This dataset represents 12 current and potential hydropower schemes across New Zealand (36 stations) with 5 schemes in the North Island (19 stations) and 7 schemes in the South Island (17 stations). Inflows or river discharge (in m³/s) are converted to power generation capacity (MWh) through the use of a conversion factor that is specific to each location (Electricity Authority 2018b).

Due to the hydrological model assumption (i.e., modelling of natural flows only, non-modelling of diverted flow through canal/pipe nor modelling of transfer between river system) and to establish a reference dataset, it was necessary to reduce the HMD historical dataset (referred to as modHMD hereafter) to a dataset that could be used for verification/validation purposes (Table 4-1). This step ensured that the hydrological model was able to represent the necessary hydrological characteristics (i.e., river discharge and total natural inflow to hydro-electric lake) for the different time scale of interest (i.e., weekly, monthly, seasonal, annual). Following analysis of the HMD datasets, the modHMD datasets contains 5 current power schemes (2 in the North Island, 3 in the South Island) and 2 potential power schemes (1 each in the North and South Islands) encompassing 24 current natural flow stations (as defined by the HMD dataset) and 8 natural flow sites. It is important to note that the modHMD covers the natural discharge/inflows to the main hydroelectricity power schemes across New Zealand and as such is relevant to the current investigation.

Table 4-1: Modified HMD dataset supporting climate change investigation.

Location	Hydropower schemes	Hydropower stations
North Island	Potential North Island scheme	Ngaruroro
	Waikaremoana	Kaitawa-Tuai-Piripaua
	Waikato	Aratiata-Ohakuri-Atiamuri- Whakamanu-Maraetai-Waipapa- Arapuni-Karapiro
South Island	Clutha	Clyde-Roxburgh
	Potential South Island schemes	Grey-Taramakau- Wairau- Hurunui-Waiau-Clarence- Cobb
	Manapouri + other SI	Manapouri-Te Anau-Monowai
	Waitaki (Mid Waitaki-Ohau chain- Tekapo)	Benmore-Aviemore-Waitaki-Ohau A- Ohau B- Ohau C- Takapo A- Tekapo B

For modelling purposes, the modHMD dataset was generated over the period 1 Jan 1971 to 31 Dec 2005, which corresponds to the historical period for CMIP5 climate change analysis. The New Zealand-wide modHMD dataset has been split as follows providing the 16 datasets for the analysis:

- North Island and South Island datasets (referred as modHMD-NI and modHMD-SI) to separate snow/ice related generation processes from real-time climate responses.
- Each dataset is split between a potential dataset (referred as -Pot) and actual generation dataset (referred as -Gen).
- Each island is separated geographically into an eastern dataset (referred as -East) and a western dataset (referred as -West). The geographical separation is based on the Southern Alps on the South Island and a line from Gisborne to Taranaki in the North Island.

The resulting datasets were split over the following three time series for the period 1971–2017:

- 1971–1985: Pre hindcast period for climate change analysis.
- 1986–2005: Hindcast period for climate change analysis.
- 2006–2017: Near future for climate change analysis.

Figure 4-1 and Figure 4-2 present the annual average and seasonal average power generation capacity frequency analysis for both the North and South Island (calculated from the modHMD dataset) calculated over hydrological years.

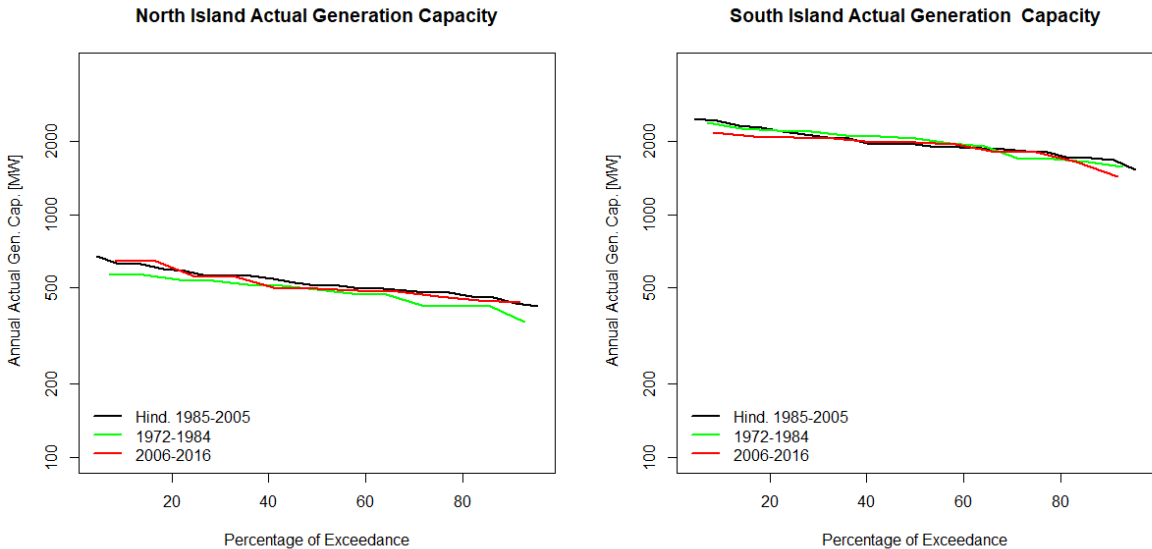


Figure 4-1: Annual average hydropower generation frequency analysis for the North Island (left panel) and the South Island (right panel). Average hydropower potential generation was generated using the modHMD dataset over the hydrological years 1972–2016.

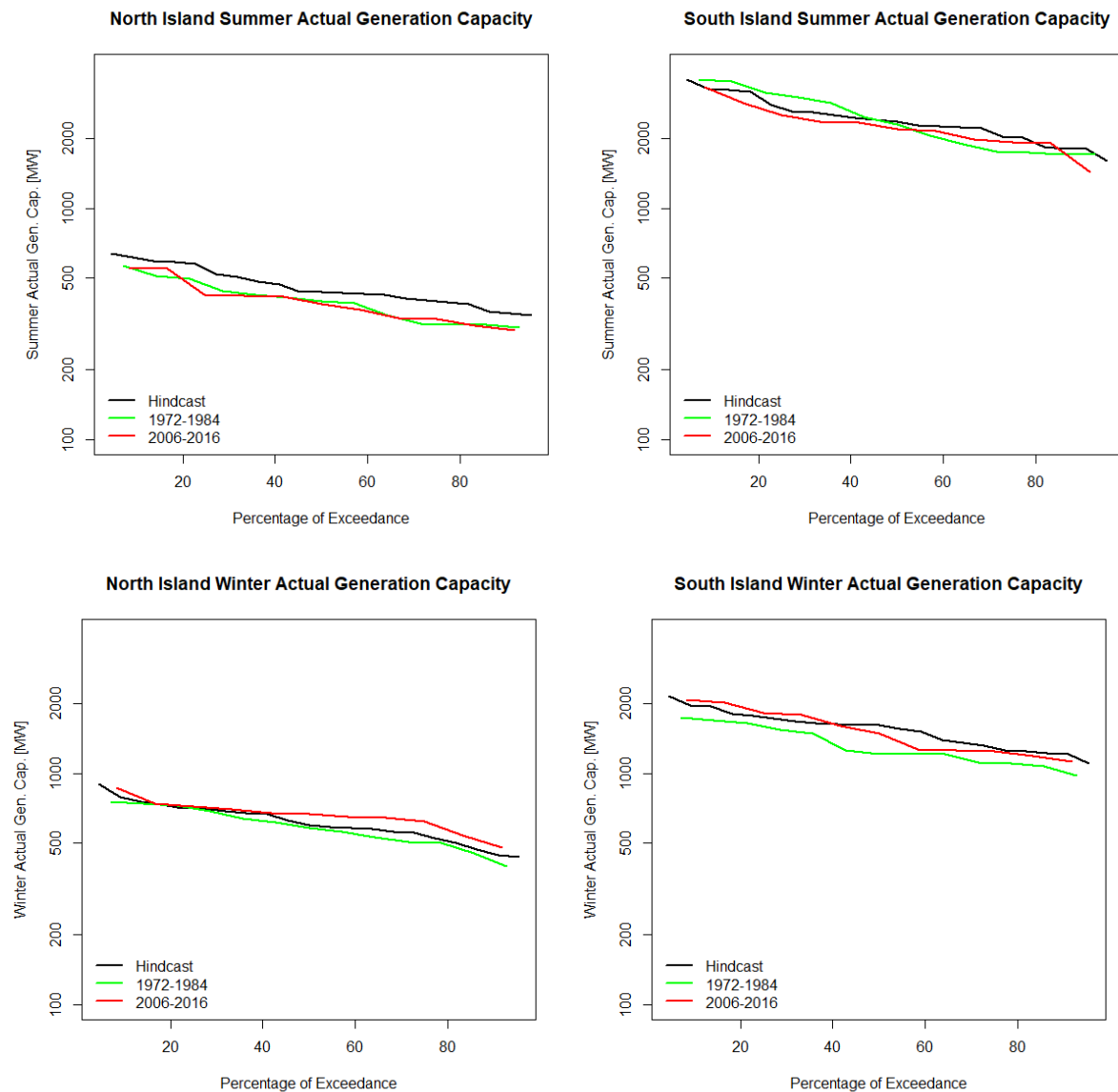


Figure 4-2: Seasonal average hydropower potential generation frequency analysis for summer (top) and winter (bottom) seasons for the North (left panels) and South (right) Islands. Average hydropower potential generation was generated using modHMD dataset over the hydrological years 1972–2016.

Analysis of the dataset across the three periods of interest indicates that:

- Hydropower potential generation capacity is dominated by the South Island contribution by more than a factor of three.
- The hindcast period (1986–2005) exhibits a lower inflow profile (hence a lower potential generation capacity profile) than the prior and later periods. This could be linked to the Interdecadal Pacific Oscillation (e.g., <https://niwa.co.nz/node/111124>) signal over the period considered, but this was not investigated as part of the analysis.
- Summer potential generation capacity remains relatively stable over the period 1972–2017 for the North Island, while the South Island exhibits a marked decrease in

generation potential capacity post-1984. The latter is thought to be associated with reduction of snow melt contribution to the South Island hydropower schemes.

- Winter potential generation capacity exhibits a different pattern with a marked reduction in the North Island’s winter potential generation capacity over the hindcast period (compared to earlier and later years). This is thought to be associated with change in rainfall pattern across the North Island in association with increased temperature resulting in lower inflow to the hydropower schemes in the North Island. The South Island is subject to the same changes as the North Island, but this results in more precipitation falling in liquid form during winter resulting in a markedly increased inflow (hence potential generation capacity) for the South Island hydropower schemes.

4.2 Hydrological bias correction

TopNet model parameterisation uses the concept of parameter multipliers, as one of the main assumptions of the model implementation is that the spatial distribution of the parameters is determined *a priori* from catchment physiographic information for the sources described above (see Section 3.2). TopNet requires the determination of seven hydrological parameter multipliers and 10 snow-related parameters for each sub-catchment (see Table 4-2). The initial values of the parameter multipliers are set to a value of 1, while snow related parameters are initialised based on previous study results for the area.

Table 4-2: Range of TopNet parameter multipliers used during calibration process.

Parameter name (internal name)	Parameter description	Calibrated range
Hydrological parameters		
Saturated store sensitivity (topmodf)	Describes exponential decrease of soil hydraulic conductivity with depth	[0.01–2] * default
Drainable soil water (swater1)	Range between saturation and field capacity	[0.05–10] * default
Plant available soil water (swater2)	Range between field capacity and wilting point	[0.05–10] * default
Hydraulic Conductivity at saturation (hydcond0)		[0.1–10000]*default
Ch_exp	Clapp-hornberger c exponent	[0.05–10] * default
Ga-psif	green-ampt wetting front suction	[0.05–10] * default
canscap	canopy storage capacity	[0.05–10] * default
canenh	canopy evaporation enhancement factor	[0.05–10] * default
Overland flow velocity (overvel)		[0.1–10]*default
Manning n	Characterises the roughness of each reach	[0.1–10] *default
Atmospheric lapse rate (atmlaps)	Change in temperature with elevation, used to adjust temperatures from climate data sites to basin centroid	[0.7–1.5] * default
Gauge Undercatch (gucatch)	Adjustment for non-representative precipitation	[0.5–1.5] * default

Parameter name (internal name)	Parameter description	Calibrated range
Snow parameters		
threshold for snow accumulation (th_accm)	Temperature threshold for snow accumulation	270.15–275.15 [K]
Threshold for snow melt (th_melt)	Temperature threshold for snow melt	269.15–274.15 [K]
snowddf	Degree-day factor for snow melt	1–10 [mm K ⁻¹ day ⁻¹]
Minddf	Calendar day of the minimum degree-day-factor day	1–366 [days]
Maxddf	Calendar day of the maximum degree-day-factor day	1–366 [days]
snowamp	Seasonal amplitude of degree-day factor for snow melt	0–5 mm K ⁻¹ day ⁻¹]
snowros	Addition in melt factor caused by rain-on-snow events	0–5 mm K ⁻¹ day ⁻¹]
dec melt	Decrease in melt due to higher albedo after fresh snow	0–5 mm K ⁻¹ day ⁻¹]
albdecy	Time decay of snow albedo	1–5 days
cv_snow	Sub-grid variability representing the distribution of the snowpack across the catchment	0–2 [-]

Due to the complex interaction between climate, landcover, and geomorphology, hydrological models generally require calibration for the model to reproduce observed hydrological behaviour and/or characteristics. Despite TopNet reproducing observed hydrological characteristics across New Zealand as a whole (see Booker and Woods 2012 and McMillan et al. 2016), model calibration is recommended to overcome catchment-specific hydrological behaviour (Zammit 2019). An alternative to calibration, is bias correction, which aims to correct the hydrological model using a simple water balance approach focussing on the following characteristics: i) long term average inflows to lakes or river discharge; and ii) long term average snow cover duration.

As part of the climate change modelling chain, a specific simple water balance bias correction focussing on reproducing the average flow conditions was developed for TopNet (Collins 2020). Figure 4-3 presents a comparison of simulated and observed hydrological statistics over the period 1986–2005. The observed statistics are calculated for a natural streamflow observation dataset (Booker 2012) and compute the mean annual discharge (QMean), representing the overall water balance of the simulated catchments, and the 7-day Mean Annual Low Flow (Q7DMALF), representing low flow hydrological behaviour being associated with ecological flow characteristics. To avoid any issues with missing information, the hydrological statistics are calculated at locations where less than 5% of observations are missing over the period 1986–2005. The simulated hydrological characteristics represent the median of the hydrological statistic calculated for each GCM driven simulation. Analysis indicates that the bias correction performance is adequate for average conditions but results in a consistent underestimation of low flows.

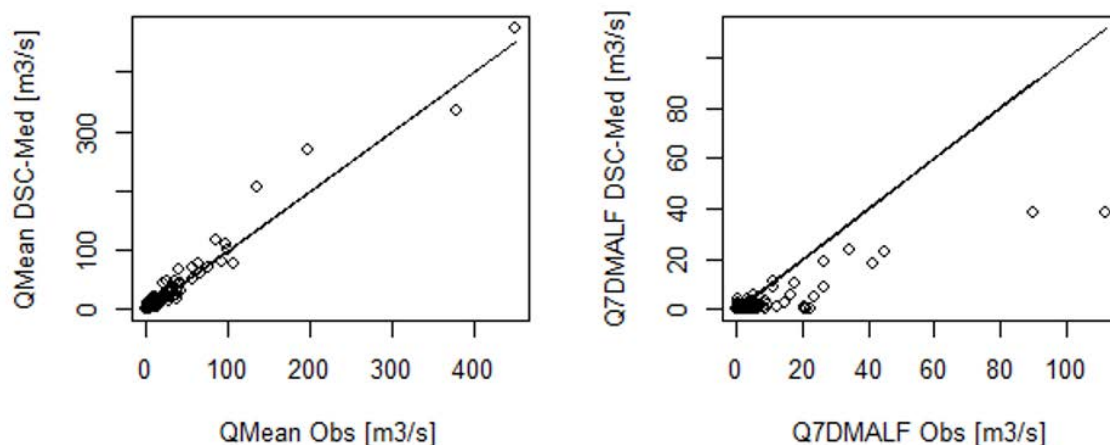


Figure 4-3: Validation of the water balance. The left panel shows annual mean discharge (QMean), while the right panel shows 7-day mean annual low flow (Q7DMALF).

To attempt to remediate this issue, the bias correction focusses on the following processes:

1. Correction of the amount of precipitation received upstream of a streamflow gauge or a hydro-lake for the locations indicated in Table 4-1. For each site we compared GCM specific simulated river discharge and natural lake inflow with associated HMD-gen timeseries (taken as observations) over the period 1985–2006. This involved comparing observed and predicted daily flow time series (to identify potential mismatches in the flow regime); observed and predicted flow duration curves (to identify potential mismatches in the statistical distribution of the flows); observed and predicted cumulative flow (to identify potential issues related to systematic bias in model simulation) and observed and predicted average flow.
2. Correction of the temperature threshold at which snow accumulates and melts upstream of a streamflow gauge or a hydro-lake for the locations indicated in Table 4-1. For each site we compared GCM specific simulated snow-cover area with snow-cover duration derived from Moderate Resolution Imaging Spectroradiometer (MODIS) satellite data (Conway et al., 2021), to represent historical snow-pack conditions.

Figure 4-4 presents the outcomes of the bias correction for a range of hydrological characteristics for lake Hawea. Use of precipitation bias correction (average reduction of 10% for lake Hawea draining catchment) and snow accumulation and melt threshold adjustment (-2 degrees), improved the model ability to generate average conditions (< 1% error for average inflows to lake Hawea). Analysis of the daily average precipitation and inflow indicates that seasonal pattern of inflows match seasonal patterns of precipitation. This result was consistent for all the modelled hydro lakes and rivers (see Appendix B).

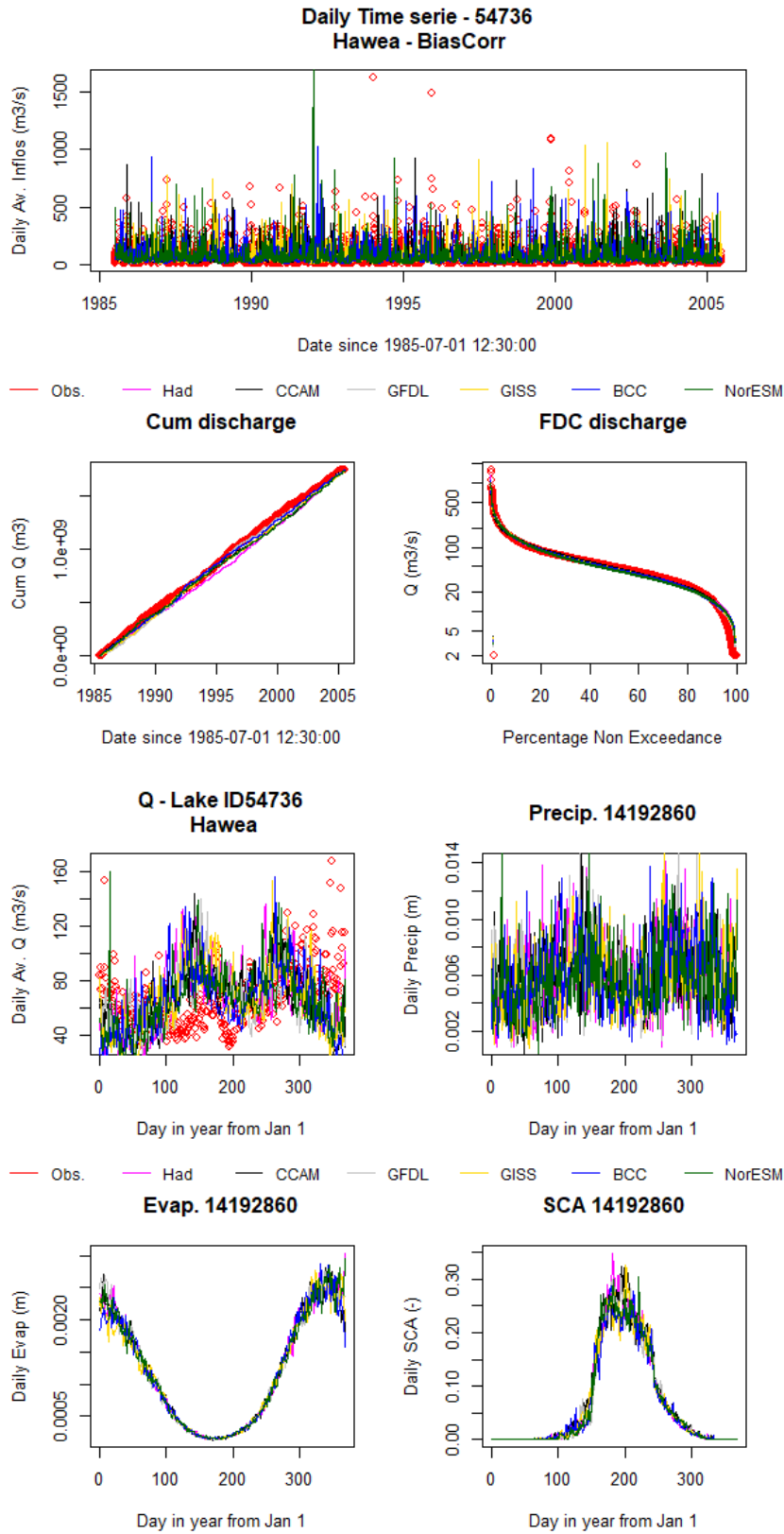


Figure 4-4: Daily hydrograph, cumulated hydrograph and flow duration curves (top) daily average inflows, precipitation, evapotranspiration and snow area (bottom) for Hawea inflows over the period 1985–2006. . Observations (black) are compared with TopNet flows driven by GCMs; HadGEM-ES (light blue), CESM1-CAM5 (blue), GFDL-CM3 (yellow), GISS-E2-R (orange), BCC-CSM1.1 (red), and NorESM1-M (dark-green).

To assess the effects of the bias correction on the hydrological simulations, we compared simulated generation over the period 1986–2005 (as shown in Figure 4-1) with bias corrected CMIP5 GCM-driven generation. Figure 4-5 shows the comparison for the North Island (upper panel) and South Island (lower panel) as time series (but this should not be understood as implying any correlation between them is expected). The models are free-running and thus expected only to simulate the distribution of results seen in the HMD-derived dataset. Quantitative analysis indicates that the CMIP5 driven simulations are generate a similar amount of power to that observed in the North Island and around 5% less power than that observed in the South Island.

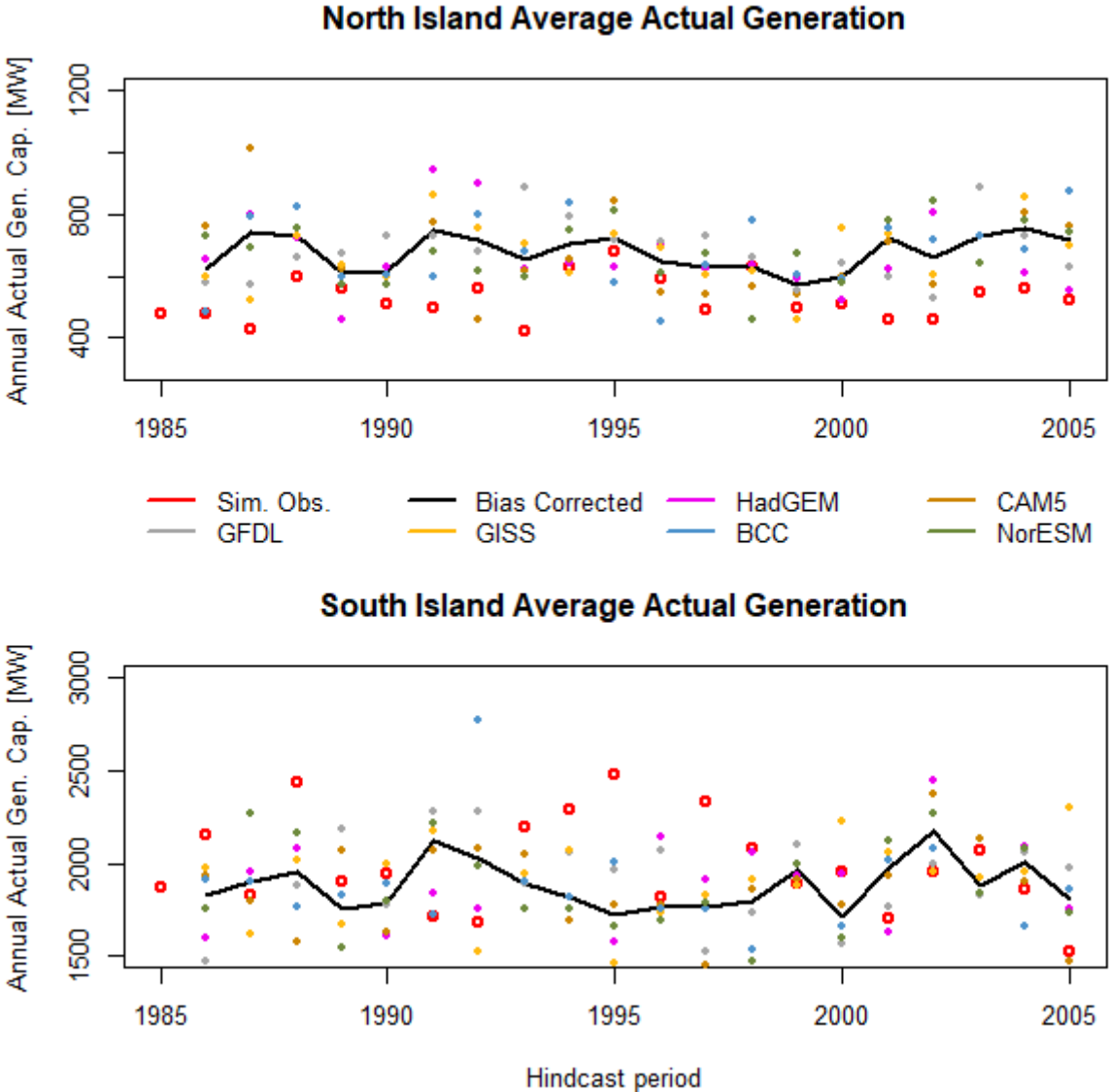


Figure 4-5: Comparison of simulated annual-average generation between HMD-gen dataset and hindcast bias-corrected CMIP5-driven for 1985–2006. North Island (top panel) and South Island (bottom panel) plots show: HMD-gen dataset (red circle); CMIP5 median island-wide actual generation (red line); TopNet flows driven by HadGEM-ES (magenta), CESM1-CAM5 (black), GFDL-CM3 (grey), GISS-E2-R (gold), BCC-CSM1.1 (blue), and NorESM1-M (dark green).

4.3 Climate change analysis

To measure the effect of climate change on the chosen variable, simulated data from the baseline period from mid-1986 to mid-2006 (20 years) are compared to four future time periods: 2021–2041 (referred to as ‘2030’), 2031–2051 (‘2040’), 2041–2061 (‘2050’), and 2051–2071 (‘2060’). The numbered year indicates the calendar year of the hydrological year starting on 1 July. The magnitude of the effect is determined by the difference between the climate/hydrological characteristics or thresholds calculated over the baseline and future periods. Three analyses are presented hereafter in regard to power generation:

- Threshold characteristic representing the 5th percentile of hydroelectric generation potential at annual-seasonal and monthly time scale.
- Time series analysis to identify consecutive hydropower generation period across reporting period.
- Frequency analysis to identify change in the distribution of hydropower generation.

For clarity only pertinent results are presented hereafter.

4.3.1 Hydropower generation threshold

Figure 4-6 presents the change in the 20-year-centred 5th percentile annual mean daily hydropower generation threshold across the North Island simulated hydropower schemes, with each 20-year period represented by a dot at its central year. Figure 4-7 presents the same analysis for the simulated South Island hydropower schemes.

Analysis of the impact of climate change on the 5th percentile annual hydropower generation threshold indicates that:

- North Island annual generation threshold exhibits a decreasing trend for most of the radiative forcing scenarios except for the lowest (RCP2.6). The decrease in the 5th percentile annual hydropower threshold is estimated to be around 10% over the period 2021–2071.
- South Island annual generation threshold exhibits an increasing trend for all radiative forcing scenarios. The increase in the 5th percentile annual hydropower threshold is estimated to be around 16% over the period 2021–2071, probably associated with increased snow melt contributing to South Island hydropower schemes.

Variability of the 5th percentile annual hydropower threshold is increasing with time and radiative forcing, generally doubling between the hindcast and 2060s period for the South Island hydropower schemes.

4.3.2 Annual

Figure 4-8 presents for each radiative forcing pathway the North Island 20-year annual mean daily hydropower generation distribution as the median across the six GCMs, for the hindcast period (1986–2005) and the four two-decade future periods as above, while Figure 4-9 presents the same analysis for the South Island hydropower generation.

Analysis of the simulations indicates:

- Future North Island hydropower generation is likely to be below hindcast North Island generation threshold for one or two years under the lowest warming scenario (over a 20year centred period) to an average of six or seven times (over a 20year period) for larger warming scenarios and with time.
- Future South Island hydropower generation is likely to be above hindcast South Island generation threshold independently of warming scenarios. This indicates that South Island hydropower generation capacity surplus is likely to increase with time and warming, likely driven by an increase glacial melt of alpine snow resource.

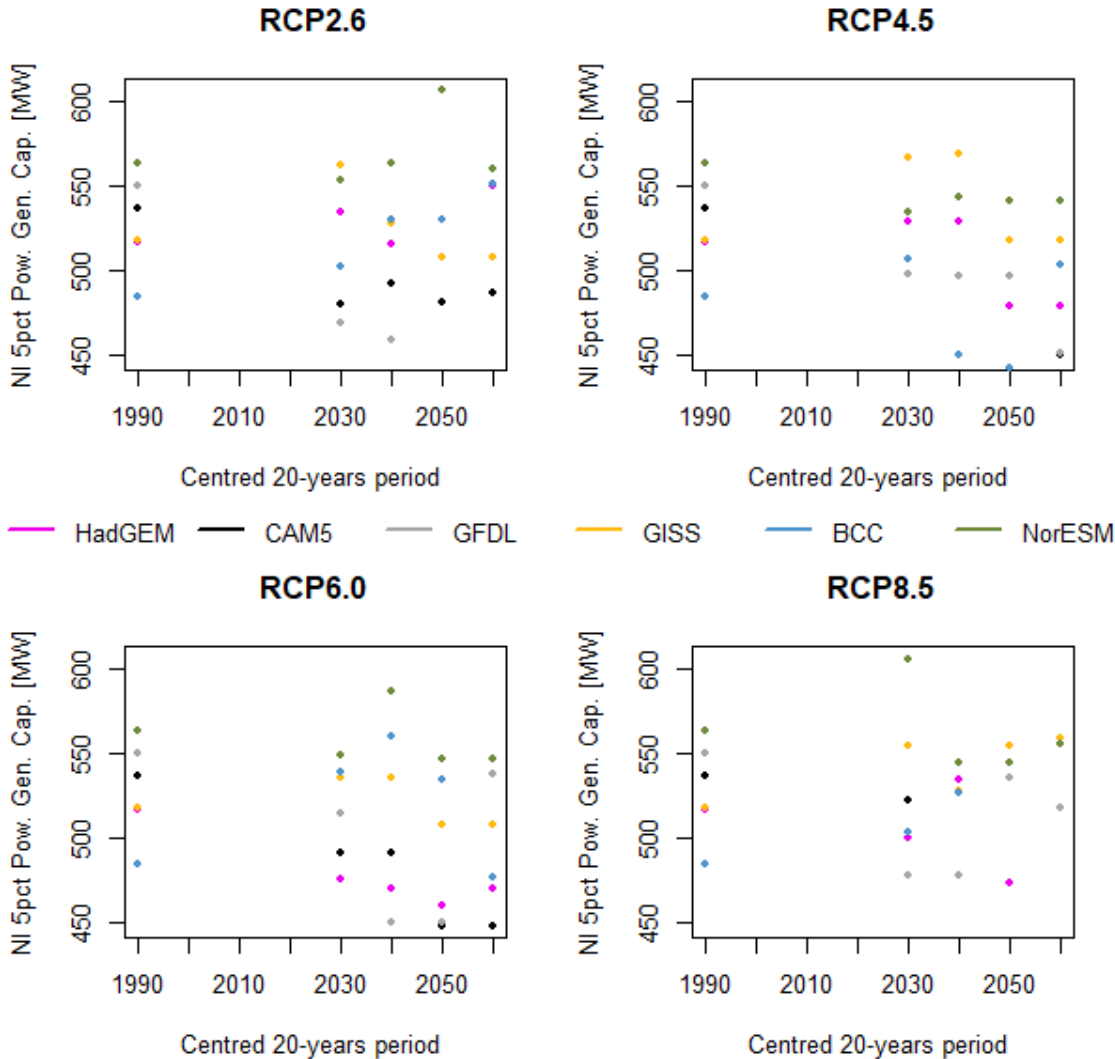


Figure 4-6: North Island 20-year centred 5th percentile annual mean hydropower generation threshold (MW) for each RCP. Calculations are for TopNet discharge driven by each GCM; HadGEM-ES (magenta), CESM1-CAM5 (black), GFDL-CM3 (grey), GISS-E2-R (gold), BCC-CSM1.1 (blue), and NorESM1-M (dark green).

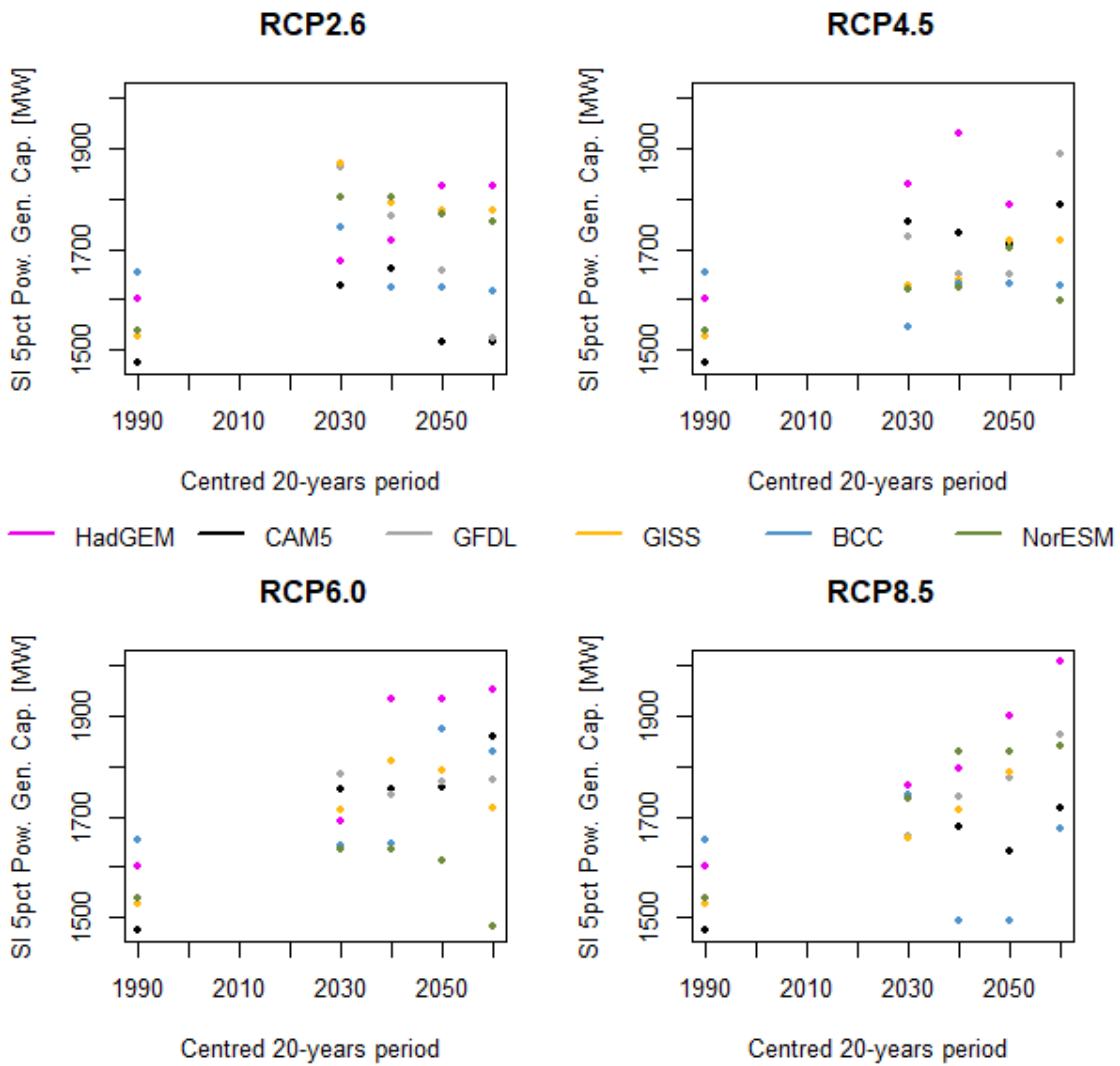


Figure 4-7: South Island 20-year centred 5th percentile annual mean hydropower generation threshold (MW) for each RCP. Calculations are for TopNet discharge driven by each GCM; HadGEM-ES (magenta), CESM1-CAM5 (black), GFDL-CM3 (grey), GISS-E2-R (gold), BCC-CSM1.1 (blue), and NorESM1-M (dark green).

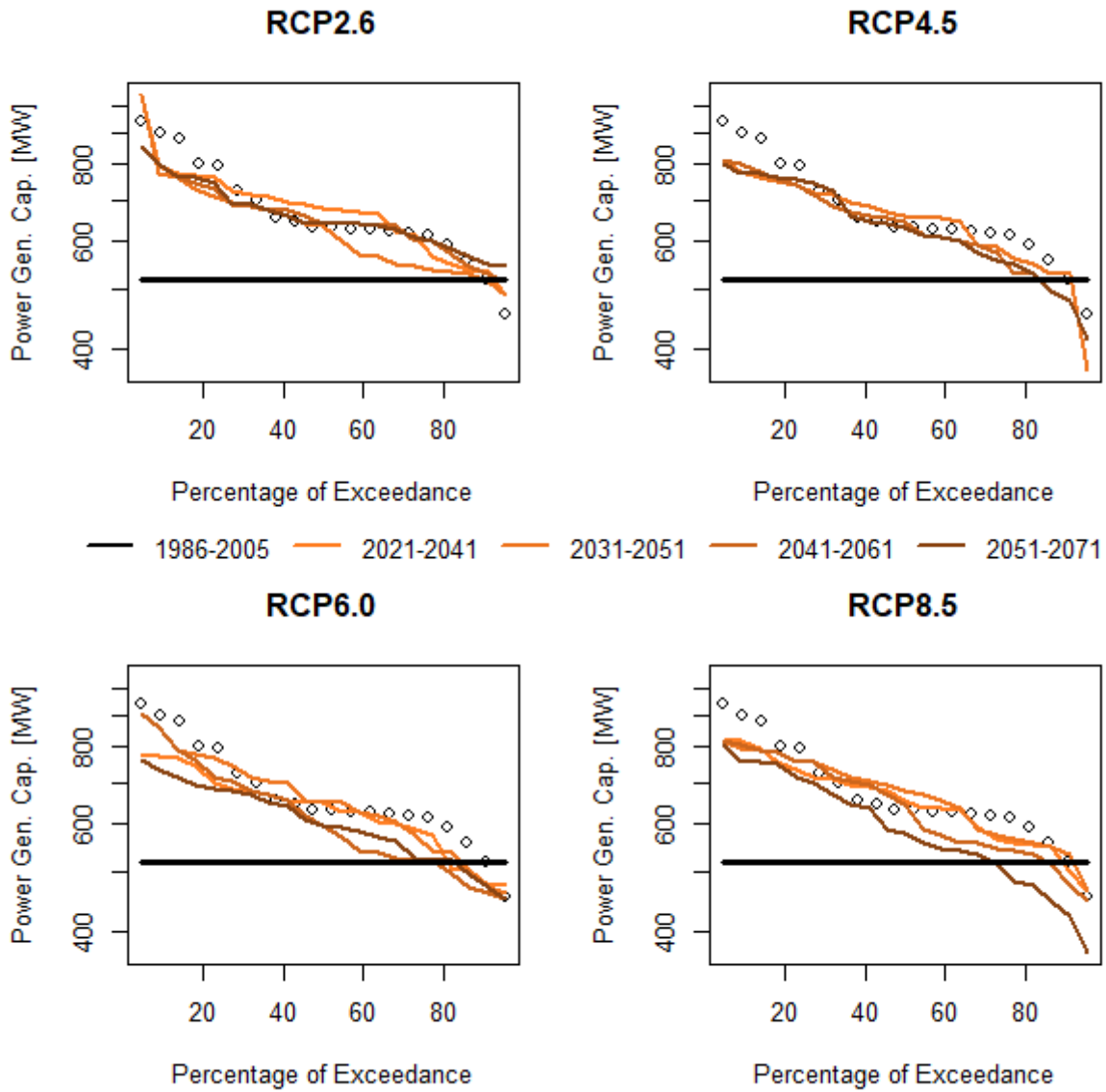


Figure 4-8: 20-year median annual mean daily hydropower generation capacity distribution curves across North Island hydropower schemes for different time periods. Shown are hindcast (1986–2005, black diamonds), future decades (brown curves, darker with time as in the legend), and North Island modelled 5th percentile annual mean daily hydropower generation (black line).

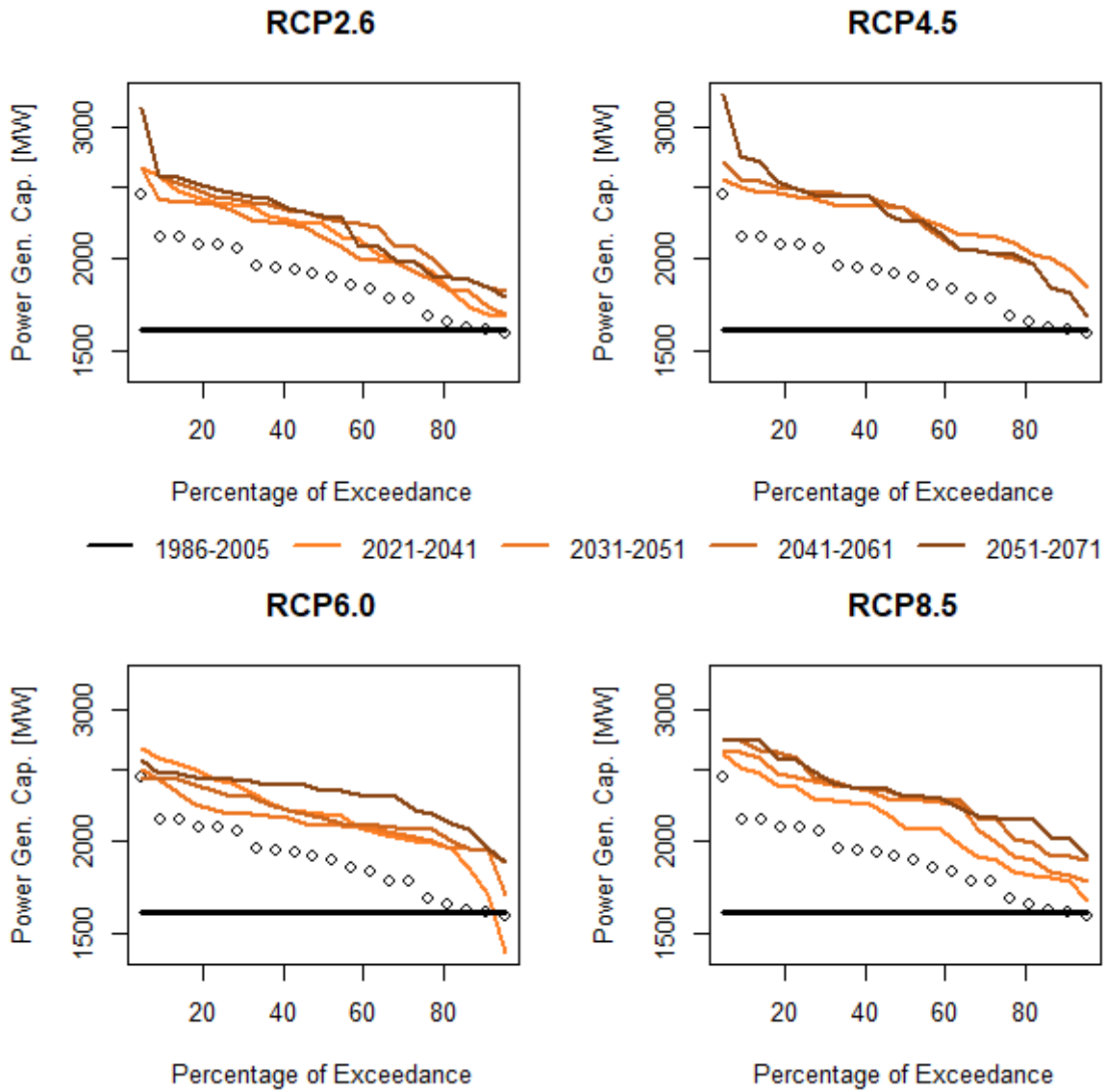


Figure 4-9: 20-year median annual mean daily hydropower generation capacity distribution curve across South Island hydropower schemes for different time periods. Shown are hindcast (1986–2005, black diamonds), future decades (brown curves, darker with time as in the legend), and South Island modelled 5th percentile annual mean daily hydropower generation (black line).

5 Wind Energy

For this report New Zealand wind generation statistics were calculated for 37 windfarms. These windfarms are listed in the table in Table A-1 and maps showing the locations are given in Figure 5-1. Generic turbine power curves similar to that used in Turner et al. (2011) for a Vestas 80 2000 kW turbine were used to calculate hourly output and these were then aggregated to weekly, monthly, and seasonal values, annual, and climate period outputs — details of these aggregations are given in Table 5-1. These temporally-aggregated generation figures were then further aggregated spatially into the two islands as well as into five sub-region (A – North of North Island, B - central North Island and most of lower North Island, C – Cook Strait region, D – the South Island north of the Waitaki River except for Marlborough, and E – the far south).

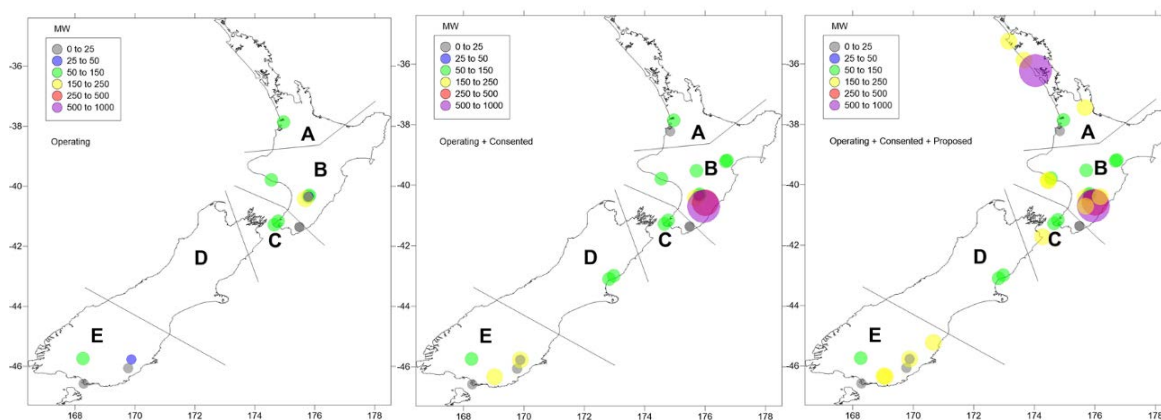


Figure 5-1: Maps showing location of wind farms for which generation scenarios were calculated in this study. The left panel shows farms that are operating as of 2021, the middle panel shows consented and operating, and the right panel shows operating, consented, and proposed.

Table 5-1: Temporal aggregation periods used in this study along with key comments.

Temporal aggregation	Base unit and comment
Weekly	Hourly, with weeks defined according to hydrological years beginning 1 June
Monthly	Hourly, with 12 30-day months from the GCMS
Seasonal	Monthly, Autumn (MAM), Winter (JJA), Spring (SON), and Summer (DJF)
Annual	Monthly, 360-day year.
Recent climate (sometimes labelled RCP10)	Hourly, 1981–2005
Future climate periods	Monthly, 2031–2060 and 2041–2070
Very recent climate	Monthly, 2018–2020 (for EA generation and high-res model gen statistics)

The aggregation and projected changes assume all the wind-farms were operating in all periods. This assumption was to isolate the change in wind generation arising out of changes in wind climate from changes due to increased capacity. The increased capacity would be due to the building of more wind farms, improved turbine technology (efficiency), and greater operating range (modern turbines can operate in conditions where the mean speeds up to around 32 m/s, 10 years ago that figure was 25 m/s). The appropriateness of this approach for the purposes here is demonstrated by the good match of wind generation estimates from NIWA’s NZ Convective Scale Model (NZCSM) (Turner et al. 2019) – a weather model, not a climate model – with the distribution of monthly wind-generation data from the Electricity Authority for the period 2018-2020; see the dashed curves in Figure 5-4 (upper panel) and Figure 5-6 (lower panel). It is also worth noting, as will be seen later in this report, that the projected annual changes in wind-generation due to climate change are typically well under 10%, which is small in comparison to the large expected increase in wind generation over the coming decades⁴ (Figure 5-1).

From the perspective of how both present and potential future wind generation integrates with hydro generation and solar power, it is useful to understand the seasonality of wind power. Figure 5-2 shows this for both North and South Islands for the recent NZCSM data. Both islands have a maximum in spring, for which average generation is about 20% above the annual mean. South Island sites have a minimum in winter but note that for both existing and potential wind farms the total generation for the North Island is about eight times larger than for the South. This is the reverse of the situation for hydro generation.

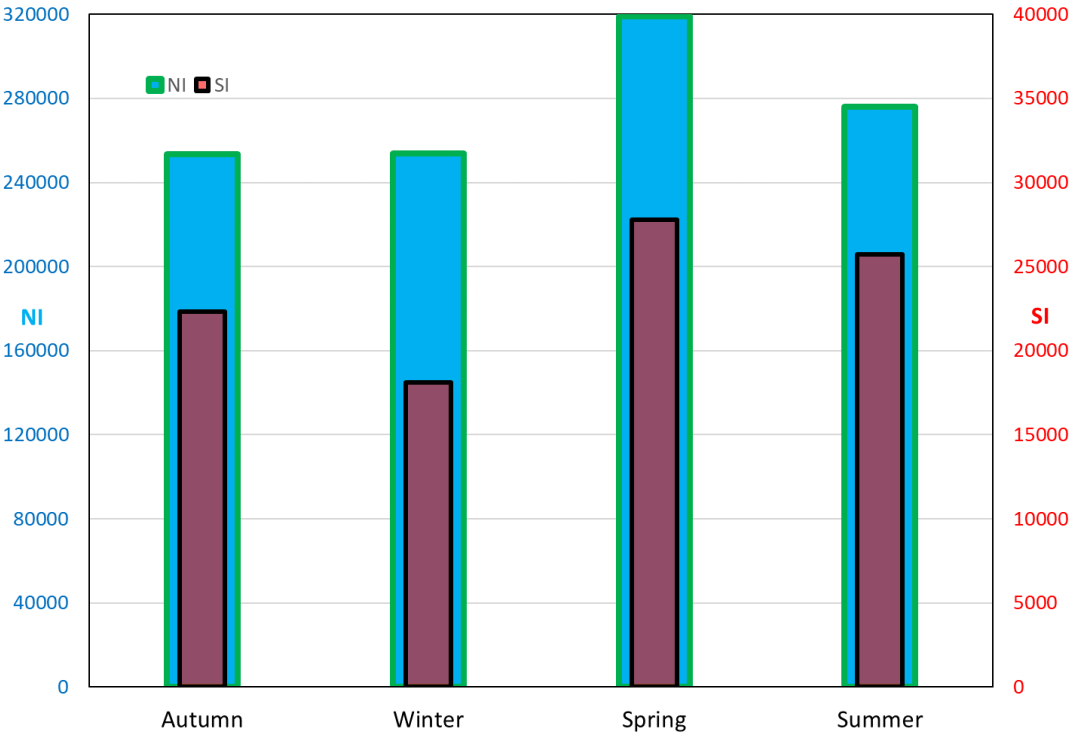


Figure 5-2: Recent (2018–2020) seasonal cycle in wind generation for each island. Note North Island wind generation capacity (left vertical scale) is around eight times that of the South Island (right vertical scale) for the distribution of present wind farms reporting generation statistics to the EA, and for the assumed future distribution of wind farms (i.e., operating, consented and proposed).

⁴ Currently around 2000 GWh and could double if consented projects proceed.

Figure 5-3 shows comparable analysis from the CMIP5 simulations. Over this longer period, summer now has the lowest wind generation in both islands. Mean South Island winter generation is very similar to spring and autumn, while the (much larger) North Island generation is higher in spring, as in the NZCSM results.

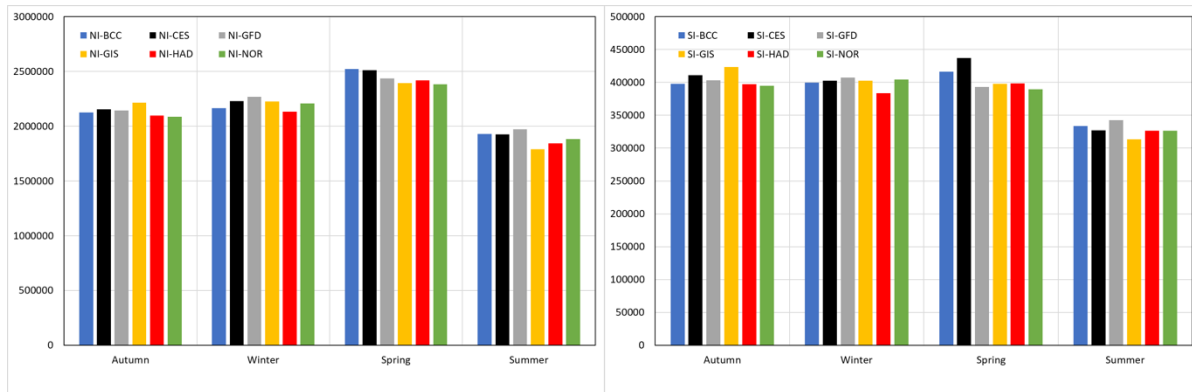


Figure 5-3: Hindcast seasonal cycle in wind generation for each island from CMIP5 models. North Island (left) and South Island (right) plots are for the assumed future distribution of wind farms (operating, consented and proposed). Note the scale difference; North Island generation projected to have around eight times the capacity of South Island.

5.1 Climate change scenario

In this section results are generally presented for the period 2031–2060. The 2041–2070 results are qualitatively similar, sometimes with a stronger response for the RCP85 pathway. In Figure 5-4 through Figure 5-7 a variety of scaled GCM projections for 2031–2060 showing the percentage of months in which generation thresholds are exceeded are provided. The plots shown, which vary by region and model, were selected to show the range of response for each RCP. Firstly, differences between the monthly percentile distribution of generation for the short 2018–2020 and the CMIP5-model 1981–2005 period are not due to issues with the representation of turbine response as NZCSM model predictions match the actual output well. The differences are most likely due to there being a greater number of windfarms and that these would be more widespread than the EA currently collects statistics for along with the much shorter 3-year period used. The results for the HadGEM2-ES model (Figure 5-4 and Figure 5-5), GISS-E2-R model (Figure 5-6), and BCC-CSM1.1 model (Figure 5-7) are presented here as these represent the range of responses modelled, with HadGEM2-ES showing the largest increases in generation and GISS-E2-R and BCC-CSM1.1 showing the largest decreases in generation.

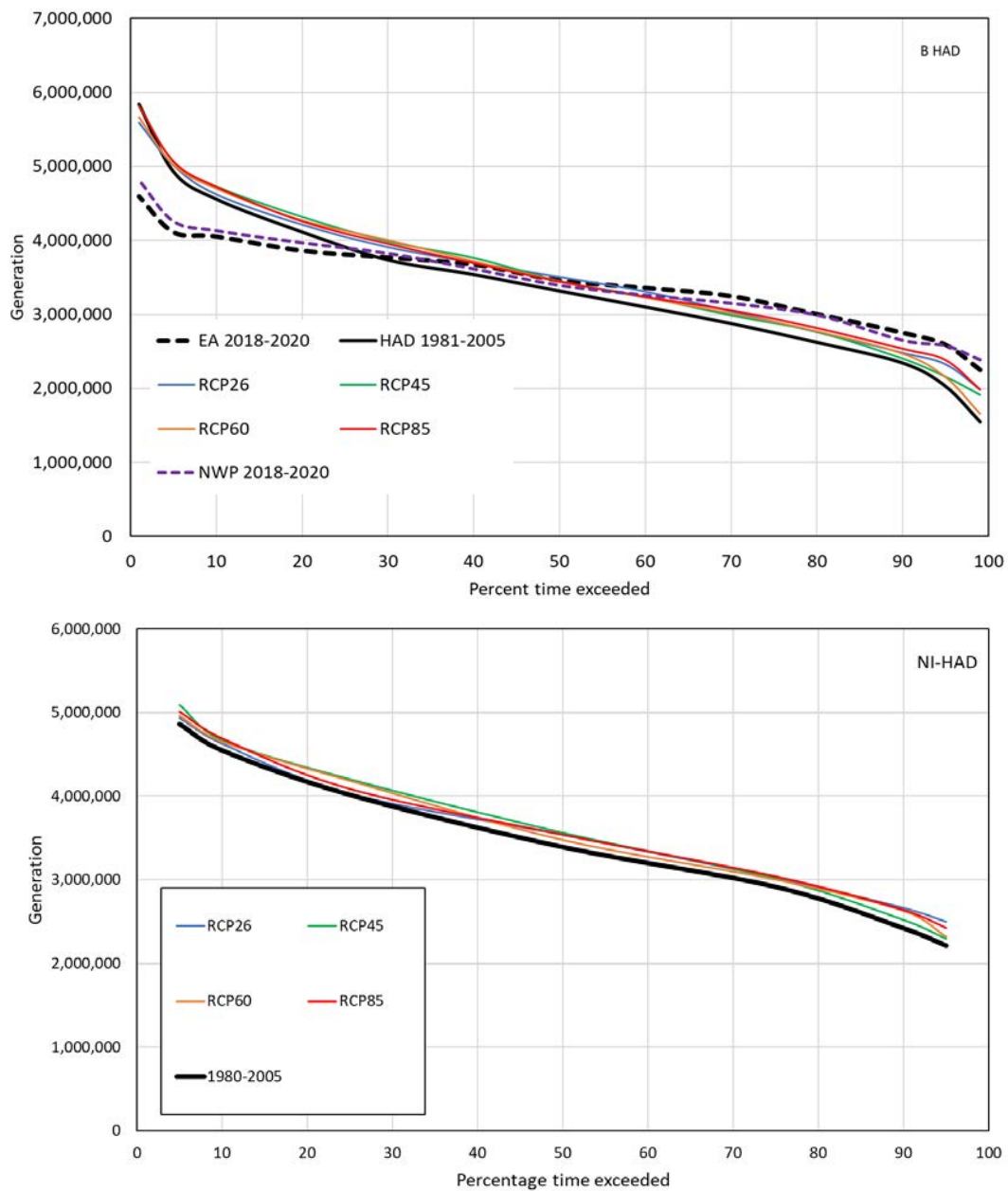


Figure 5-4: Scaled Hadley Centre GCM projections for 2031–2060 for the percentage of months exceeding specified generation (kWh) for the North Island. The upper panel is for Region B (refer Figure 5-1) and lower panel for the whole North Island. The scaling accounts for windfarm distribution (Appendix A) and turbine response. Also presented in the upper panel are the curves for actual generation for six region B windfarms sourced from the Electricity authority for the period 2018–2020 as well as forecasts from NIWA’s 1.5 km Numerical Weather Model (NZCSM).

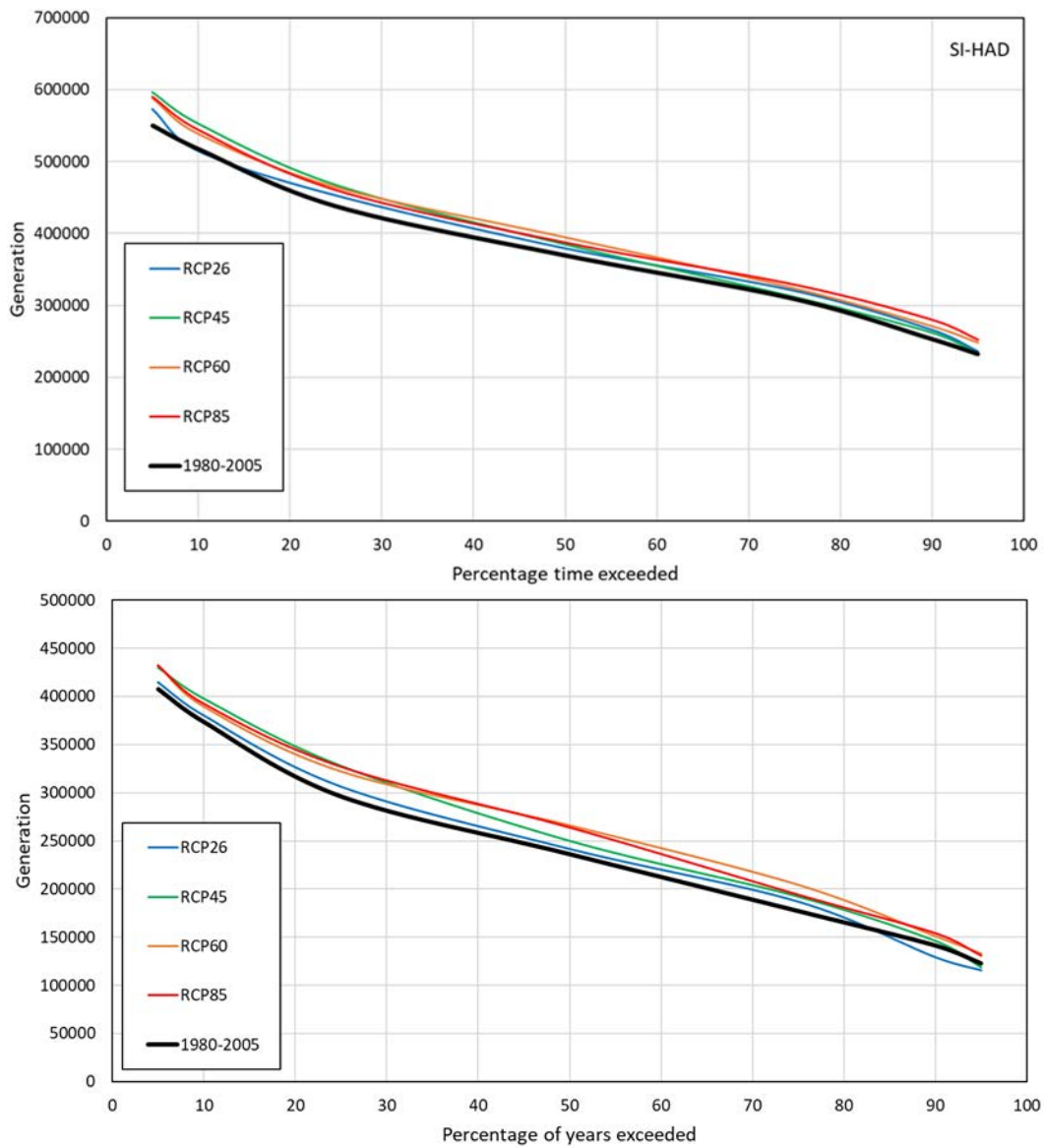


Figure 5-5: Scaled Hadley Centre GCM projections for 2031–2060 for the percentage of months exceeding specified generation (kWh) for the South Island. The upper panel is for the whole South Island, and the lower panel for region E. The scaling accounts for windfarm distribution (Appendix A) and turbine response.

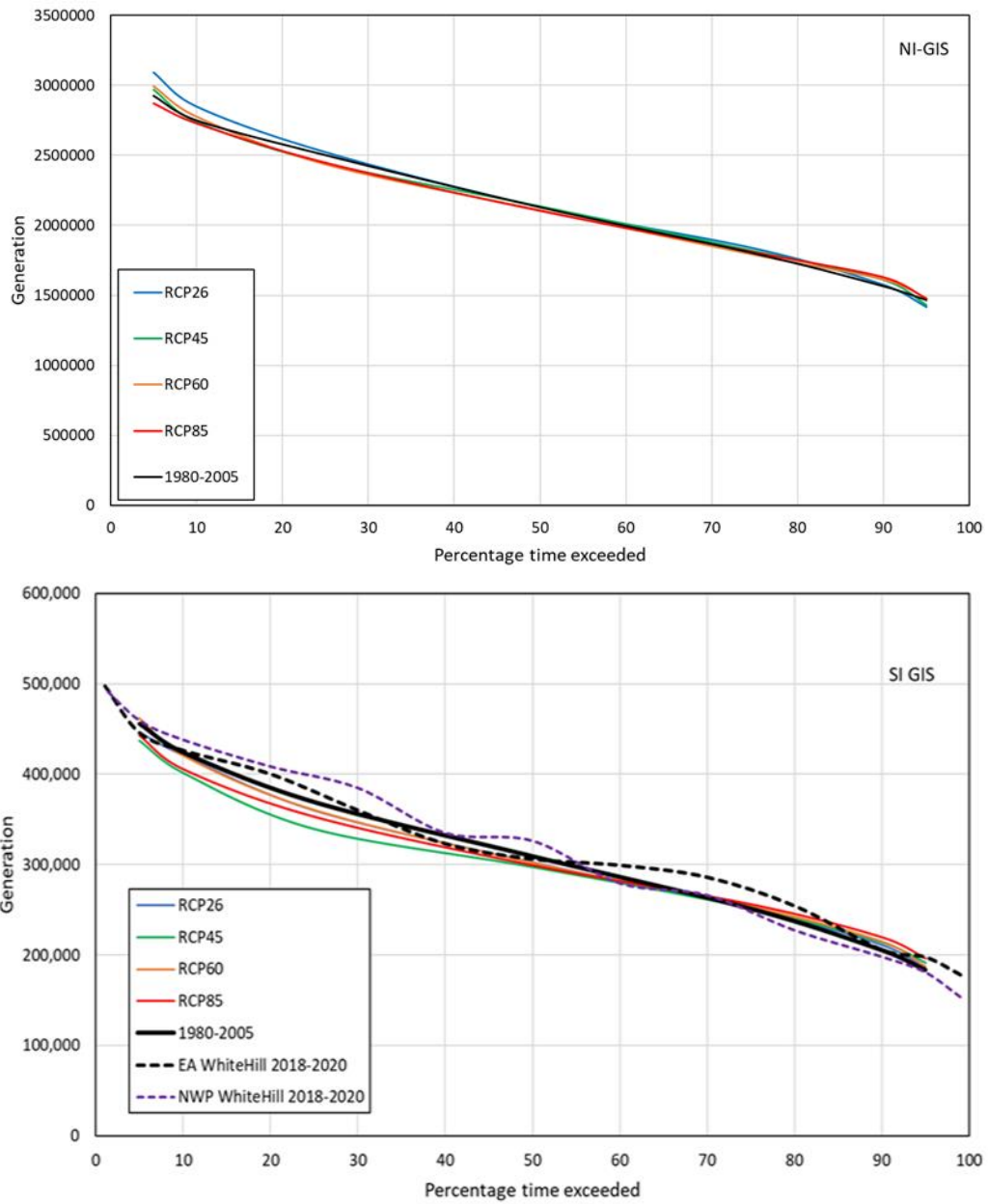


Figure 5-6: Scaled GIS GCM projections for 2031–2060 for the percentage of months exceeding specified generation (kWh) for the North (upper panel) and South (lower) Islands. Also shown in the lower panel are the curves for actual generation for the White Hill windfarm sourced from the Electricity authority for the period 2018–2020 as well as forecasts from NIWA’s 1.5 km Numerical Weather Model (NZCSM).

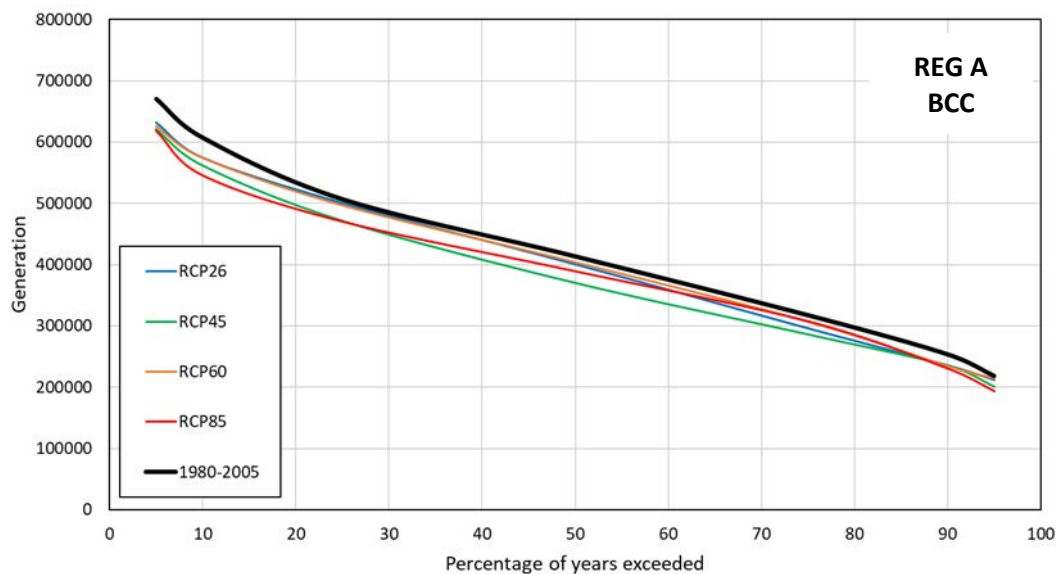


Figure 5-7: Scaled BCC GCM projections for 2031–2060 for the percentage of months exceeding specified generation (kWh) for Region A.

Figure 5-8 summarises more succinctly the percent changes (2031 to 2060 vs 1981–2005) at the exceedance thresholds of 95%, 50%, and 5% in generation for each RCP scenario. Here changes are shown for each model and grouped by the six CMIP5 models. This demonstrates that the models do show very different projections. In terms of the 5th percentile plots (i.e., low-generation months) which are of most concern – there is more consensus for increases in wind generation in the South Island of 1–5% and especially from 2041 to 2070.

The changes in variance for each island for the period 2031–2060 versus 1981–2005 are shown in Figure 5-9. Here we are examining possible scale of changes in month-to-month volatility. There seems to be little congruity between models for any overall change in North Island variance with several models indicating a decrease and several others an increase. For the South Island the Hadley Centre model shows large increases in variance – possibly a reflection of the projected increase in overall generation for that model – but overall, no consensus is seen between the models.

Seasonal changes for each model for the period 2031–2060 are shown for the North Island (Figure 5-10) and South Island (Figure 5-11). For all RCP's there is an increase in spring generation in both islands with the strongest signal being in the South Island. For other seasons, there seems to be an overall tendency for decreased wind generation (less than 5% change) in summer and autumn and a slight increase in North Island winter wind generation (again less than 5%). Similar results (not shown) were seen for 2041–2070, and for Region E the changes were qualitatively similar to that of the South Island but of around twice the magnitude, suggesting again that springtime generation in the south will increase but there is also a risk for decreased autumn production coinciding with low autumn inflows and exacerbating dry year conditions.

Finally within the wind section, Figure 5-12 and Figure 5-13 show the range and average of the six CMIP5 model projected annual changes for each RCP for both islands (Figure 5-12) for the two climate periods 2031–2060 and 2041–2070.



Figure 5-8: Per cent changes (2031 to 2060 vs 1981–2005) in wind generation for each RCP scenario grouped by the six CMIP5 models. The left-hand column is for the North Island and the right-hand side the South Island. The upper panel is for the 95th percentile (i.e., high generation months exceeded 5% of the time), the second row is for median generation (exceeded 50% of the time), the bottom two rows are for the 5th percentile (i.e., low production months) for 2031–2060 and 2041–2070 respectively.

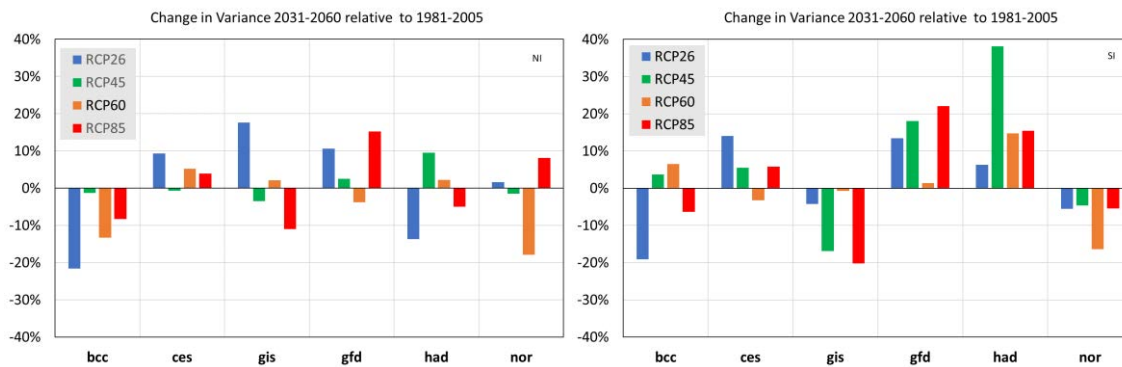


Figure 5-9: Per cent changes (2031 to 2060 vs 1981–2005) for in monthly variance of generation for each RCP scenario grouped by the six CMIP5 models. The left-hand column is for the North Island and the right-hand column the South Island.

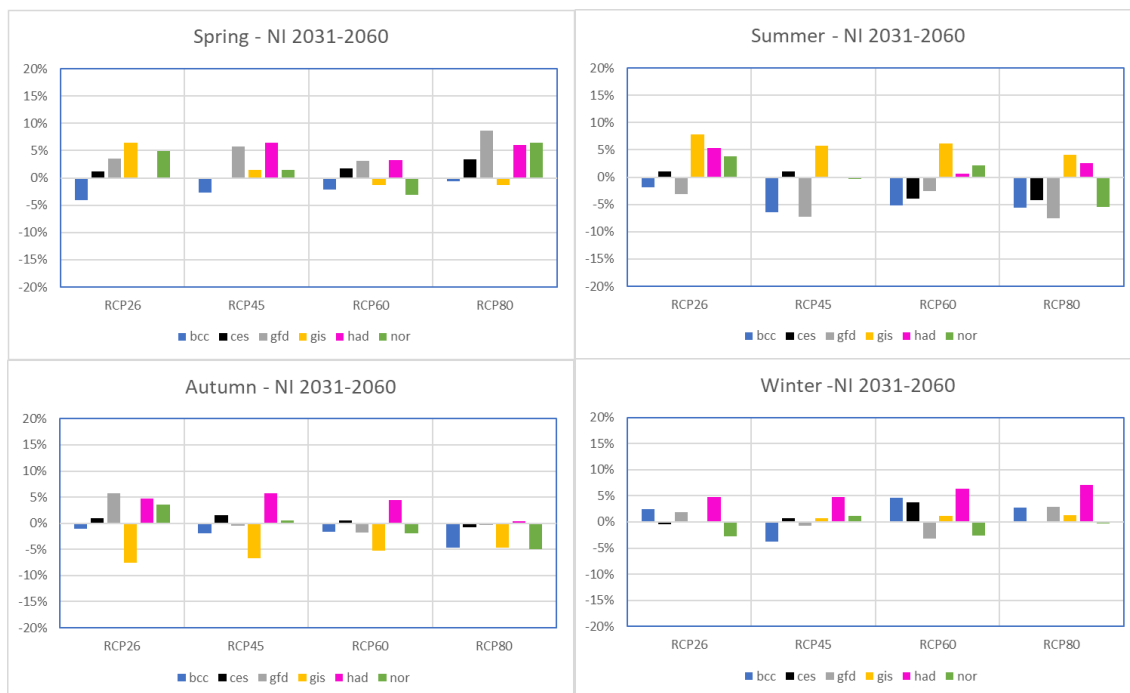


Figure 5-10: Relative changes (1981–2005 to 2031–2060) in North Island seasonal wind generation for each CMIP5 model as grouped by RCP.

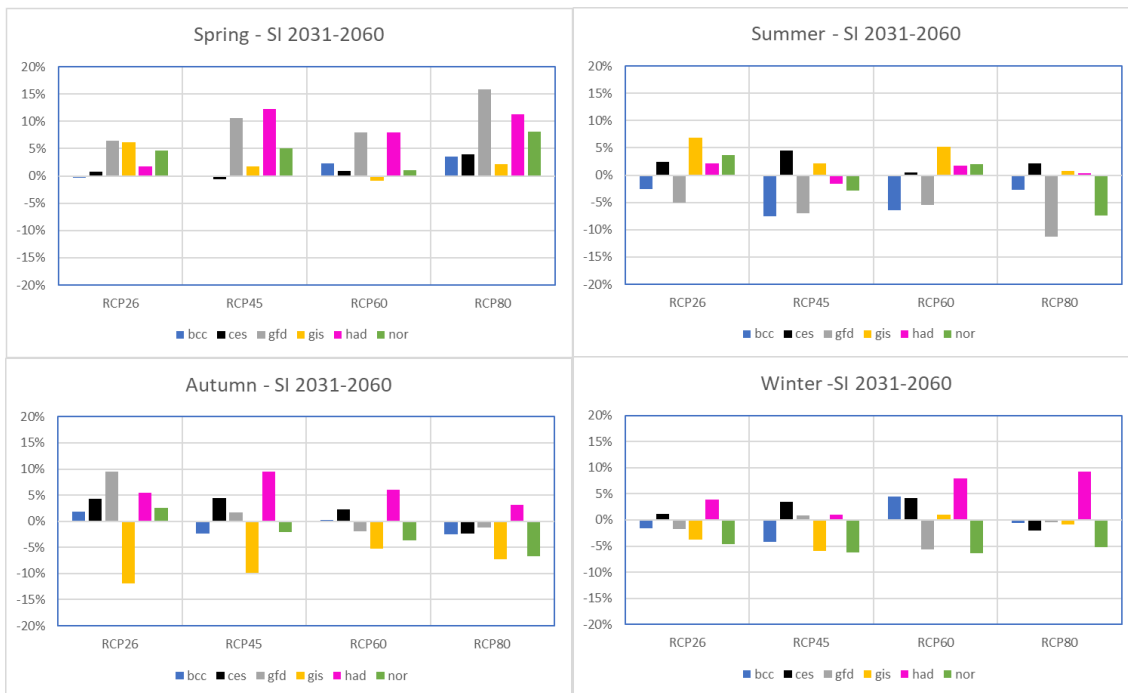


Figure 5-11: Relative changes (1981–2005 to 2031–2060) in South Island seasonal wind generation for each CMIP5 model as grouped by RCP.

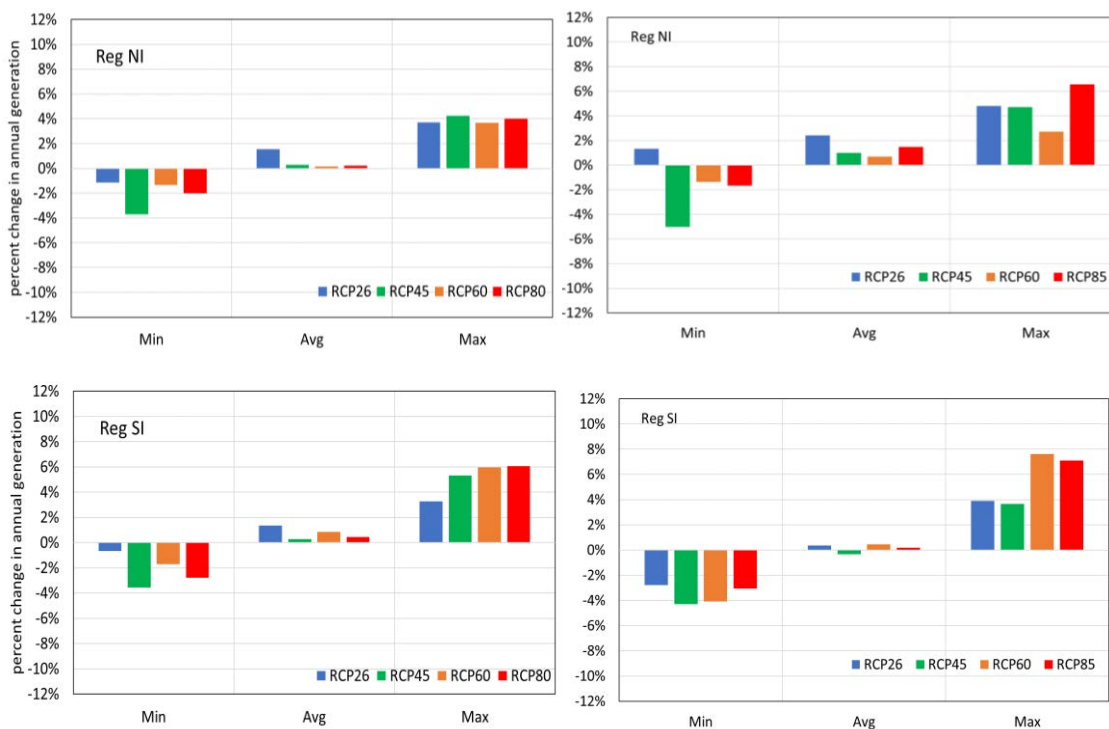


Figure 5-12: The minimum, average and maximum per cent change from 1981–2005 to future wind generation due to climatic changes in wind over the 6 CMIP5 GCMs. Changes are presented for each RCP scenario for North Island (top panels) and South Island (bottom panels), and for 30-year climate periods 2031–2060 (left panels) and 2041–2070 (right panels).

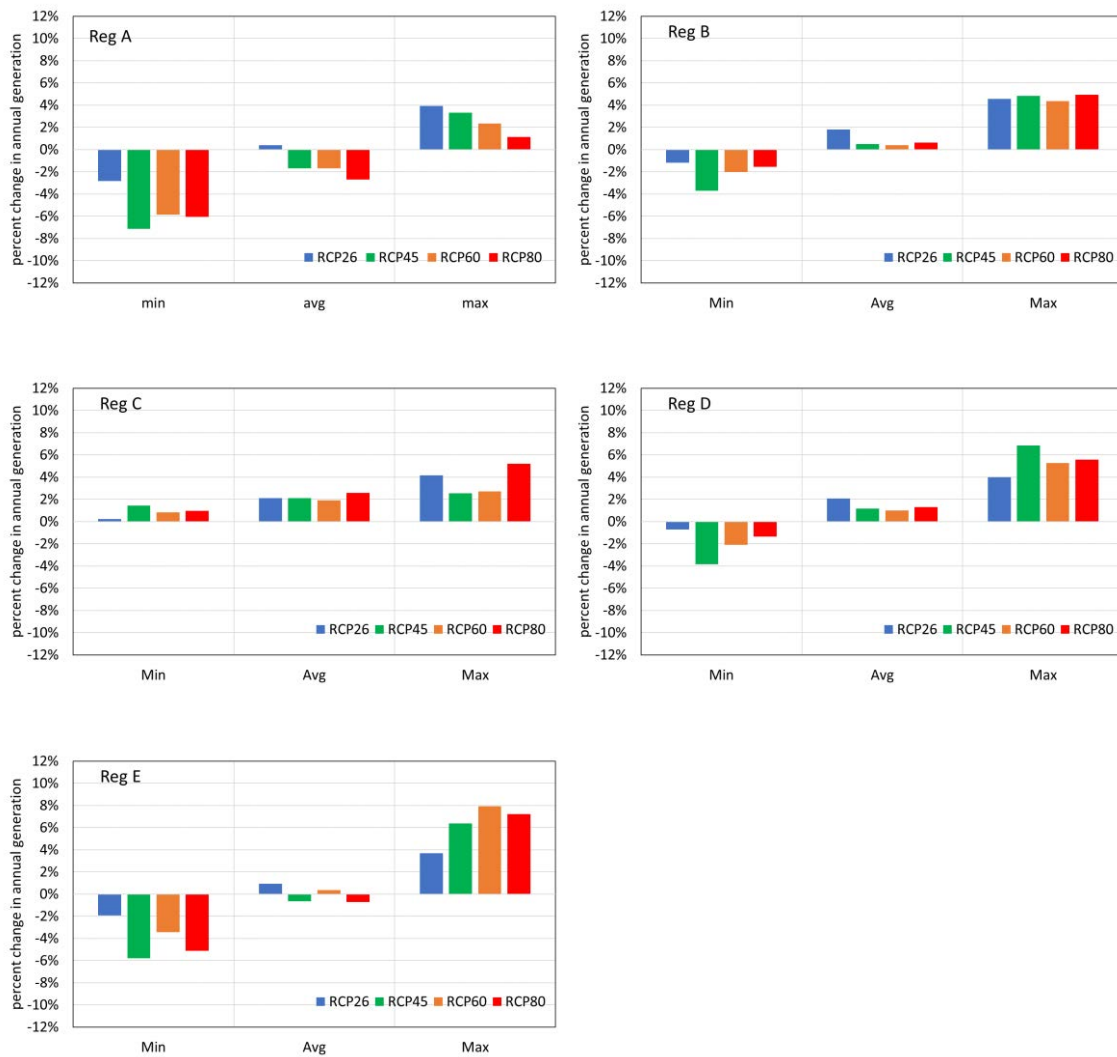


Figure 5-13: The minimum, average and maximum percent change from 1981–2005 to future wind generation due to climatic changes in wind over the 6 CMIP5 GCMs. Changes are presented for each of the 5 regions for the 30-year climate period 2031–2060 with upper left being Region A, upper Right region B, middle left Region C, middle right Region D, and bottom left Region E.

The same plots but just for 2031–2060 for the five regions are shown in (Figure 5-13) 2041–2070 were similar – but stronger in magnitude. We see both increases and decreases in generation are projected for each RCP, interestingly there is a consensus for increased generation (range 1 to 6%) for all models for all RCP’s in Region C (Cook Strait).

Overall, there may be more wind in spring in the far south, and possible autumn reductions, but such changes are minor compared to increased capacity from more modern turbines and new and dispersed wind farm construction.

6 Solar Energy

Solar energy at present accounts for less than 0.3% of NZ electricity generation, but that could change rapidly with economic or political direction as the lead time for new generation is short. Rooftop installation requires only a building permit, and even solar farms are quick to plan and construct by comparison with any other source of power at utility scale. The last year has seen announcements of solar farms in Northland, Waikato, Coromandel, Bay of Plenty, and Taupō that would add more than 2% to the country's generation, and they are expected before the end of 2023.

Because solar generation even at utility scale is relatively uncontentious, the regular Electricity Authority records showing planned and consented future generation has shown no solar energy at all. It is therefore not possible to base scenarios on such plans as for hydroelectricity and wind. Instead, we envisage solar generation to be distributed around the country approximately in proportion to population. This would inevitably apply if much of the installation is rooftop solar, both residential and commercial. It also appears to be applicable to solar farms for grid supply; all current plans are for installations close to the existing grid, and in turn to population centres.

Whereas hydroelectric dams and onshore wind farms are located according to topography and climatology, there is little constraint with solar photovoltaics (PV). Figure 6-1 shows annual average global horizontal irradiance (GHI) for NZ compared with its antipodes in Europe.

First, it is worth noting that Germany has 40 GW of rooftop PV capacity, but nowhere in Germany has greater annual average GHI than Invercargill. In this sense, nowhere in NZ could be described as unsuitable for solar energy.

Global Horizontal Irradiation (GHI)

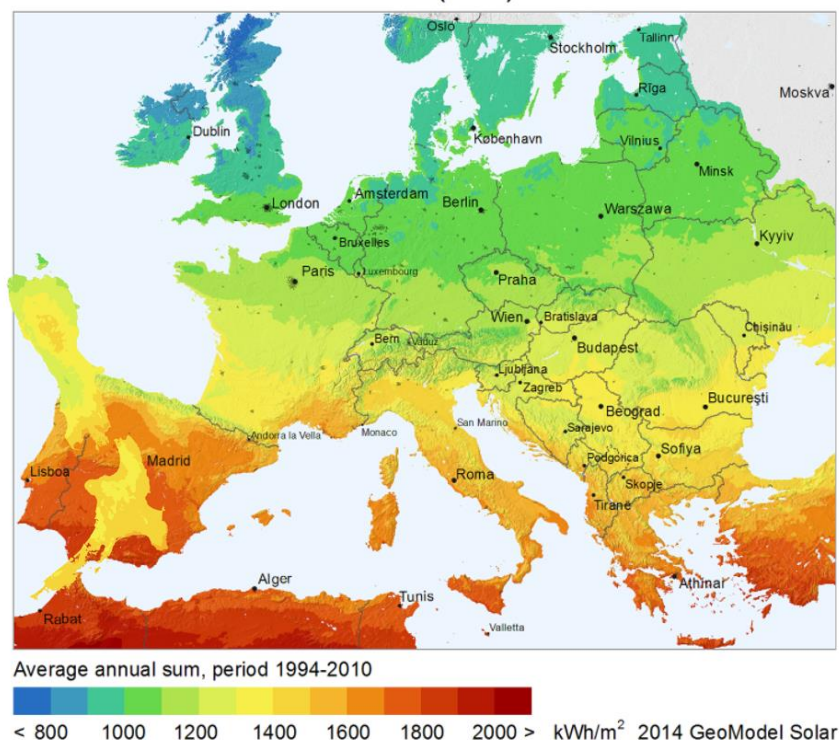


Figure 6-1: Annual average global horizontal irradiance for Aotearoa-New Zealand compared with its antipodes. Note the New Zealand map superimposed on Spain The New Zealand data are from NIWA analysis of pyranometer data in the NZ Climate Database. European data are derived by SolarGIS from satellite data.

Second, the figure shows relatively little variation in GHI in New Zealand, from just under 1200 to over 1500 kWh/m² per year. Areas like Northland, the Bay of Plenty, Nelson-Marlborough, and Central Otago have relatively high GHI, but no populated areas are poor prospects. Rakiura is one of the lowest areas for annual irradiance, but its reliance on diesel generation at much higher cost make it one of the best candidates for solar generation, subject to the cost-effectiveness of storage.

A third consideration is that GHI is not in exact proportion to the generation of PV panels, for several reasons. One is that rooftop panels are typically tilted to roof pitch, and tilting them northward decreases the effect of latitude, while tilting toward the east or west can shift the peak to earlier or later in the day. For most sites total annual generation is greatest for panels tilted up as much as 40° between north and north-west; the latter because in NZ afternoons are clear more often than mornings are. Nevertheless, the greatest economic benefit can arise from even steeper tilt angles if winter power is more valuable than summer. A further effect is that PV panel efficiency falls with rising temperature; in winter and in cooler climates they make better use of incident GHI.

As a final consideration, new solar farms now tend to use single-axis tracking, with panels mounted on a shaft that runs from north to south and rotates to follow the sun. The direct beam radiation is then incident near normal to the panels at sunrise and sunset, but at higher incidence angle around noon. This results in daily generation that is more uniform across daylight hours for unobscured sun, and somewhat higher than for fixed panels, but it can increase the summer-winter difference because the panels are not tilted toward the sun during the peak period around noon.

Considering all these effects, we have treated generation as simply proportional to GHI, but the ratio of summer to winter generation should be considered flexible within a limited range. The difference in day length alone means that summer generation will usually be at least twice that in winter, and for panels close to horizontal the summer generation is three to four times higher.

The radiation data used for the historical analysis, analogous to the HMD data for hydroelectricity, are for the 18 climate zones shown in Figure 6-2, represented by the identified sites. The datasets were collated and carefully curated to develop Typical Meteorological Years (TMYs), which are widely used to represent NZ climates for building energy simulation. The TMYs are also used by NIWA's online solar energy calculator, and they were recently updated using 31 years of data from 1990 to 2020 inclusive. Each TMY provides a synthetic year of hourly data for temperature, humidity, wind speed and direction, and solar radiation expressed as both GHI and its separate diffuse and direct components inferred from GHI.

With the separate components of radiation, plus temperature and wind speed, it is possible to model the performance of solar panels, whether fixed or tracking. As noted above, we have modelled generation as simply proportional to total GHI, but this could be changed if there is a need to refine the solar model, such as to account for a possible predominance of solar farms with tracking arrays.

The NZ TMYs were originally developed for the Energy Efficiency and Conservation Authority (EECA) to use in their Home Energy Rating Scheme. For administrative ease, the climate zone boundaries were chosen to coincide with those of Territorial Local Authorities (TLAs). For the present study, to distribute solar generation according to population density, we used a table of TLA populations from the NZ Ministry of Statistics (<https://www.stats.govt.nz/topics/population-estimates-and-projections>) to calculate weights for each TMY climate zone from the population of TLAs that each comprised. The TMY population weights were then combined into the same five regions as for wind analysis, plus totals for the North and South Islands and for the country.

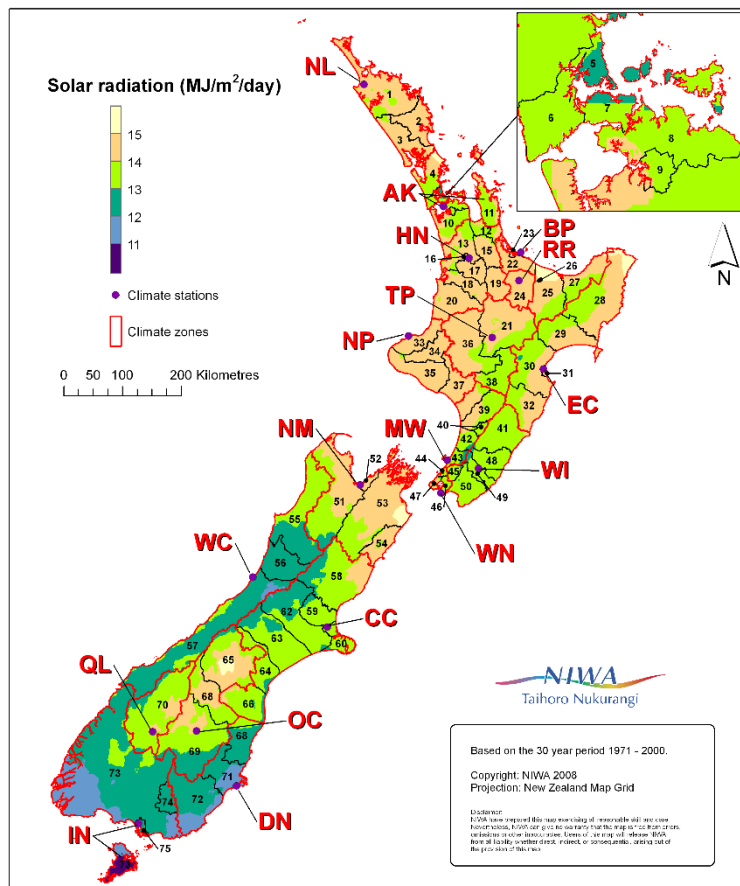


Figure 6-2: Climate zones for NZ. The zones outlined in red represent NZ climates in terms of Territorial Local Authorities as outlined in black. The locations labelled by two-letter codes are the climate stations used.

As apparent from a comparison with Figure 6-1, the colours of Figure 6-2 exaggerate the contrast in values. Mean daily integrals of GHI are expressed in the SI unit of megajoules (MJ), but it is usually conceptually simpler to work in kW-hours, noting that 1 kWh = 3.6 MJ.

With no firm figures for anticipated NZ solar generation capacity by 2050, we base our analysis below on 2 kWp per person, or 5 kWp on each home.

In this context, the ‘p’ denotes system capacity; the generation with normal-incident bright sunlight. In fact, this nominal capacity is not the limiting generation of an individual system, which can be higher when the sun is unobscured and surrounded by bright cloud. Such ‘cloud enhancement’ can result in irradiance up to 40% higher than bright sunlight for periods of a few minutes, but the effect is much reduced over longer periods as the enhancement is more than countered by times of obscured sun. Similarly, enhancement is unlikely in spatial averages over many systems.

The 2 kWp per person corresponds to 10 GWp for the country. Whether that generation is distributed on rooftops or includes substantial solar farms has implications for the distribution network, but it makes little difference to the analysis here.

Note that in either case the average yield of solar systems is typically 15-20%. Over a year, it is dark half the time, the sun is at a low angle to the panels some of the time, and it is obscured by cloud 30–40% of the time in Aotearoa. The net effect is that the notional 10 GWp of solar generation will on average deliver 1.5–2.0 GW, or 13–17 TWh per year.

6.1 Historical solar flux

Figure 6-3 shows the historical generation if each of two million homes in NZ had a solar PV array of 5 kWp, or the equivalent 10 GWp of solar PV were distributed in proportion to population density in 2020 as described above. The large contrast between North and South Islands is mostly a result of the distribution of population, with little effect from geographical differences in solar flux. It is nonetheless significant in the sharp contrast with hydroelectric generation, of which about 75% is in the (southern) South Island. As shown in Section 5, present and potential future wind capacity is, like solar, concentrated in the North Island, with the best land-based resource in the central belt.

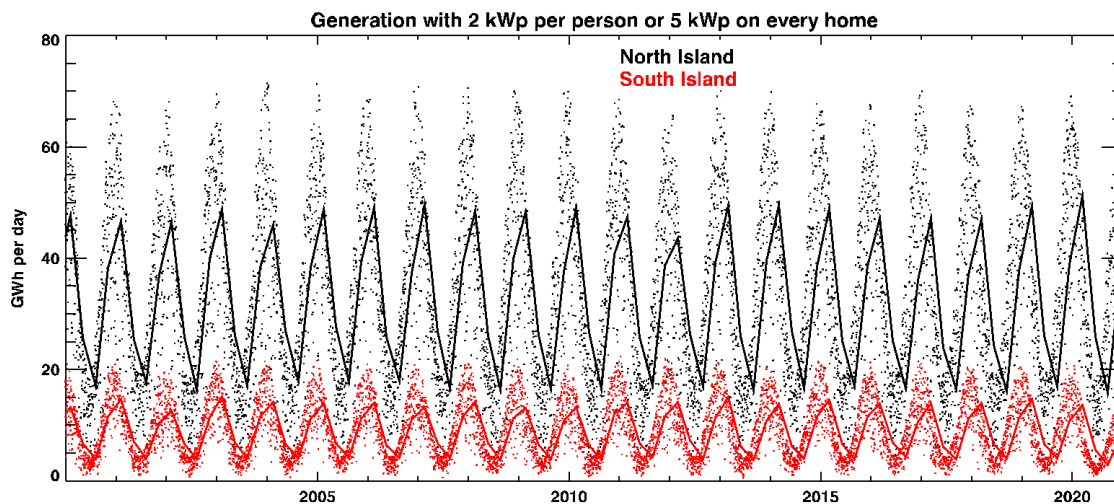


Figure 6-3: Historical solar generation for 10 GWp of PV systems distributed in proportion to population. Symbols are individual daily values, solid lines are seasonal means, for North (black) and South (red) Islands.

Superimposed on the symbols in Figure 6-3 showing potential daily PV generation, the solid lines connect seasonal means, but the relation of the two needs some consideration. Without the implicit storage of hydro generation, wind and solar power are instantaneous, even requiring some buffering to be considered at daily time scales, let alone weekly or longer. At present that buffering is possible by varying hydro flow, but with much greater wind and solar generation that may not be possible.

Some fixed battery storage is likely, but the expected fleet of electric vehicles (EV) provide the most obvious store, if as expected they are predominantly battery EV (BEV). For example, two million BEV each with 50 kWh capacity, sufficient for 300 km range, would represent 100 GWh of storage. The present 4.6 million light vehicles in NZ each average 14,000 km per year, or 38 km per day, so they are stationary 95% of the time. If even 20% of two million BEVs are plugged in – at home, at work, in car parks – and available for vehicle-to-grid (V2G) supply, that would represent 20 GWh of storage and nearly 3 GW of rapidly variable supply. We can envisage an electronically managed marketplace whereby such power arbitrage could be effective and worthwhile for the owners of parked vehicles, even to two or three times the above estimate. Together with fixed batteries, either purpose-built or retired from older BEV, it seems plausible that V2G can balance an average 6 GW of variable wind and solar power with 4 GW of hydro and geothermal generation, as envisaged in Section 2. It is then reasonable to consider the relative seasonal supply of wind, solar, and hydro power.

Section 2 concluded that the present 'dry year' problem is a dry autumn in river flows, leading to low hydro storage in winter. The very large contrast in solar generation between summer and winter will greatly accentuate this difference, even if high wind generation capacity helps to counteract it through being reasonably uniform over the seasons.

On the other hand, a large increase in solar generation in NZ would mean regular oversupply in summer relative to mean consumption. The implication might be that the country could save on hydro generation over summer and routinely go into autumn with all hydro storage full.

6.2 Climate change scenario

The climate change scenarios for solar energy follow the same pattern as the above for hydro and wind, with the mean daily GHI extracted from the six CMIP5 models interpolated to the locations of the representative sites for the TMYS.

As a first step, analogous to the bias correction for relating projected flows from the models and TopNet to hydro generation, we compare potential solar generation computed from measured GHI to that calculated from the hindcast model runs. It is not meaningful to compare the measured time series with free-running models, but we can expect that the distribution of values will be comparable. This question is addressed in Figure 6-4, which shows histograms of the historical and model hindcast data. The frequency is expressed as occurrences in each 1 GWh step in the 31 years; the duration of the historical dataset shown by solid lines, coloured by season. Dashed lines show the corresponding frequencies (scaled to the same duration) in hindcast data, coloured by model.

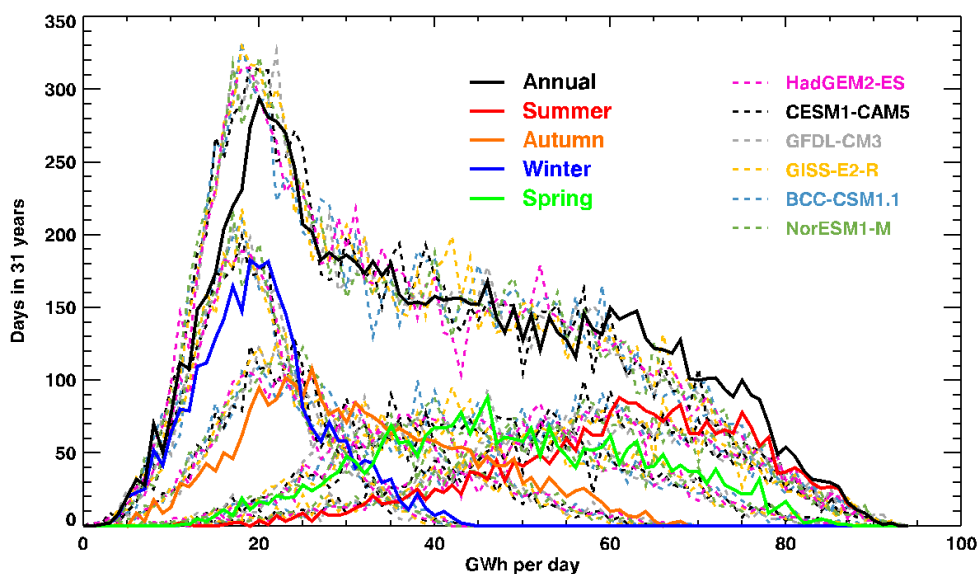


Figure 6-4: Histograms of potential generation for 10 Gwp distributed PV in NZ, annually and by season. Thick solid lines are from measurements; dotted lines are the six CMIP5 models in hindcast mode.

It is apparent that all the models show essentially the same distribution of solar output, both annually and by season. The models all show a similar small bias to lower daily solar flux than measured, and it is relatively uniform across seasons. We find that scaling all model values up by 8% brings both annual and seasonal distributions into close alignment, but we do not make this adjustment in the analysis that follows. As all model projections for the different RCP scenarios are compared with the corresponding model in hindcast mode, relative differences would be unaffected.

For the comparison between future scenarios and periods, and especially for the correlations with hydroelectricity and wind, we sought a measure of solar variability that is more uniformly distributed. For this, we fit the generation (historical, model hindcasts, and future scenarios) on the required time scale (weekly, monthly, or seasonal) with a statistical model of the form:

$$E = E_0 + E_1 y + \sum_{k=1}^3 [E_{Ck} \cos(2\pi ky) + E_{Sk} \sin(2\pi ky)] \quad (1)$$

where y is decimal year from the mid-point, and k indexes annual, 6-month, and 4-month cycles.

An example is shown in Figure 6-5 for the NorESM1-M model and RCP8.5, with the model (red) fitted to monthly means (green).

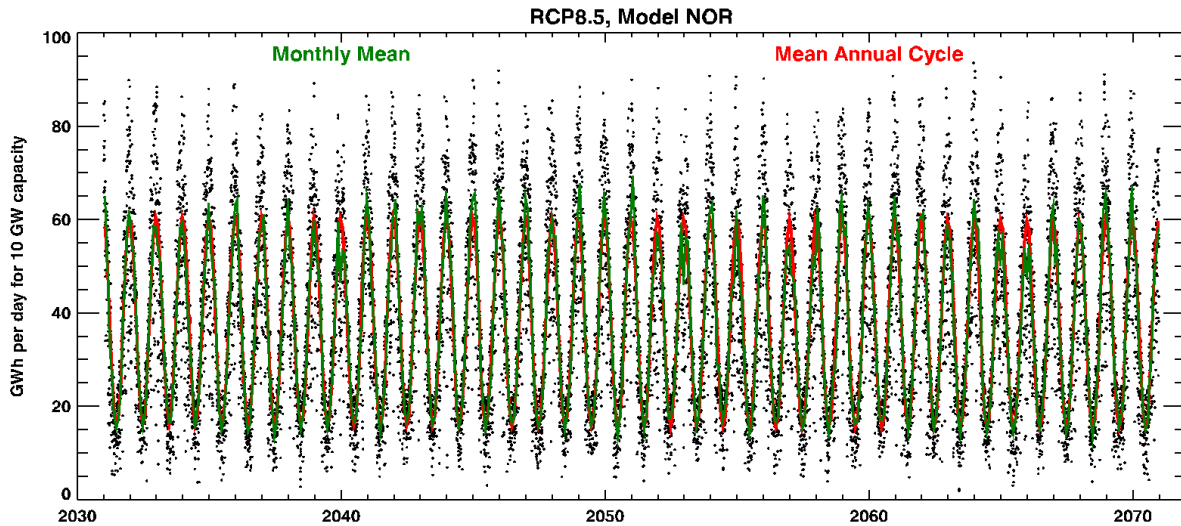


Figure 6-5: Daily and monthly mean PV generation for NorESM1-M model, RCP 8.5, assuming 10 GWp. The figure illustrates the daily variability (black symbols), monthly means (green) and the mean annual cycle (red) as described by statistical fit.

We then compute residuals, as the difference between monthly (or weekly or seasonal) means and the statistical model. The residuals again have a strong seasonality (larger differences in summer), but expressed as a fraction of the model they are approximately homoscedastic (constant variance), as illustrated in Figure 6-6 for CMIP5 model BCC-CSM1.1 and RCP2.6. Though it represents only one example, we find similar homoscedasticity of the proportionate residuals for all models and RCPs.

Thus, we arrive at a description of the solar generation as a mean annual cycle with any linear trend, plus residuals (weekly, monthly, or seasonal) that are uniform over seasons and over decades as a fraction of the mean cycle and trend. The distribution of fractional residuals is Gaussian to a good approximation, as demonstrated with Q-Q plots (not shown).

Classical statistical measures, including correlation analysis, routinely assume independently identically distributed (usually normal) random variates. Here we have satisfied the second, third, and fourth assumptions. In time series of geophysical variables, temporal independence is often inexact at most; indeed, some predictability from autocorrelation is expected. We explore this below, and in the correlation of comparable measures for hydro and wind generation in Section 7, but first we compare the mean generation, trend, and amplitudes between models and RCPs.

Table 6-1 shows the mean NZ solar generation (annual average in 2000 for the hindcast period or 2050 for the four RCPs) in each of the CMIP5 GCMs relative to the mean of all of them for the corresponding RCP. It shows that there is little variation between the models in mean solar flux.

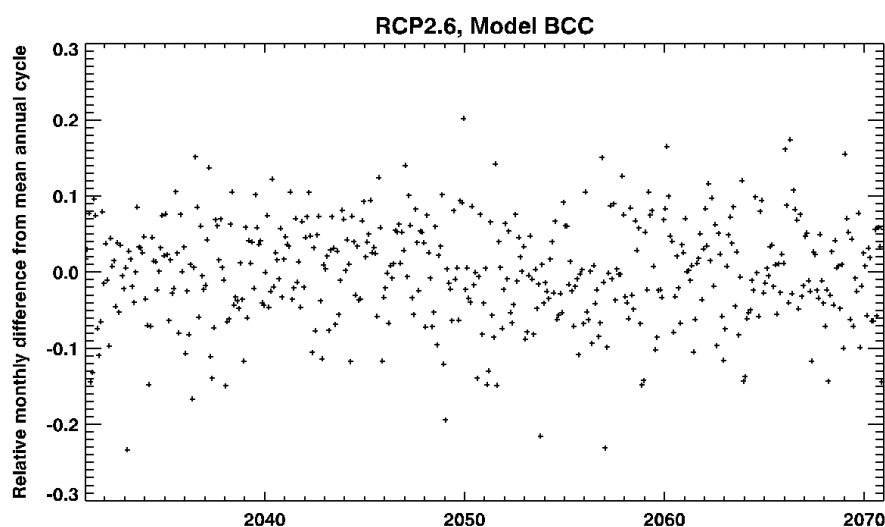


Figure 6-6: Relative monthly residuals from mean annual cycle for BCC-CSM1.1, RCP 2.6. The distribution is the same between and within years, and approximately normal, making this a good parameter for analysis.

Table 6-1: CMIP5 model solar means relative to overall mean. Differences in per cent.

Model	Hindcast	RCP 2.6	RCP 4.5	RCP 6.0	RCP 8.5
BCC-CSM1	1.40	0.51	0.87	-0.40	0.52
CESM1-CAM5	0.07	0.44	0.41	0.88	0.57
GFDL-CM3	0.51	0.32	-0.31	0.12	-0.34
GISS-E2-R	-0.39	0.03	-0.11	-0.58	-1.20
HadGEM2-ES	0.35	-0.71	0.22	0.28	0.46
NorESM1-M	-0.07	-0.71	-0.97	-0.65	-1.54

The changes in mean solar generation for NZ from the hindcast period to the mid-point of the 2031–2070 projections are shown in Table 6-2. Four of the six models at least show consistency in the sign of the change (increase or decrease) between different RCPs, but it does not scale with the radiative forcing, and it is not consistent between models. Most changes are less than 1 per cent, and at that level would not be detectable in 2050 from a comparison with past data; whatever the state of measurement then, present measurements cannot define the national solar flux to within this level of uncertainty.

Table 6-2: CMIP5 model solar mean changes from 2000 to 2050. Differences in per cent.

Model	RCP 2.6	RCP 4.5	RCP 6.0	RCP 8.5
BCC-CSM1	-0.88	-0.52	-1.78	-0.87
CESM1-CAM5	0.37	0.33	0.81	0.49
GFDL-CM3	-0.19	-0.82	-0.39	-0.85
GISS-E2-R	0.42	0.28	-0.20	-0.81
HadGEM2-ES	-1.05	-0.13	-0.06	0.11
NorESM1-M	-0.64	-0.91	-0.58	-1.47

As described, the statistical model for each combination of GCM and RCP contains a term for trend per year over the simulation period, either 1981-2006 (hindcast) or 2031–2071. Those trends, relative to their mean across all models, are shown in Table 6-3. Again, there is little variation, and they show little consistency with the projected changes over five decades as in Table 6-2. Instead, we regard all of them as the natural variability in free-running models that do not differ measurably from each other in projected mean solar flux.

Table 6-3: CMIP5 model solar trends per decade relative to model mean. Differences in per cent.

Model	Hindcast	RCP 2.6	RCP 4.5	RCP 6.0	RCP 8.5
BCC-CSM1	0.27	0.22	-0.12	0.36	-0.22
CESM1-CAM5	-0.17	-0.05	-0.25	0.35	-0.04
GFDL-CM3	-0.33	0.16	-0.20	-0.00	0.06
GISS-E2-R	-0.95	0.04	0.32	-0.00	-0.13
HadGEM2-ES	-0.79	0.21	-0.32	0.04	0.14
NorESM1-M	-0.99	0.22	-0.12	-0.19	-0.63

As a final consideration, Table 6-4 shows the differences in the amplitude of the annual cycle of solar power, all relative to the mean amplitude for all GCMs and RCPs. Once again, the differences are below the threshold for measurement, at least for the present.

Table 6-4: CMIP5 model solar annual cycle amplitudes relative to overall mean. Differences in per cent.

Model	Hindcast	RCP 2.6	RCP 4.5	RCP 6.0	RCP 8.5
BCC-CSM1	0.04	0.14	1.50	-0.70	2.52
CESM1-CAM5	-1.22	0.87	-0.29	0.83	1.28
GFDL-CM3	0.35	1.00	0.48	0.64	0.16
GISS-E2-R	-0.57	-1.12	0.44	-1.59	-0.73
HadGEM2-ES	0.34	-2.26	1.36	0.87	1.41
NorESM1-M	0.19	-1.06	-0.94	-1.47	-2.48

From all of the above, we conclude that the different GCMs and RCPs do not project changes in solar flux for NZ that should be considered in planning for future electricity generation. If such changes do eventuate, they will be from causes that are not included in present simulations. Such changes are not impossible; they might arise from large volcanic eruptions, from solar flux modification with geoengineering, or the like. Increased solar flux through cleaner air resulting from global electrification would be less relevant for NZ's already clean air.

In assessing the future need for increased hydroelectric storage in NZ, the important implications of solar energy all relate to how much solar capacity is installed, whether summertime solar generation can be used to manage hydro storage, and the development path of other energy storage technologies like hydrogen and ammonia production from electricity. Depending on their development path and 'experience curve', they may be cost-competitive with a pumped hydro scheme for generation. This could be accentuated if solar generation produces a large summer surplus that effectively makes electricity free for any storage technology.

7 Combined Hydro, Wind, and Solar

7.1 Monthly generation

The three renewable energy datasets were combined into three 20-year time series for calendar years (Jan–Dec, rather than hydrological years Jun–May) 1986–2005, 2031–2050, and 2051–2070. Figure 7-1 shows the monthly hindcast and future generation (for RCP 4.5), for all six GCMs, of each energy type in the North (upper panel) and South (lower) Islands. Square symbols denote monthly hydro generation, diamonds are wind, and the solid lines are solar generation, with the median and 2.5% to 97.5% range across all models shown for hindcast values. Hydroelectricity and wind energy are coloured by GCM model, showing the variability between the free-running models. Solar data are shown as black lines to distinguish them from hydro and wind, but again all six models are shown; the spread in solar generation between models is minimal compared to the range for wind and hydro, and as compared to the strong annual cycle for solar.

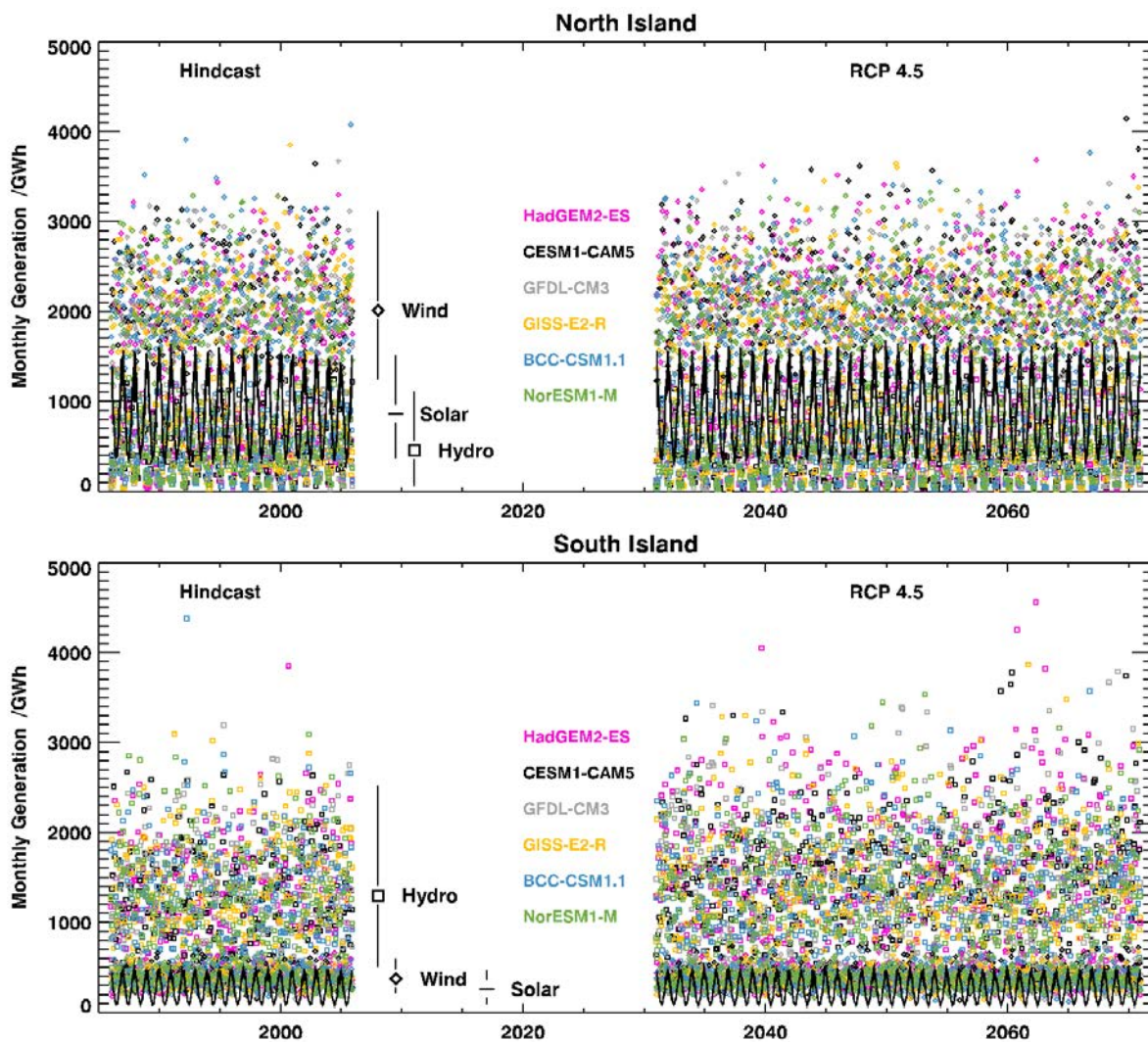


Figure 7-1: Projected monthly hydro, wind, and solar generation for North and South Islands with six GCMs for hindcast and future RCP 4.5. Diamonds show wind and squares show hydro, both coloured by GCM as shown. Solid lines are solar, in black for all GCMs. Symbol labels show median and 2.5% to 97.5% range.

The monthly generation shown in Figure 7-1 assumes, for both hindcast and future, only the existing ‘actual’ NZ hydroelectric capacity of 5.58 GWp listed for the HMD, rather than any new hydro dams. Hydrological flows for both hindcast and future scenarios are bias-corrected as described in Section 4.2. South Island hydro generation is more than three times that of the North Island.

As shown in Table A-1, the projected wind generation is for a total capacity of 10 GWp, half of it offshore. This total is about 10 times present wind generation capacity, reflecting a need for at least another 4 GW of renewable generation by 2050 (MBIE 2019). With installed capacity of 10 GWp, the average wind generation for the country is 3.4 GW, or 2450 MWh per month. The monthly variability is proportionately less than for hydro, and most importantly, the North Island wind generation is about five times that of the South Island; the reverse of the distribution of hydroelectric capacity.

The solar figures also assume 10 GWp, as described in Section 6, corresponding to 2 kWp per person or 5 kWp per home. With the assumption of fixed PV panels on rooftops, the average yield from 10 GWp is 1.6 GW, or 1150 GWh per month. Average yield will be higher if, continuing a trend of announcements in the last year, much of the PV installation is in the form of solar farms with single-axis-tracking bifacial panels. Still, the capacity is entirely notional, representing a 100-fold increase from present solar PV capacity in recent Electricity Authority figures. The assumed capacity is still less than IEA expectations for OECD countries (IEA 2021b), and it might readily be exceeded by 2050.

The assumed generation capacity of each type is not critical if we consider just linear correlations, which are unchanged if the capacities are scaled by constant factors.

Figure 7-2 shows scatter plots of hindcast monthly hydro, wind, and solar generation with assumptions as above. These are the same data as in Figure 7-1, plotted against each other for each North - South pair. Axis ranges are the same for both islands for each type of generation to facilitate comparability between different panels. Note that the range for solar generation is half that for hydro and wind, but it can be scaled according to the assumed rate of PV installation.

In the upper right of each plot are the linear correlation coefficients for each GCM, and the range that they span is listed in the table. For ease of reference, the table has the same spatial distribution as the scatter plots to which the figures refer.

The same analysis for future generation in 2031–2050 and 2051–2070, and for each of the four RCPs, shows similar results, as illustrated in Figure 7-3 for RCP 6.0 in the period 2051–2070. The order of correlations between the models varies, showing that the variation itself has little predictive value. For completeness, Appendix C shows plots and tabulated values corresponding to Figure 7-3 for both the 2031–2050 and 2051–2070 periods, and for all four RCPs. To maintain the sequence, Figure C-7 repeats Figure 7-3.

In all such plots and analyses, there is substantial correlation between South Island hydro generation and North Island wind, and comparably strong anticorrelation between North Island hydro and solar generation in both islands. However, the latter sounds a warning about the nature of such correlation. As evident in Figure 7-1, and previously in Figure 6-3 and Figure 6-5, monthly solar generation in both islands for a widely distributed network is very strongly seasonal, so the anticorrelation with monthly-average North Island hydro flows simply reflects that the latter have the reverse seasonality – they are low in summer and high in winter.

To distinguish the effect on correlations of seasonality, we fitted the model described by Equation (1), in Section 6.2, to monthly totals for each of the three generation types. The fitted cycles are shown in Figure 7-4 for each generation type, island, and model for the hindcast values.

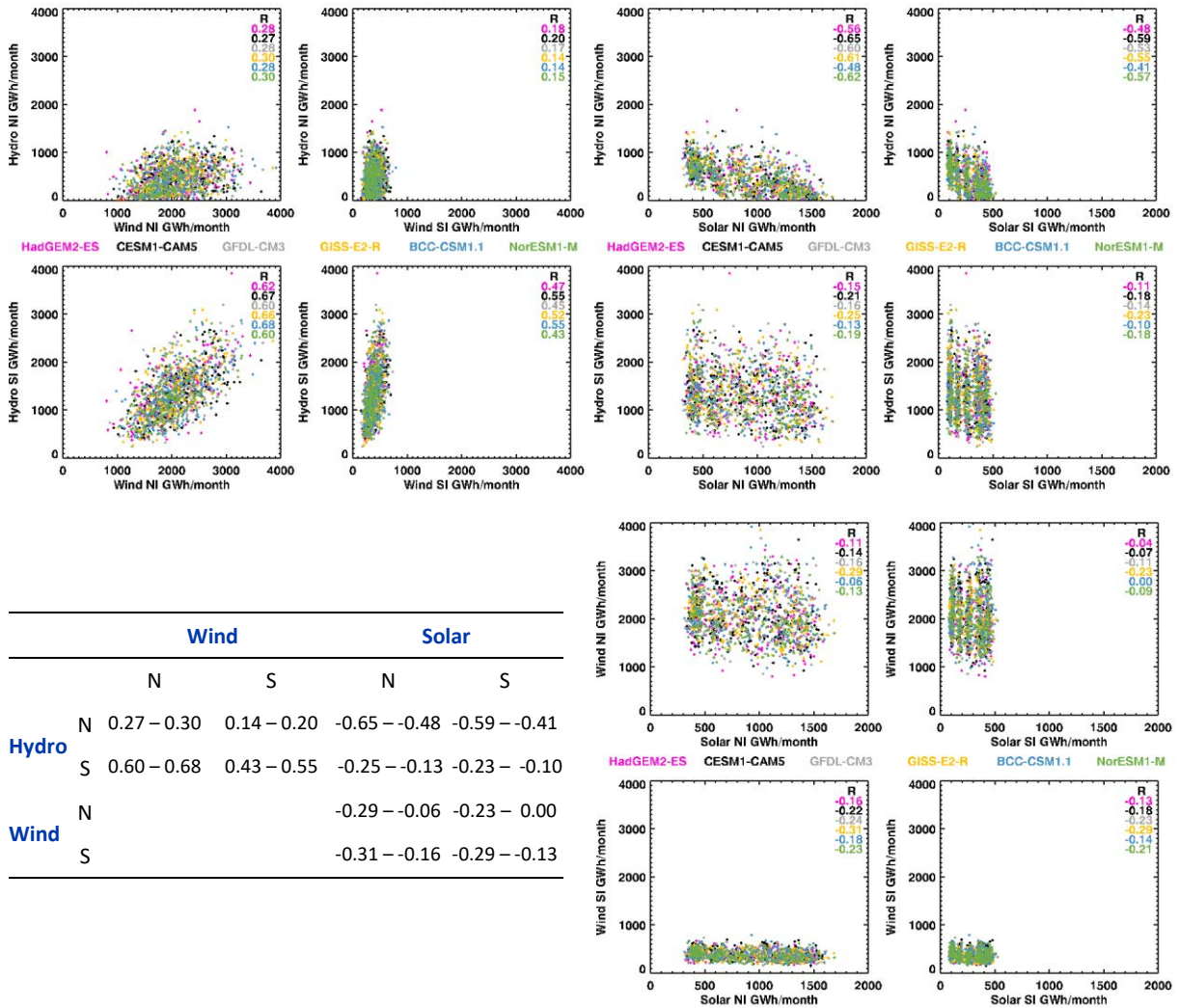


Figure 7-2: Correlations of hindcast monthly hydro, wind, and solar generation by island for the six CMIP5 models. Linear correlation coefficients are shown within plots, and the ranges summarised in the table.

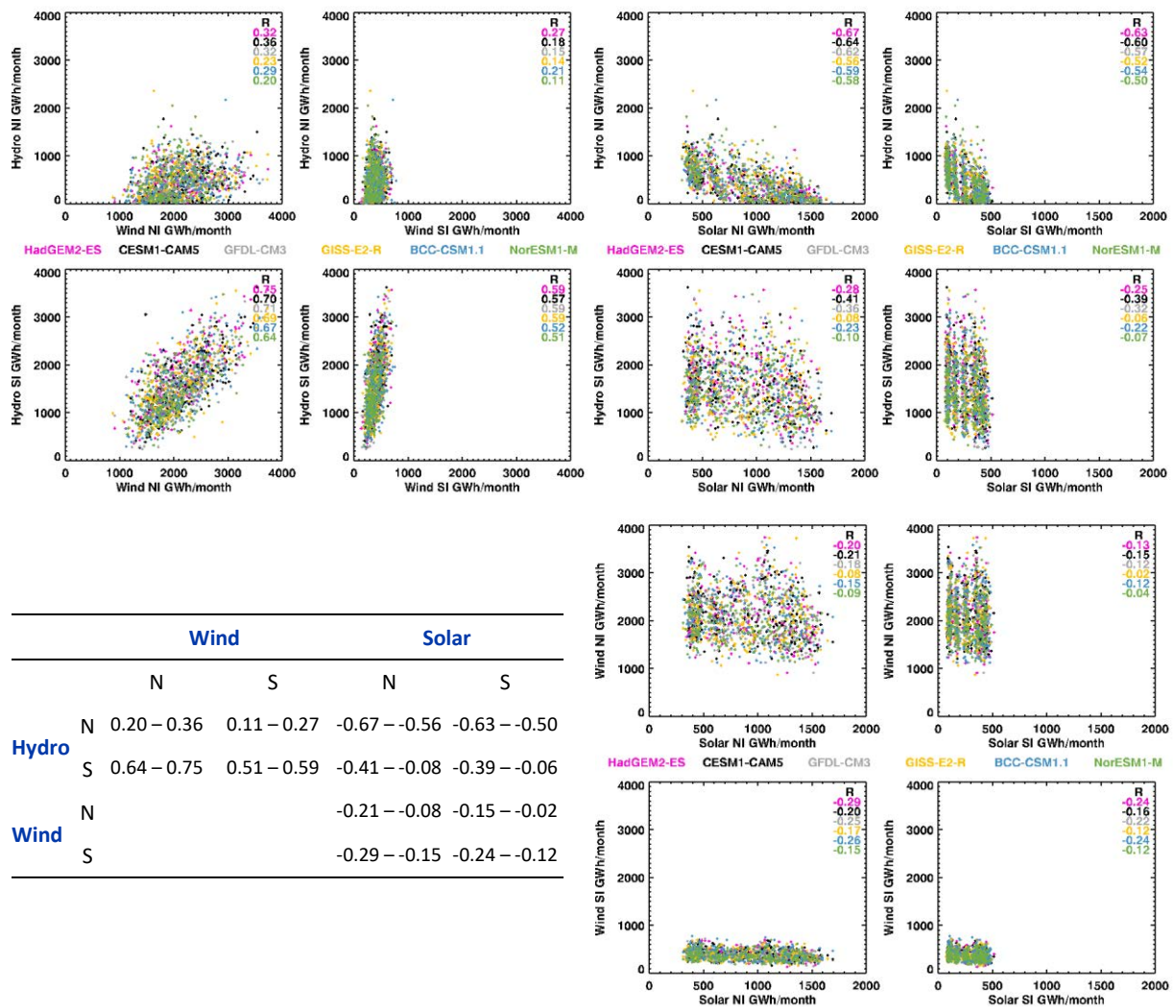


Figure 7-3: Correlation of projected 2051–2070 monthly North and South Island hydro, wind, and solar generation for RCP 6.0 in the six CMIP5 models. Linear correlation coefficients for each GCM are shown within plots, and the ranges summarised in the table.

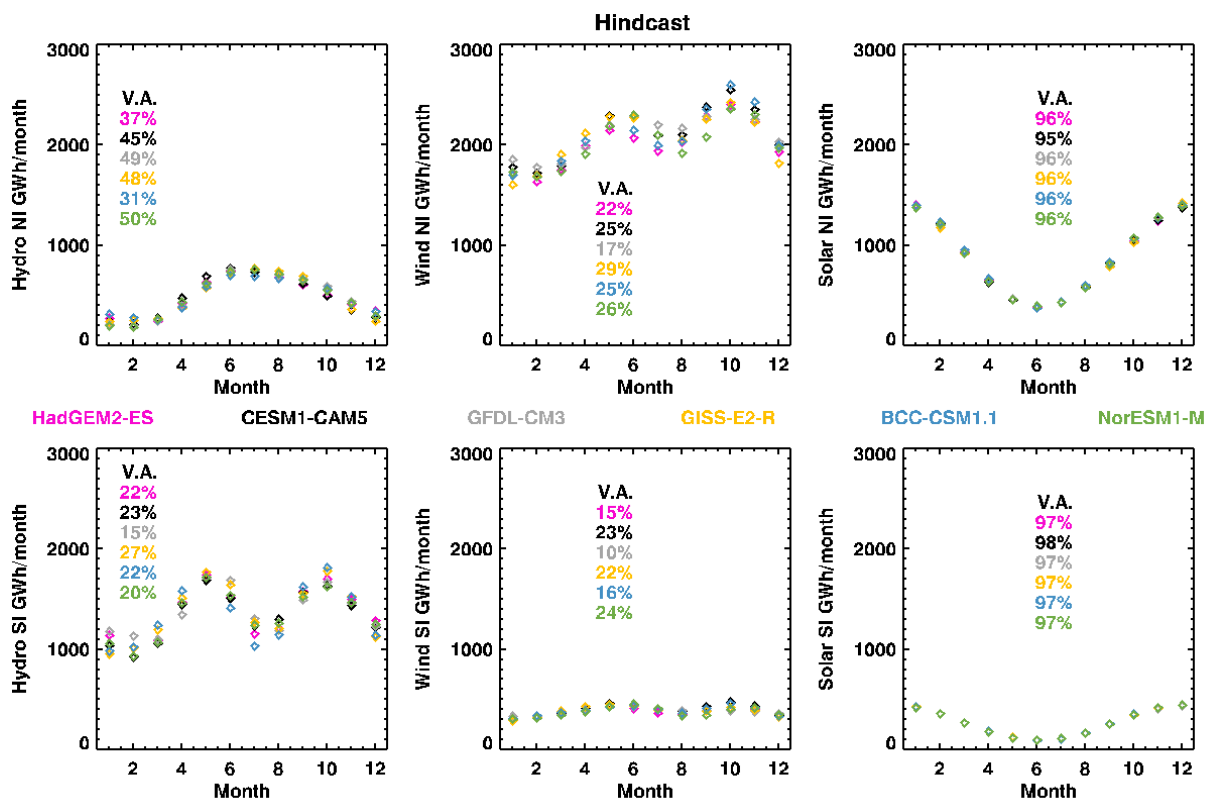


Figure 7-4: Seasonality of hydro, wind, and solar generation for North and South Islands in hindcast monthly totals. The model given by Equation (1) was fitted to each of the CMIP5 models, as colour-coded. For comparability, the Y axis scale in all plots is the same. Figures listed in each plot show the proportion of variance in monthly values attributable to the statistical fits of seasonal variation.

The separate plots in Figure 7-4 all have the same scale on the Y axis to facilitate comparison between them. Within each plot, the percentages in the upper left show how much of the total variance in monthly generation is explained by seasonal variation. As apparent from Figure 7-1, monthly solar generation from a distributed network is very strongly seasonal with little residual variation. As calculated from the CMIP5 models and TopNet accumulations, the variation in North Island hydro generation is also dominated by the seasonal cycle, though not nearly as strongly.

The mean seasonalities in Figure 7-4 change little in the future outlooks, as illustrated in Figure 7-5 and Figure 7-6. These figures show respectively the 2031-2050 seasonalities in RCP 4.5 and those for 2051-2070 in RCP 6.0. The eight-parameter model of Equation (1) was fitted separately for the three periods and to each of the six models, but the patterns are similar to those of Figure 7-4. Because of that similarity, some reduction of the eight parameters \times three periods \times six models is possible if deeper analysis of mean behaviour, rather than residuals, is required.

Across hindcast and future periods it is clear that, for the assumed 2050 generation capacity, the dominant sources are South Island hydroelectricity and North Island wind. The correlation of these two, as noted in Figure 7-2 and Figure 7-3, is also apparent in their seasonal cycles; both are highest in spring and low in summer. Whereas North Island hydro peaks in winter in the model datasets, South Island hydro is lowest in winter. A coincident local minimum in North Island wind accentuates the correlation between South Island hydro and North Island wind seen in Figure 7-2 and Figure 7-3.

Though less apparent at the shared scale of the y-axes in Figure 7-4 to Figure 7-6, South Island wind shows a similar seasonality to North Island wind. Thus, for both wind and solar energy, the annual cycle is similar in both islands. The expectation is that most new wind and solar generation capacity will be in the North Island, conveniently closer to where demand is greatest.

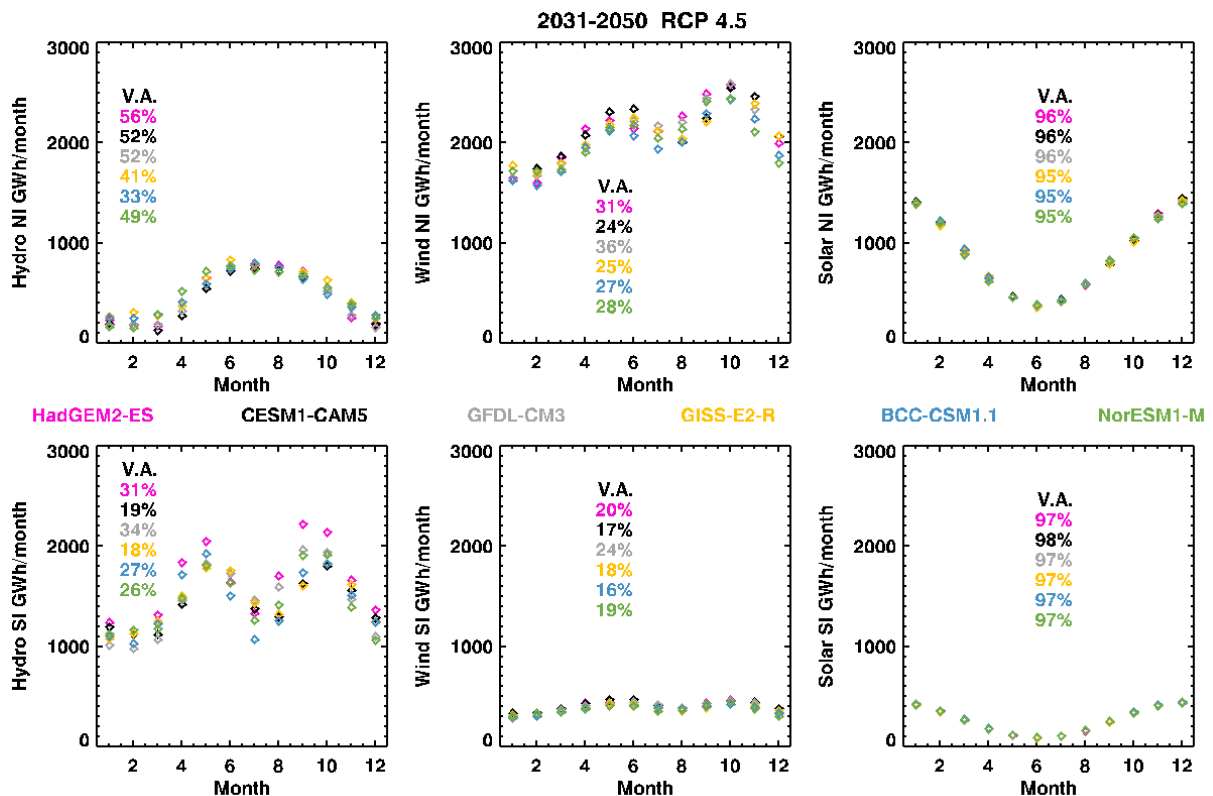


Figure 7-5: Seasonality of hydro, wind, and solar generation for the North and South Islands in 2031-2050 RCP 4.5 monthly totals. As in Figure 7-4, the model was fitted to each of the CMIP5 models, as colour-coded. Figures in each plot show the proportion of variance in monthly values attributable to the fitted seasonality.

In the seasonality of future scenarios of Figure 7-5 and Figure 7-6, relative to Figure 7-4, there is some increase in mean winter and spring hydro generation in the South Island, especially in some models. To clarify this shift, Figure 7-7 summarises the seasonality of the dominant North Island wind and South Island hydro sources by combining values for all six CMIP5 models. The symbol shows the mean of the six, while the vertical lines cover the range.

With the three types of generation in the two islands separated into seasonal cycle and residual difference, we can examine the correlations of the latter, as shown in Table 7-1. The residuals represent the extent to which any type of generation is greater or less than average for that time of year. If there is a tendency, in present or projected future climates, for low hydro flows to coincide with less wind or sun then we might expect that to be apparent in the correlation of residuals.

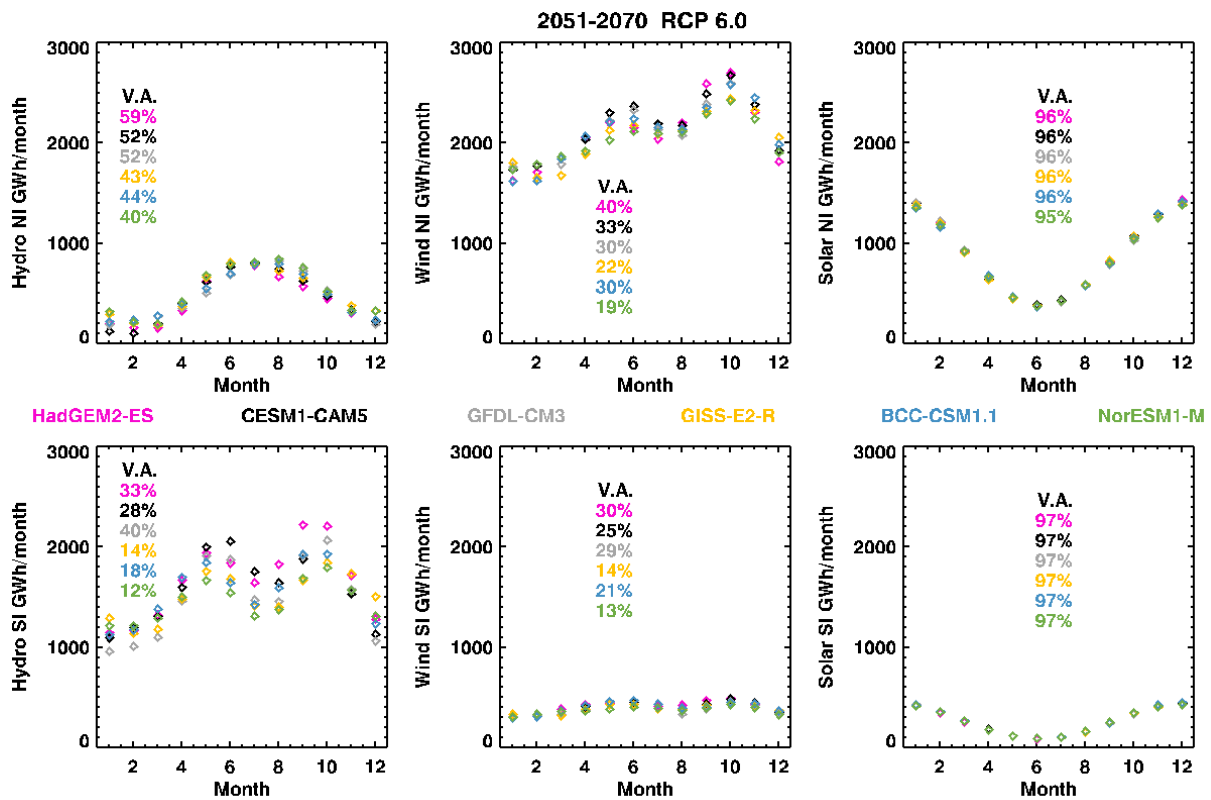


Figure 7-6: Seasonality of hydro, wind, and solar generation for the North and South Islands in 2051-2070 RCP 6.0 monthly totals. The model of was fitted to each of the CMIP5 models, as colour-coded. Figures in each plot show the proportion of variance attributable to the fitted seasonality.

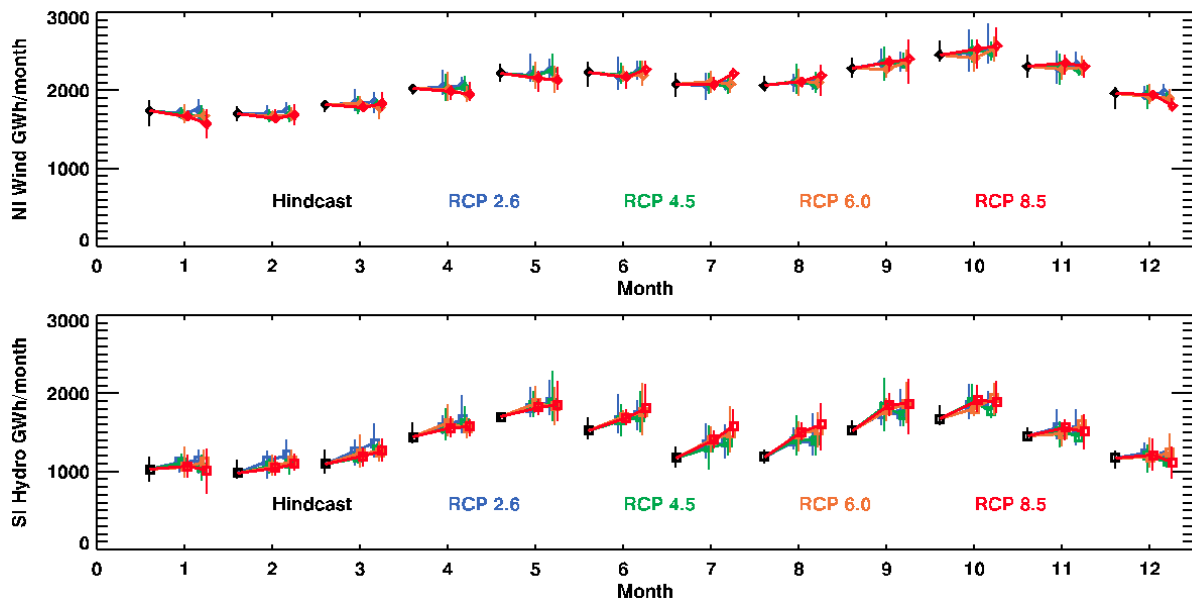


Figure 7-7: Seasonality of North Island wind and South Island hydro from hindcast to future projections for the four RCs. The symbol shows the mean for all six CMIP5 models, while the vertical lines show their range.

Table 7-1: Correlations between residual variation in hindcast monthly generation. The residuals from subtraction of the annual cycle (and any trend) show the extent to which any month is wetter or drier, windier or calmer, and clearer or cloudier than usual.

Residual	Wind		Solar		
	N	S	N	S	
Hydro	N	0.05 – 0.19	-0.09 – 0.07	-0.43 – -0.34	-0.27 – -0.18
	S	0.53 – 0.63	0.35 – 0.48	-0.11 – 0.01	-0.17 – -0.02
Wind	N		0.05 – 0.14	0.17 – 0.32	
	S		0.14 – 0.23	0.17 – 0.31	

First, we can largely discount solar generation from such consideration. The correlation of solar residuals on either island with those for wind are small, and the anticorrelation of residuals for solar and hydro generation are small to negligible except in the North Island for both. Even there it is only moderate, and the residuals for solar are only about a tenth of the mean cycle in magnitude, as was shown in Figure 6-6. For a widely-distributed solar generation network, monthly generation is expected to be highly predictable, but strongly concentrated around the summer months.

We can thus expect that solar generation from summer through autumn can be used to reduce hydro generation at that time, thus ensuring any hydro storage is full before the critical winter period. It may also be that surplus summer solar generation supports production of hydrogen and perhaps ammonia. Their economic viability would be much enhanced if summer wholesale power prices are very low because of much larger solar capacity.

Plots corresponding to Figure 7-3 for both the 2031–2050 and 2051–2070 periods, and for all four RCPs, are shown in Appendix C. In all of them there is positive correlation between hydro and wind, especially for the most important two, South Island hydro and North Island wind. As shown in Table 7-1 for hindcast data, much of this correlation persists in the residuals. Table 7-2 shows the South Island hydro – North Island wind correlations for total generation (from figures in Appendix C), and Table 7-3 shows the residual variation relative to the mean seasonal behaviour shown in Figure 7-4.

For each period, RCP, and model, the percent change in correlation from hindcast is shown in smaller figures. Some of the difference will be spurious, because both hindcast and projected future values are from free-running models that will vary from run to run. The percentage figures do highlight that some models (especially GFDL-CM3 and HadGEM2-ES) show more consistently increasing correlation in Table 7-1. However, even for a given model, the change is not uniform with time (earlier period to later) or clearly related to radiative forcing (RCP figure).

The same analysis applied to the correlation of residuals, as in Table 7-3, shows even less consistency. There seems to be no clear reason to think that future patterns of monthly rainfall into South Island hydro lakes and monthly North Island wind generation will differ from past values in the coincidence of highs or lows of both. The present tendency for moderate correlation ($R \sim 0.5$) between them is possibly representative of future climates.

Table 7-2: Correlation of monthly South Island hydro generation with North Island wind. Linear correlation coefficients for each GCM, and the mean of all six, are shown for hindcast data and each future RCP. The change in correlation from hindcast to projected future is expressed as per cent in smaller font.

		HadGEM2		CESM-CAM		GFDL-CM3		GISS-E2-R		BCC-CSM		NorESM		Mean	
Hindcast		0.62	%	0.67	%	0.60	%	0.66	%	0.68	%	0.60	%	0.64	%
2031-2050	RCP 2.6	0.61	-1	0.57	-15	0.67	11	0.67	1	0.62	-8	0.70	15	0.64	0
2051-2070	RCP 2.6	0.67	8	0.71	6	0.64	6	0.62	-4	0.58	-15	0.52	-13	0.62	-2
2031-2050	RCP 4.5	0.69	12	0.67	0	0.68	13	0.62	-5	0.66	-2	0.66	9	0.67	4
2051-2070	RCP 4.5	0.67	8	0.70	4	0.64	7	0.66	0	0.68	0	0.65	7	0.67	4
2031-2050	RCP 6.0	0.68	10	0.64	-3	0.65	8	0.71	8	0.60	-11	0.50	-16	0.63	-1
2051-2070	RCP 6.0	0.75	20	0.70	3	0.71	17	0.69	5	0.67	-1	0.64	6	0.69	8
2031-2050	RCP 8.5	0.67	8	0.71	6	0.69	15	0.64	-2	0.72	5	0.65	7	0.68	6
2051-2070	RCP 8.5	0.69	11	0.64	-4	0.67	11	0.64	-2	0.63	-7	0.67	11	0.66	2

Table 7-3: Correlation of residuals for South Island hydro with North Island wind. Linear correlation coefficients are shown for each GCM, and the mean of all six, in hindcast and for each future RCP. The change in correlation from hindcast to future values is expressed as per cent in smaller font.

		HadGEM2		CESM-CAM		GFDL-CM3		GISS-E2-R		BCC-CSM		NorESM		Mean	
Hindcast		0.55	%	0.59	%	0.56	%	0.54	%	0.63	%	0.53	%	0.57	%
2031-2050	RCP 2.6	0.56	3	0.53	-9	0.57	1	0.53	0	0.60	-4	0.60	12	0.57	0
2051-2070	RCP 2.6	0.63	15	0.65	10	0.62	10	0.55	2	0.53	-16	0.45	-14	0.57	1
2031-2050	RCP 4.5	0.62	14	0.60	1	0.56	0	0.55	2	0.62	-1	0.57	7	0.59	3
2051-2070	RCP 4.5	0.60	9	0.63	6	0.54	-3	0.61	13	0.62	-2	0.62	16	0.60	6
2031-2050	RCP 6.0	0.60	9	0.53	-9	0.61	7	0.65	21	0.52	-18	0.47	-12	0.56	0
2051-2070	RCP 6.0	0.62	14	0.63	5	0.59	5	0.65	21	0.63	0	0.61	14	0.62	9
2031-2050	RCP 8.5	0.57	4	0.61	2	0.58	3	0.57	6	0.67	5	0.56	6	0.59	4
2051-2070	RCP 8.5	0.52	-5	0.53	-11	0.60	6	0.55	2	0.59	-7	0.55	2	0.55	-2

7.2 Weekly generation – hydro-wind correlations

Weekly wind-hydro correlations for various regions and between regions have been noted by generation companies in the past in confidential briefings. For example, it is well known that there is a large variation in weekly output in the range of 10 to 250% of average, with low persistence from week to week (i.e., not much autocorrelation). The same week-to-week behaviour is seen in simulations of future climates. Additionally, it was noted in the industry report that hydro-wind correlations are greater over longer time periods, e.g., New Zealand annual hydro-wind generation correlations were around 0.7–0.8, which is twice that of weekly hydro-wind correlations. These relationships are also seen for future climate scenarios (Figure 7-8). It is also reassuring that the models broadly reproduce the various regional hydro generation vs regional wind generation correlations. Generally, the CMIP5-based hydro-wind correlations are somewhat higher than the station-based correlations. This is not too surprising given the resolution of the regional climate

model simulations (i.e., downscaled results which use CMIP5 model as boundary conditions) and more localised influences on station winds.

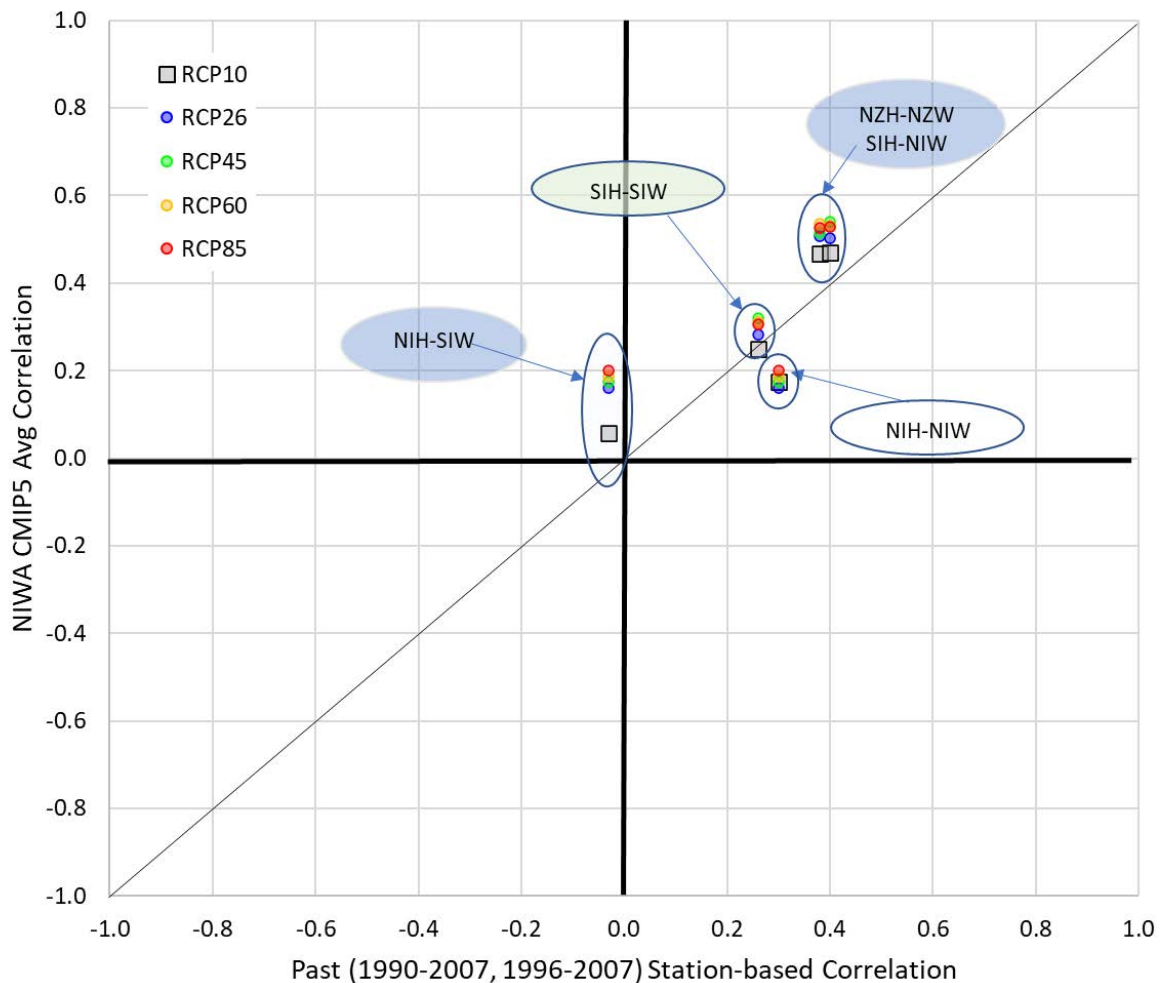


Figure 7-8: Comparison of various CMIP5 hydro - wind correlations by island for four RCP's plus hindcast vs a previous climate station-based correlation analysis. The past analysis (for industry) covered periods 1990–2007, and 1996–2007. Symbols falling on the diagonal line would represent identical correlations. In the legend, 'RCP10' denotes hindcast data.

Figure 7-9 shows the absolute change (2051–2070 vs 1986–2005) in hydro region-wind region correlation for each CMIP5-based model for various pairs of regions. Key points to note here are how the NZ hydro-wind correlation is dominated by South Island hydro and North Island wind and the increase in correlation for the Hadley and GFDL models.

Finally, the average over all CMIP5 models of the absolute change (2051–2070 from 1986–2005) in hydro - wind correlations for each RCP is shown in Figure 7-10. It shows the largest increases in correlation for North Island hydro and South Island wind, however these correlations are generally very low. Change for the whole country depends mostly on the important South Island hydro – North Island wind combination.

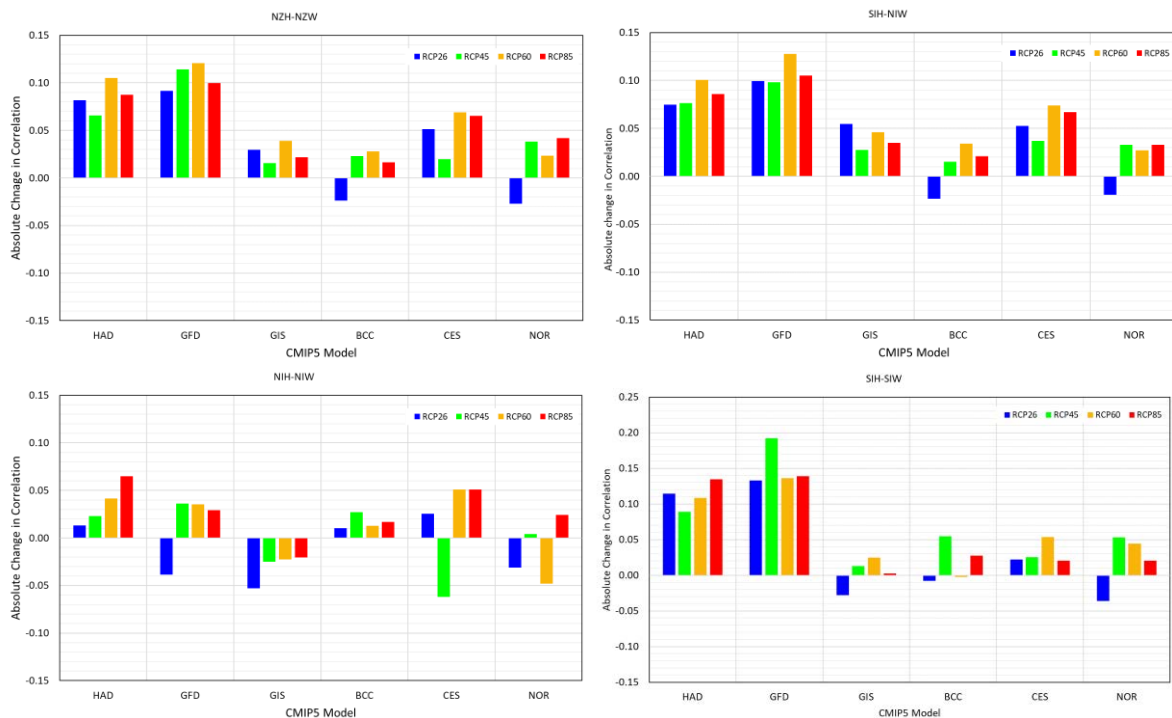


Figure 7-9: Change in hydro - wind correlation by island for each CMIP5 model and RCP scenario. Plots show the absolute change in correlation from 1986–2005 to 2051–2070 for NZ hydro with NZ wind (top left); South Island hydro with North Island wind (top right); North Island hydro with North Island wind (bottom left); and South Island hydro with South Island wind (bottom right).

7.3 Possible further analyses with present datasets

In Section 2, and especially Figure 2-2, we showed that the ‘dry year’ problem was closely aligned with autumn river flows, even without any representation of hydro storage. In future decades, by the time a substantial pumped hydro scheme at Lake Onslow or elsewhere could be completed, electricity demand is likely to be at least 80% higher, with most of the extra supply from wind and solar generation. The solar generation will be strongly seasonal, but the summer surplus may well mean that any hydro storage can be full at the end of summer.

With that assumption, and agreement on how much wind and solar generation should be assumed, the above datasets at either monthly or weekly resolution could be combined with estimated demand. The latter would ideally come from historical data, adjusted for any expected change in pattern, but even a constant demand figure might be sufficient.

By integrating the balance of supply minus demand over the autumn and winter periods, we would calculate the peak energy deficit in GWh for the above scenarios and models. The frequency and amounts by which this exceeded present storage would help inform the required capacity of pumped hydro schemes. Though obviously less satisfactory than a simulation that fully integrates storage and lag times, analysis as described may help to bracket a more detailed study. It would be a relatively straightforward extension of the present work.

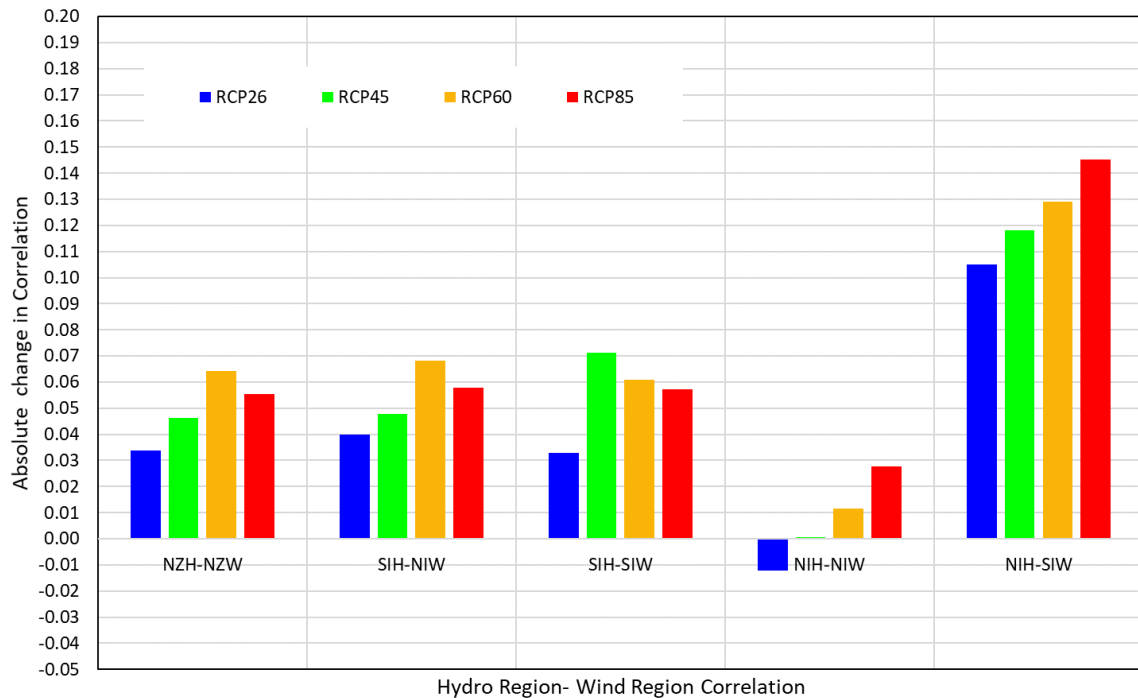


Figure 7-10: Average change in hydro-wind correlations from hindcast to 2051–2070 for each RCP scenario. Bars coloured by RCP show the average over all CMIP5 models of the absolute change in correlation for NZ and for island pairs as labelled. The total is dominated by the South Island hydro – North Island wind pair.

7.4 Possible refinements and new datasets

For the specific question of how severe future dry years may be, it could be better to consider more complex correlations (e.g., quantile non-linear) looking specifically at potential change in seasonality, especially of the lowest percentiles.

It may also be more reliable to develop bias correction targeting average and low flow characteristics for the hydro lakes, rather than the overall range. This is suggested by Figure 4-3, which shows that otherwise simulations can be valid for mean flows but consistently underestimate low flows. In the NZ Battery context that could result in projected shortages being greater than in reality.

The hydro analysis in terms of generation potential has assumed that the current HMD relationship in conversion of inflows to MWh at each hydro lake will remain the same in the future. A sensitivity analysis of the stationarity of the conversion is recommended as climate change will result in changes in weather patterns and likely affect the relative generation production of the various hydro schemes.

As a further check, it would be valuable to carry out an analysis of the current and future natural system in regards of inflows to hydro lakes, without the use of the current HMD relationship. This will provide an analysis on how the natural system is likely to behave in the future and could assess the possibly increased importance of smaller hydro lakes to the system. For example, currently simulated North Island hydro generation is highly dependent on Lake Taupō inflow and all generation capacity to the 11 subsequent power stations is derived from Taupō inflows. As those power stations cover a large spatial domain, changed weather patterns could lead to increased capture by the distributed nature of the Waikato power scheme. This would reduce reliance on Lake Taupō for generation

capacity. Similar analysis can be carried out for Clyde-Manapouri and the Waitaki system in the South Island.

Finally, all the above analysis has been based on six GCMs providing boundary conditions for the one regional climate model. We have treated the six GCMs as sampling the space of possible futures under each RCP, but we cannot be certain how well they do so. An alternative would be to use a resource like *Weather at Home* Happi simulations (happimip.org). This is a physics-based climate model that, used in conjunction with climate change scenarios through the NZ Earth System Model, could generate a true large ensemble (thousands) of climate scenarios. These would then be used to assess the tails of distribution that characterise the dry year problem.

8 Concluding remarks

In the introduction we posed a number of questions that arise from the prospect of 100% renewable electricity generation and the implications of hydro inflow variation. Here we summarise how the findings in this report answer those questions.

8.1 Is a dry year characterised by historical inflow variation still appropriate?

Examination of the HMD data identified that past dry years all corresponded to low autumn inflows. The seasonality of hydro flows appears to change little in the future scenarios. The projected hydro generation at lowest flows may increase by around 10% in the North Island, and by up to 16% in the South Island, for which hydro generation is at least three times greater. These are nevertheless much smaller changes than the expected increase in demand and the additional wind and solar generation capacity needed to achieve 100% renewable electricity.

If the hydroelectric fraction of New Zealand's total generation falls from 55% to around 30% by 2050, as in the assumptions above, the parameters that define a dry year will change. Excess solar generation in summer will allow hydro storage to be high going into autumn. Wind generation is less variable from year to year than rainfall into the hydro catchments, reducing the impact of a dry year if wind flows are normal. However, hydroelectricity remains the only form of renewable energy for power generation with significant storage and dispatchability. There is none for wind and solar; geothermal generation runs at near capacity for economic reasons; and biofuels (especially wood waste used for process heat and cogeneration) are likely to remain a small component of New Zealand's generation profile. Unless or until chemical storage such as with hydrogen or ammonia production becomes competitive, low hydro flows will continue to be a concern for security of electricity supply in winter. This concurs with conclusions of a recent discussion paper from the Electricity Authority's Market Development Advisory Group (MDAG, 2022).

8.2 Does reliance on renewable generation sources exacerbate the dry year problem?

For the expected number and distribution of wind farms in New Zealand 20–30 years hence, wind generation is less variable from year to year than hydro generation. For this reason, a large amount of new wind generation should reduce the relative importance of dry years. However, there is a positive correlation between hydro generation in the largest source area - the South Island – and wind generation (particularly in the north Island). The positive correlation of around 0.5 at weekly or monthly time scales suggests that wind generation will not reduce the impact of low rainfall years by much.

The other large source of new generation – solar energy – has quite different implications. Because of its scalability, and the suitability of most of NZ for solar energy capture, future solar generation is likely to be widely dispersed. It is highly variable at short time scales locally, and of course entirely diurnal, so its integration into the national electricity grid necessarily assumes that it will be buffered at time scales of minutes to days; most probably in fixed-batteries or car batteries with vehicle-to-grid supply. With that assumption, we can consider it alongside hydro and wind at weekly or monthly time scales, and in that context it is reliably seasonal. Nonetheless, electricity storage in batteries, whether in vehicles or fixed, will not be useful for inter-seasonal storage.

The most important implication of a large amount of solar generation capacity for addressing the dry year problem is that the expected summer peak in solar generation will probably obviate any

concern about dry summers leading to a winter shortage. With a large amount of solar generation operating the country can expect to enter autumn with all hydro lakes storage full.

8.3 Do future correlations between hydro inflows and wind flows, for example, mean the required battery solution needs to be larger or smaller?

The future correlations between hydro inflows and wind generation are not clearly different from present correlations in the six GCM-based analyses considered here. The required storage capacity of a NZ Battery will depend on future demand and on how much of that is met with wind generation. For the scenario considered in this report, wind generation would increase ten-fold from the present and be nearly three times the supply from both present and currently consented wind generation capacity. We also assume that demand would increase by 80% or more. Because the seasonality of wind generation is correlated with hydro generation, especially the much-larger South Island hydro, the extra supply and demand will present some of the same risk of seasonal shortage. If the linear correlation between South Island hydro and North Island wind of 0.5 were to apply equally across the distribution of hydro flows, we might roughly estimate that it would mean hydro storage would need to increase to at least 1.5 times present capacity. Such an assumption is probably unjustified, but we can perhaps assess that with bias-corrected hydro inflow data. More likely, some further analysis as suggested in Sections 7.3 and 7.4 may be needed.

Again, increased solar generation has other implications. The large excess of generation in summer will often greatly exceed the rate at which hydro storage can be increased, even with a putative Lake Onslow. It could store energy only at a rate comparable to its suggested generation rate of 1 GW, whereas the summer excess from solar generation could be 10 GW or more, depending on installed capacity. The result will be that electricity prices in NZ will often fall to zero, though not into negatives as already occurs in places like Spain or Queensland where thermal generation has to be kept running for when the sun sets. With free electricity, energy storage as hydrogen or ammonia may be cost-competitive with a pumped hydro scheme. The likelihood of that hinges on the development path of such chemical storage and the resulting economics, which are both well outside the scope of this study. What we can say from the seasonality and present cost-competitiveness of solar generation is that the physical pre-conditions (as described in Section 6) will certainly apply.

9 References

- Bandaragoda, C., Tarboton, D.G., Woods, R.A. (2004) Application of TOPNET in the distributed model intercomparison project. *J. Hydrol.*, 298:178-201.
- Bentsen, M., (2013) The Norwegian Earth System Model, NorESM1-M – Part 1: Description and basic evaluation of the physical climate. *Geosci. Model Dev.*, 6, 687–720.
<https://doi.org/10.5194/gmd-6-687-2013>
- Beven, K.J., Lamb, R., Quinn, P., Romanowicz, R., Freer, J. (1995) TOPMODEL. In: *Computer Models of Watershed Hydrology*, edited by: Singh, V.P., Water Resour. Publ., Highlands Ranch, Colorado, 627–668.
- CCC (He Pou a Rangi the Climate Change Commission) (2021) Ināia Tonu Nei: a low emissions future for Aotearoa. <https://www.climatecommission.govt.nz/our-work/advice-to-government-topic/inaia-tonu-nei-a-low-emissions-future-for-aotearoa/>
- Clark, M.P., Rupp, D.E., Woods, R.A., Zheng, X., Ibbitt, R.P., Slater, A.G., Schmidt, J., Uddstrom, M.J. (2008) Hydrological data assimilation with the ensemble Kalman filter: Use of streamflow observations to update states in a distributed hydrological model. *Advances in Water Resources*, 31(10): 1309-1324. 10.1016/j.advwatres.2008.06.005
- Collins, D. (2020) New Zealand river hydrology under late 21st century climate change. *Water*, 12, 2175; doi:10.3390/w12082175
- Conway, J., Carey-Smith, T., Cattoen-Gilbert, C., Moore, S., Sirguey, P., Zammit, C. (2021) Simulations of seasonal snowpack duration and water storage across New Zealand. *Weather and Climate*, vol 41, issue 1, pp 72-89
- Electricity Authority (2018a) Hydrological Modelling Dataset. Report 2a: 2018 HMD Flow series comparison with 2015. WSP report 3-53422.00 for Electricity Authority.
- Electricity Authority (2018b) Hydrological Modelling Dataset. Report 2: Flow series description and methodology. WSP report 3-53422.00 for Electricity Authority.
- Electricity Authority (2018c) Electricity in New Zealand. <https://www.ea.govt.nz/about-us/media-and-publications/electricity-new-zealand/>
- Electricity Authority (2019) Power stations proposed at 20190924.
https://www.emi.ea.govt.nz/Wholesale/Datasets/Generation/Generation_fleet/Proposed
- Goring, D.G. (1994) Kinematic shocks and monoclinal waves in the Waimakariri, a steep, braided, gravel-bed river. *Proceedings of the International Symposium on Waves: Physical and Numerical Modelling*, University of British Columbia, Vancouver, Canada, 21–24 August, 1994, pp. 336–345.
- Griffies, S. M. (2011) The GFDL CM3 Coupled Climate Model: Characteristics of the Ocean and Sea Ice Simulations, *Journal of Climate*, 24(13), 3520-3544.
<https://journals.ametsoc.org/view/journals/clim/24/13/2011jcli3964.1.xml>

- Ibbitt, R.P., Woods, R. (2002) Towards rainfall-runoff models that do not need calibration to flow data, in: Friend 2002 – Regional Hydrology: Bridging the Gap Between Research and Practice, edited by: van Lanen, H. A. J. and Demuth, S., IAHS Publ., 274, 189–196.
- IEA (International Energy Agency) (2021a) Net Zero by 2050: A Roadmap for the Global Energy Sector. <https://www.iea.org/reports/net-zero-by-2050>
- IEA (2021b) World Energy Outlook 2021. <https://www.iea.org/reports/world-energy-outlook-2021>
- IPCC (2014) Climate Change 2014: Synthesis Report. Contribution of Working Groups I, II and III to the Fifth Assessment Report of the Intergovernmental Panel on Climate Change: 151 pp.
- Jones, C. D. (2011) The HadGEM2-ES implementation of CMIP5 centennial simulations. *Geosci. Model Dev.*, 4, 543–570. <https://doi.org/10.5194/gmd-4-543-2011>
- McMillan, H., Clark, M., Bowden, W.B., Duncan, M.J., Woods, R. (2011) Hydrological field data from a modeller’s perspective. Part 1: diagnostic tests for model structure. *Hydrol. Process.* 25 (4), 511–522.
- McMillan, H.K., Hreinsson, E.O., Clark, M.P., Singh, S.K., Zammit, C., Uddstrom, M.J. (2013) Operational hydrological data assimilation with the recursive ensemble Kalman Filter. *Hydrol. Earth Syst. Sci.*, 17, 21-38.
- McMillan, H.K., Booker, D.J., Cattoen, C. (2016) Validation of a national hydrological model. *Journal of Hydrology*, 541: 800-815. 10.1016/j.jhydrol.2016.07.043.
- MDAG (2022) Price discovery under 100% renewable electricity supply. <https://www.ea.govt.nz/assets/dms-assets/29/01-100-Renewable-Electricity-Supply-MDAG-Issues-Discussion-Paper-1341719-v2.4.pdf>
- Meehl, G. A. (2013) Climate Change Projections in CESM1(CAM5) Compared to CCSM4, *Journal of Climate*, 26(17), 6287-6308. <https://journals.ametsoc.org/view/journals/clim/26/17/jcli-d-12-00572.1.xml>
- MfE (2018) Climate Change Projections for New Zealand: Atmosphere Projections Based on Simulations from the IPCC Fifth Assessment, 2nd Edition. Wellington: Ministry for the Environment. <https://environment.govt.nz/assets/Publications/Files/Climate-change-projections-2nd-edition-final.pdf>
- MBIE (Ministry of Business, Innovation and Employment) (2019) Electricity demand and generation scenarios: Scenario and results summary. <https://www.mbie.govt.nz/dmsdocument/5977-electricity-demand-and-generation-scenarios>
- Mullan, A. B., Stuart, S. J., Hadfield, M. G., Smith, M. J. (2010) *Report on the Review of NIWA’s ‘Seven-Station’ Temperature Series*. NIWA Information Series No. 78. Wellington, p. 55.

- Newsome, P.F.J., Wilde, R.H., Willoughby, E.J. (2000) Land Resource Information System Spatial Data Layers, Technical Report, Palmerston North, Landcare Research NZ Ltd., New Zealand.
- NZ Government (2019) Climate Change Response (Zero Carbon) Amendment Act 2019. <https://www.legislation.govt.nz/act/public/2019/0061/latest/whole.html>
- Schmidt, G. A. (2014) Configuration and assessment of the GISS ModelE2 contributions to the CMIP5 archive, *J. Adv. Model. Earth Syst.*, 6, 141– 184, <https://doi.org/10.1002/2013MS000265>
- Snelder, T.H., Biggs, B.J.F. (2002) Multiscale river environment classification for water resources management. *Journal of the American Water Resources Association*, 38:1225-1239.
- Sood, A. (2014) Improved bias corrected and downscaled regional climate model data for climate impact studies: Validation and assessment for New Zealand. Retrieved from www.researchgate.net/publication/265510643_Improved_Bias_Corrected_and_Downscaled_Regional_Climate_Model_Data_for_Climate_Impact_Studies_Validation_and_Assessment_for_New_Zealand
- Transpower (2020) Whakamana i Te Mauri Hiko: Empowering our Energy Future. <https://transpower.co.nz/sites/default/files/publications/resources/TP%20Whakamana%20i%20Te%20Mauri%20Hiko.pdf>
- Wu, T. (2014) An overview of BCC climate system model development and application for climate change studies. *Journal of Meteorological Research*, 28, 34–56. <https://doi.org/10.1007/s13351-014-3041-7>

Appendix A Wind farms considered in this report

Table A-1: Wind farms used in this report; name, region (see Figure 5-1), island, number of turbines, turbine capacity, total capacity, start year, status, and operator. The status indicators are as of 2021 and are; O operating, C consented, P proposed, H hypothetical.

Name	Reg	I*	No	Turbine Capacity (MW)	Farm Capacity (MW)	Year	Status	Operator
Ahipara	A	NI	50	3.0	150	2040	P	Meridian
Omamari	A	NI	50	3.0	150	2040	P	TiltRenewables
Rototuna	A	NI	200	2.5	500	2040	P	Meridian
Offshore	A	NI	500	5.0	2500	2040	H	VirtualNIWA
Kaimai	A	NI	50	3.0	150	2040	P	Ventus
Offshore	A	NI	500	5.0	2500	None	H	VirtualNIWA
TeUku	A	NI	28	2.3	64	2011	O	Meridian
Taumatotara	A	NI	5	2.0	10	2024	C	Ventus
Harapaki	B	NI	40	3.3	130	2023	C	Meridian
Titikura	B	NI	20	3.0	60	2023	C	Meridian
Central Wind	B	NI	40	3.3	130	2021	C	Meridian
Waipipi	B	NI	31	4.3	133	2020	O	TiltRenewables
Offshore	B	NI	50	3.0	150	2040	H	VirtualNIWA
Te Apiti	B	NI	55	1.7	91	2004	O	Meridian
Tararua 3	B	NI	31	3.0	93	2007	O	TiltRenewables
Tararua 2	B	NI	55	0.7	36	2004	O	TiltRenewables
Tararua 1	B	NI	48	0.7	32	1999	O	TiltRenewables
Te Rere Hau	B	NI	97	0.5	48	2008	O	NZWindFarms
Waitahora	B	NI	50	3.0	150	2040	P	Contact
Turitea	B	NI	60	3.6	222	2020	O	Mercury
Puketoi	B	NI	100	3.2	318	2023	C	Mercury
Castle Hill	B	NI	280	3.1	860	2023	C	Genesis
Mt Munro	B	NI	50	3.0	150	2040	P	Meridian

Mill Creek	C	NI	26	2.3	60	2014	O	Meridian
West Wind	C	NI	62	2.3	143	2009	O	Meridian
Hau Nui 2	C	NI	8	0.6	5	2004	O	Genesis
Hau Nui 1	C	NI	7	0.6	4	1996	O	Genesis
Cape Campbell	C	SI	50	3.0	150	2040	P	Mercury
Hurunui	D	SI	25	3.0	76	2023	C	Meridian
MtCass	D	SI	30	3.1	93	2025	C	MainPower
Mt Stalker	E	SI	50	3.0	150	2040	P	WaitakiWind
White Hill	E	SI	29	2.0	58	2007	O	Meridian
Mahinerangi 2	E	SI	50	3.2	160	2025	C	TiltRenewables
Mahinerangi 1	E	SI	12	3.0	36	2011	O	TiltRenewables
MtStuart	E	SI	9	0.9	8	2009	O	Pioneer
Kaiwera Downs	E	SI	80	3.0	240	2024	C	TiltRenewables
Slopedown	E	SI	50	3.0	150	2040	P	GenesisEnergy
Flat Hill	E	SI	8	0.8	7	2015	O	Pioneer

*NI- North Island; SI – South Island

Appendix B Hydrological bias-correction for each hydro system considered

The result of hydrological bias correction for each hydro-power scheme defined in Table 4-1.

Waikaremoana hydropower scheme

Bias corrected Lake Waikaremoana mean inflows error calculated to be around 0.5 % [-1%, 1%] across the 6 GCMs.

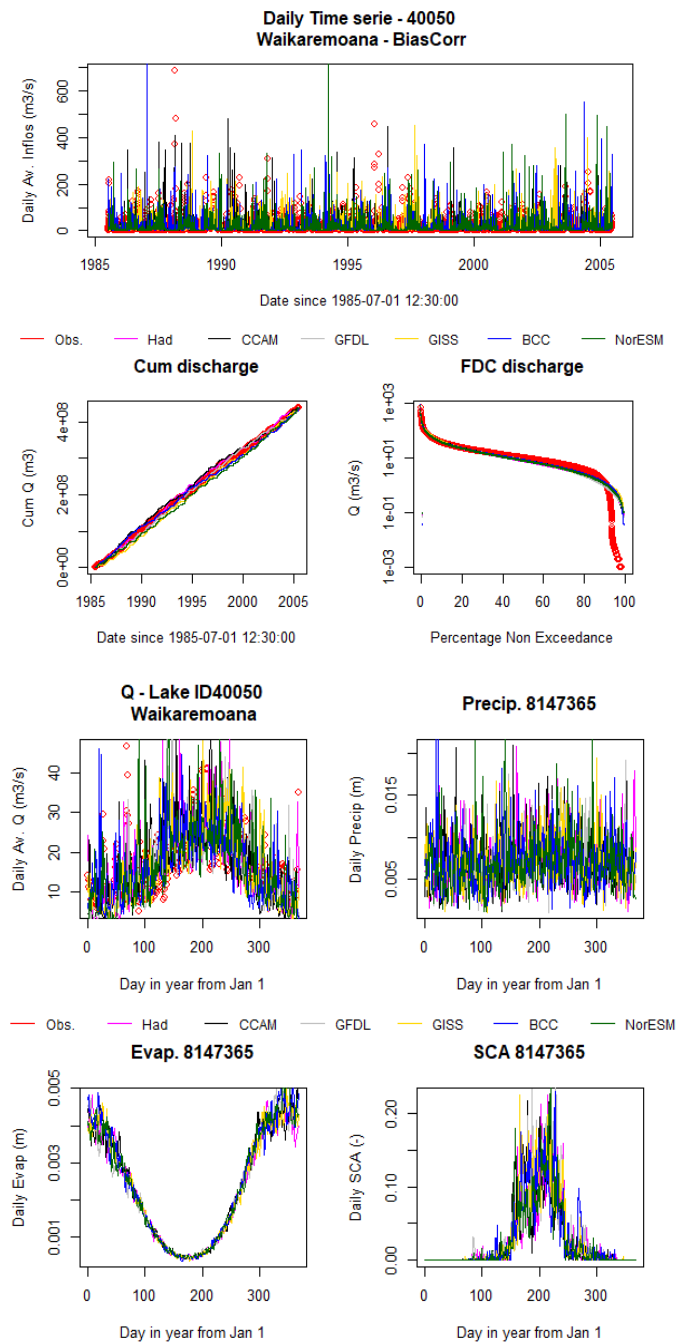


Figure B-1: Daily hydrograph, cumulated hydrograph and flow duration curves (top) daily average inflows, precipitation, evapotranspiration and snow area (bottom) for Lake Waikaremoana inflows over the period 1985–2006. Observations (black) are compared with TopNet flows driven by GCMs; HadGEM-ES (light blue), CCSM1-CAM5 (blue), GFDL-CM3 (yellow), GISS-E2-R (orange), BCC-CSM1.1 (red), and NorESM1-M (dark-green).

Taupo hydropower scheme

Bias corrected Lake Taupo mean inflows error calculated to be around 3.5 % [3%, 4%] across the 6 GCMs.

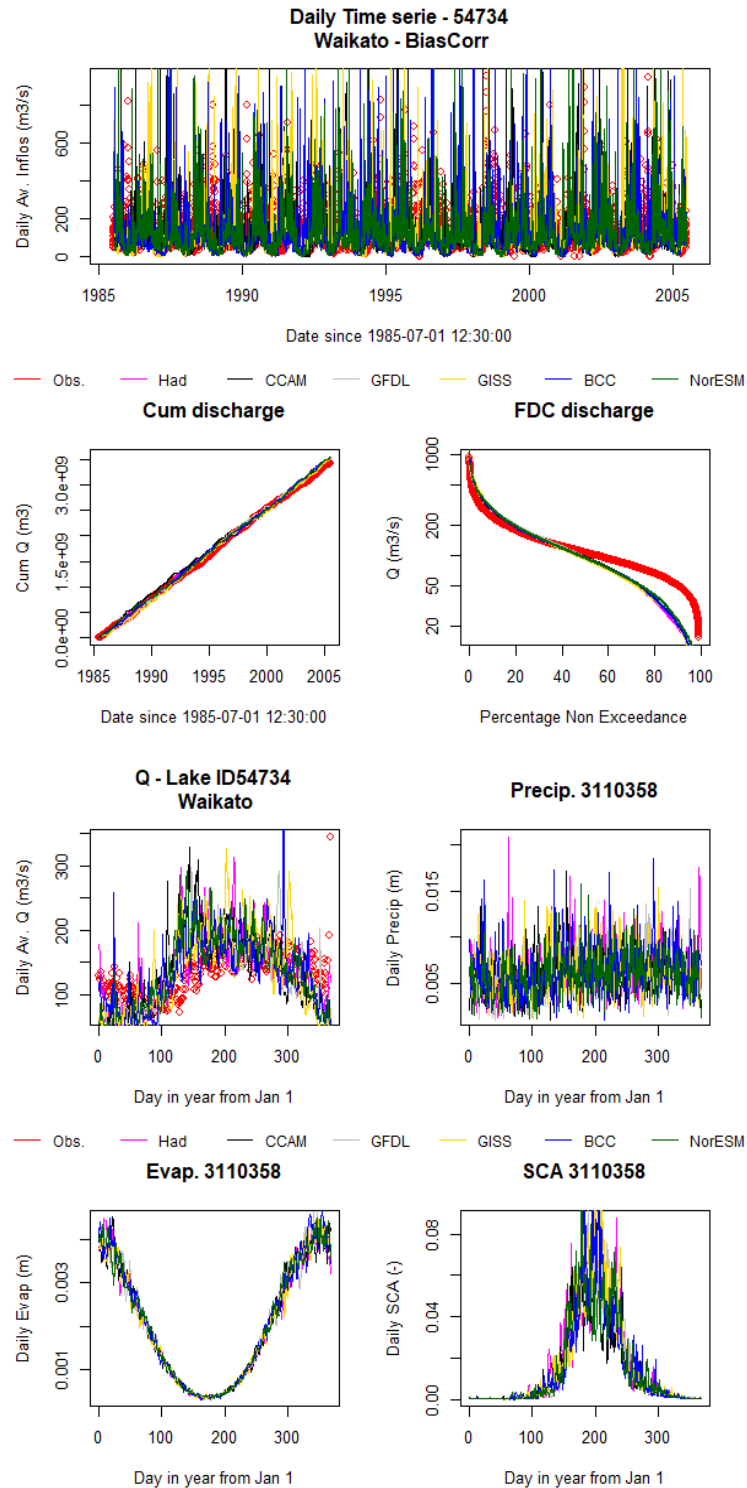


Figure B-2: Daily hydrograph, cumulated hydrograph and flow duration curves (top) daily average inflows, precipitation, evapotranspiration and snow area (bottom) for Lake Taupo inflows over the period 1985–2006. Observations (black) are compared with TopNet flows driven by GCMs; HadGEM-ES (light blue), CESM1-CAM5 (blue), GFDL-CM3 (yellow), GISS-E2-R (orange), BCC-CSM1.1 (red), and NorESM1-M (dark-green).

Cobb hydropower scheme

Bias corrected Lake Taupo mean inflows error calculated to be around 0.25 % [-1%, 1%] across the 6 GCMs.

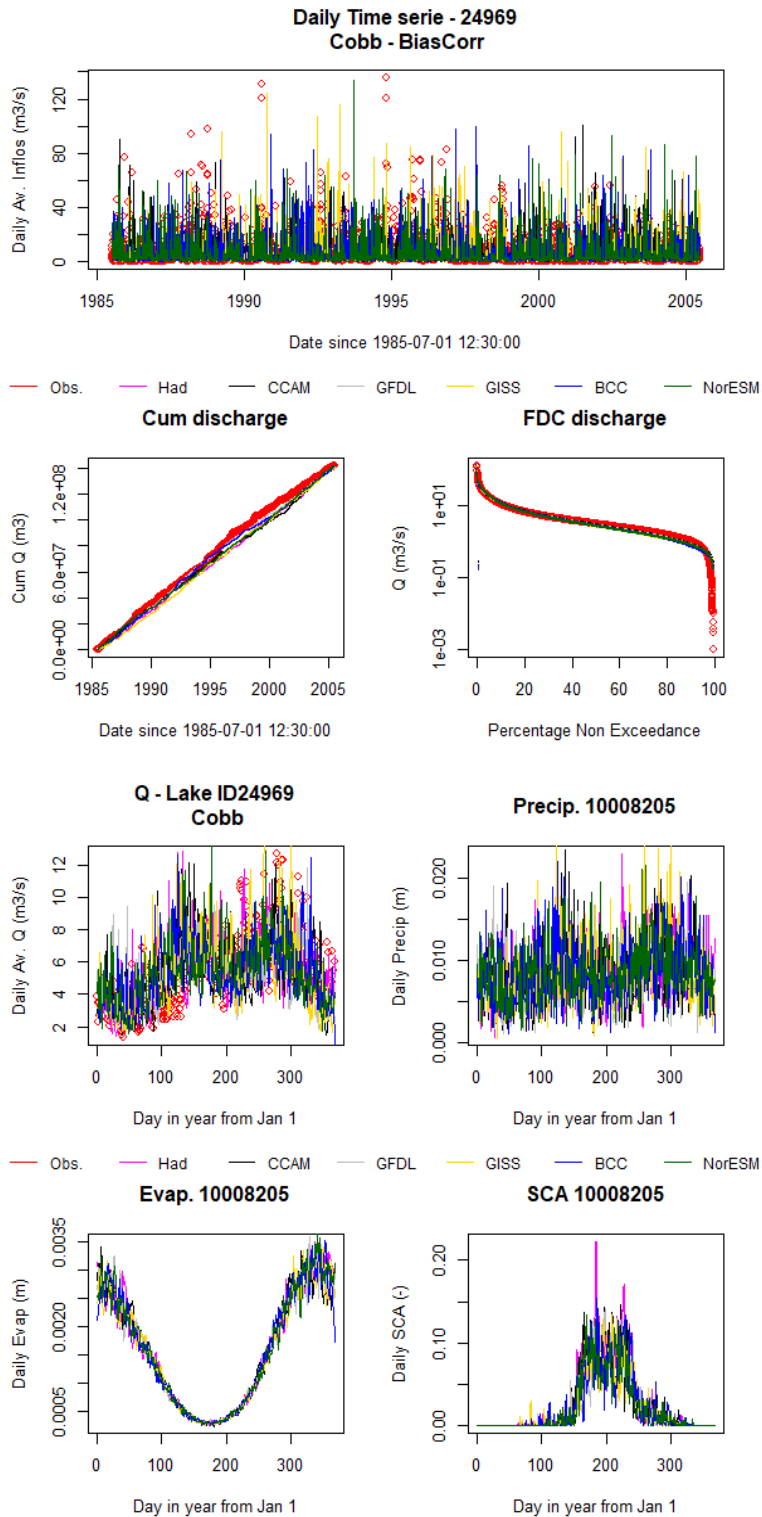


Figure B-3: Daily hydrograph, cumulated hydrograph and flow duration curves (top) daily average inflows, precipitation, evapotranspiration and snow area (bottom) for Lake Cobb inflows over the period 1985–2006. Observations (black) are compared with TopNet flows driven by GCMs; HadGEM-ES (light blue), CESM1-CAM5 (blue), GFDL-CM3 (yellow), GISS-E2-R (orange), BCC-CSM1.1 (red), and NorESM1-M (dark-green).

Waitaki power scheme

Bias corrected Lake Ohau mean inflows error calculated to be around 2 % [2%, 2%] across the 6 GCMs.

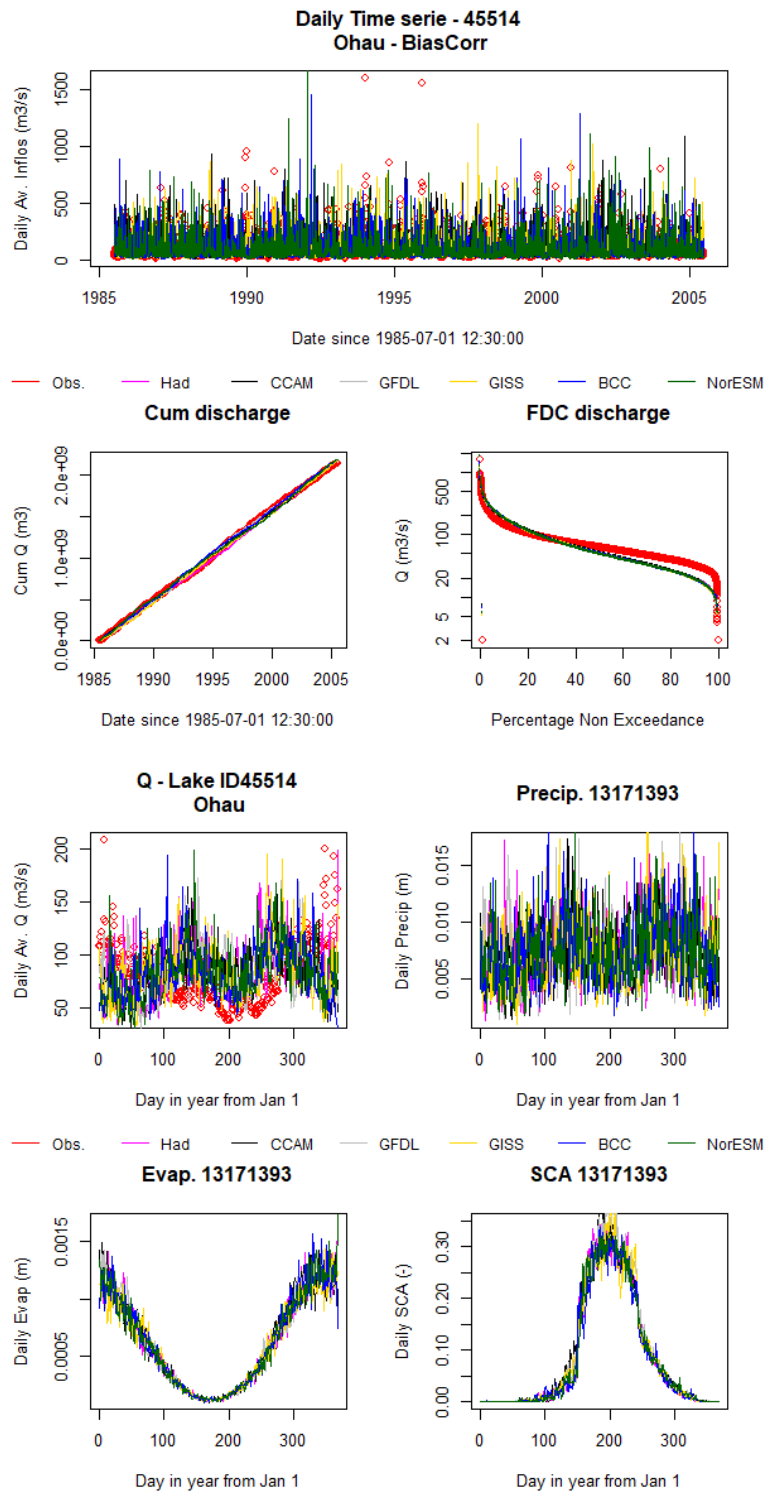


Figure B-4: Daily hydrograph, cumulated hydrograph and flow duration curves (top) daily average inflows, precipitation, evapotranspiration and snow area (bottom) for Lake Ohau inflows over the period 1985–2006. Observations (black) are compared with TopNet flows driven by GCMs; HadGEM-ES (light blue), CESM1-CAM5 (blue), GFDL-CM3 (yellow), GISS-E2-R (orange), BCC-CSM1.1 (red), and NorESM1-M (dark-green).

Bias corrected Lake Pukai mean inflows error calculated to be around 1 % [0%, 2%] across the 6 GCMs.

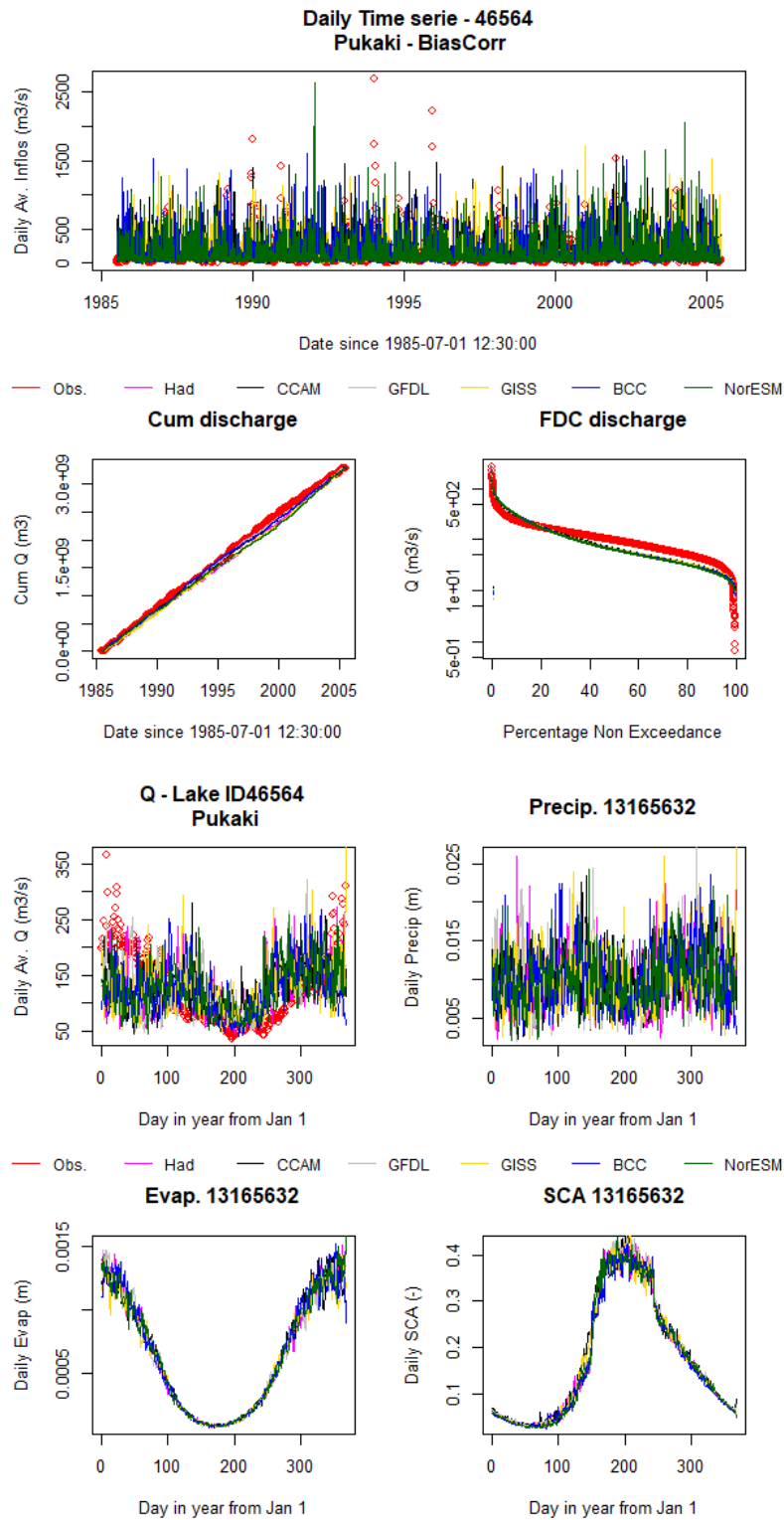


Figure B-5: Daily hydrograph, cumulated hydrograph and flow duration curves (top) daily average inflows, precipitation, evapotranspiration and snow area (bottom) for Lake Pukai inflows over the period 1985–2006. Observations (black) are compared with TopNet flows driven by GCMs; HadGEM-ES (light blue), CESM1-CAM5 (blue), GFDL-CM3 (yellow), GISS-E2-R (orange), BCC-CSM1.1 (red), and NorESM1-M (dark-green).

Bias corrected Lake Tekapo mean inflows error calculated to be around 0 % [0%, 0%] across the 6 GCMs.

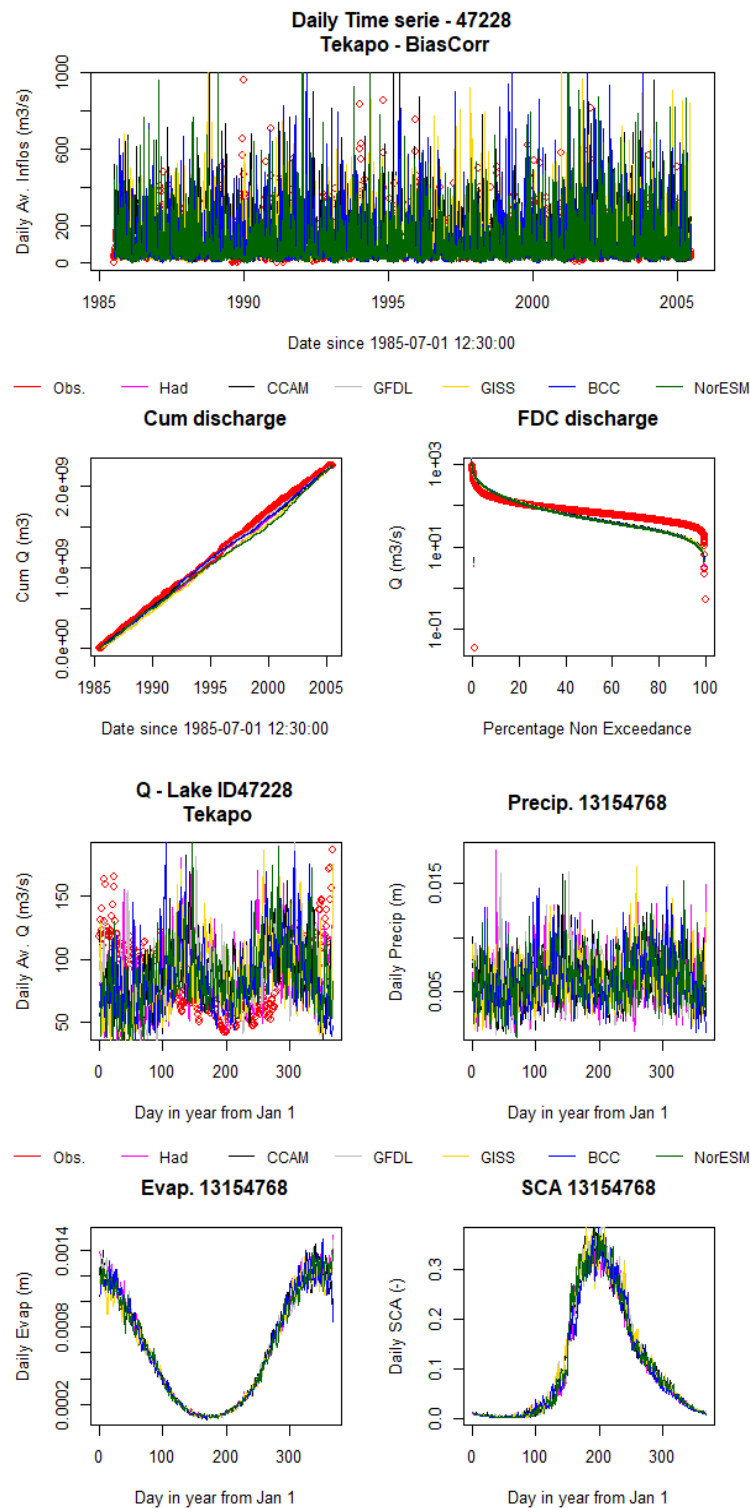


Figure B-6: Daily hydrograph, cumulated hydrograph and flow duration curves (top) daily average inflows, precipitation, evapotranspiration and snow area (bottom) for Lake Tekapo inflows over the period 1985–2006. Observations (black) are compared with TopNet flows driven by GCMs; HadGEM-ES (light blue), CESM1-CAM5 (blue), GFDL-CM3 (yellow), GISS-E2-R (orange), BCC-CSM1.1 (red), and NorESM1-M (dark-green).

Clutha hydro-power scheme

Bias corrected Lake Hawea mean inflows error calculated to be around -1 % [-1%, 0%] across the 6 GCMs.

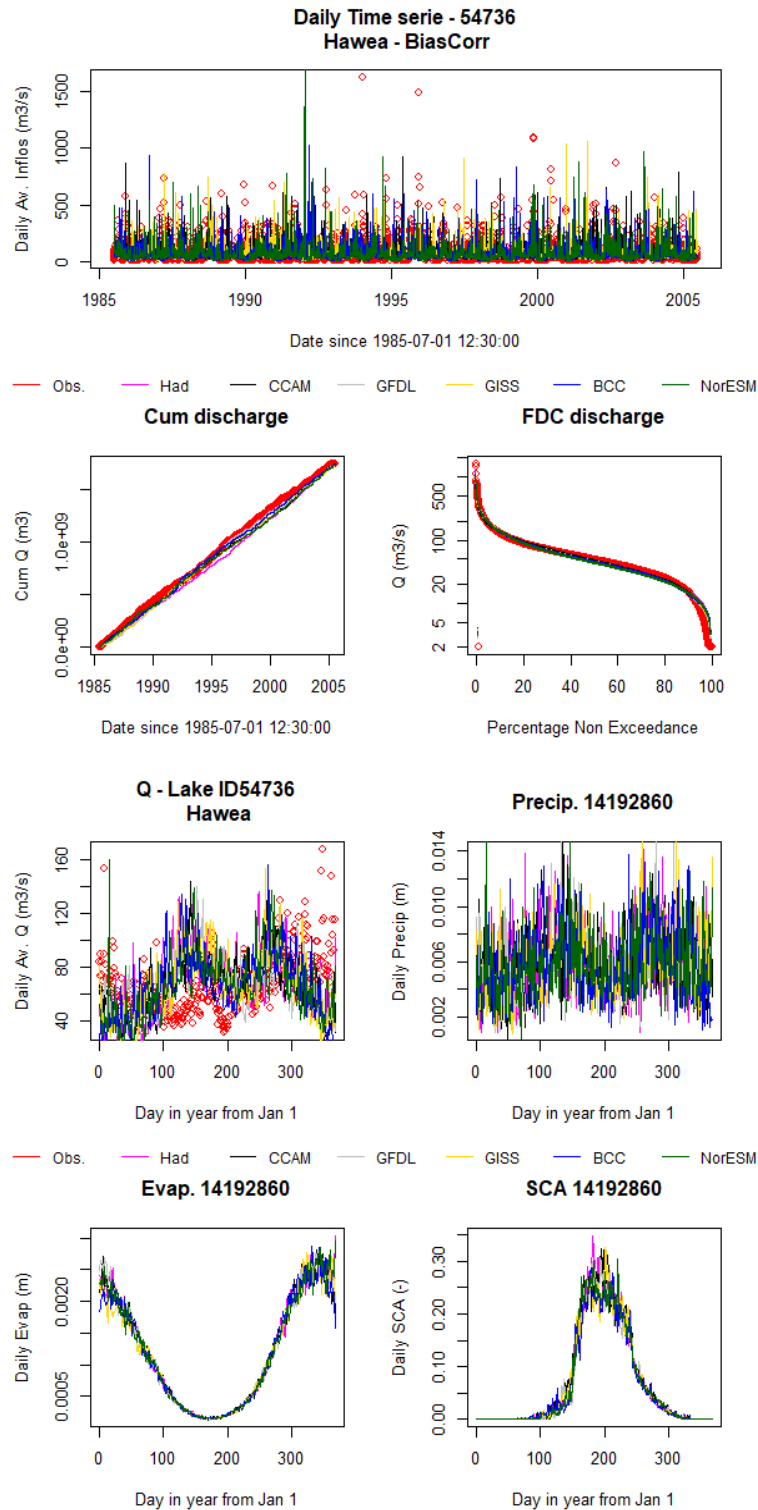


Figure B-7: Daily hydrograph, cumulated hydrograph and flow duration curves (top) daily average inflows, precipitation, evapotranspiration and snow area (bottom) for Lake Hawea inflows over the period 1985–2006. Observations (black) are compared with TopNet flows driven by GCMs; HadGEM-ES (light blue), CCSM-CAM5 (blue), GFDL-CM3 (yellow), GISS-E2-R (orange), BCC-CSM1.1 (red), and NorESM1-M (dark-green).

Manapouri hydro-power scheme

Bias corrected Lake Monowai mean inflows error calculated to be around -4 % [-4%, 4%] across the 6 GCMs.

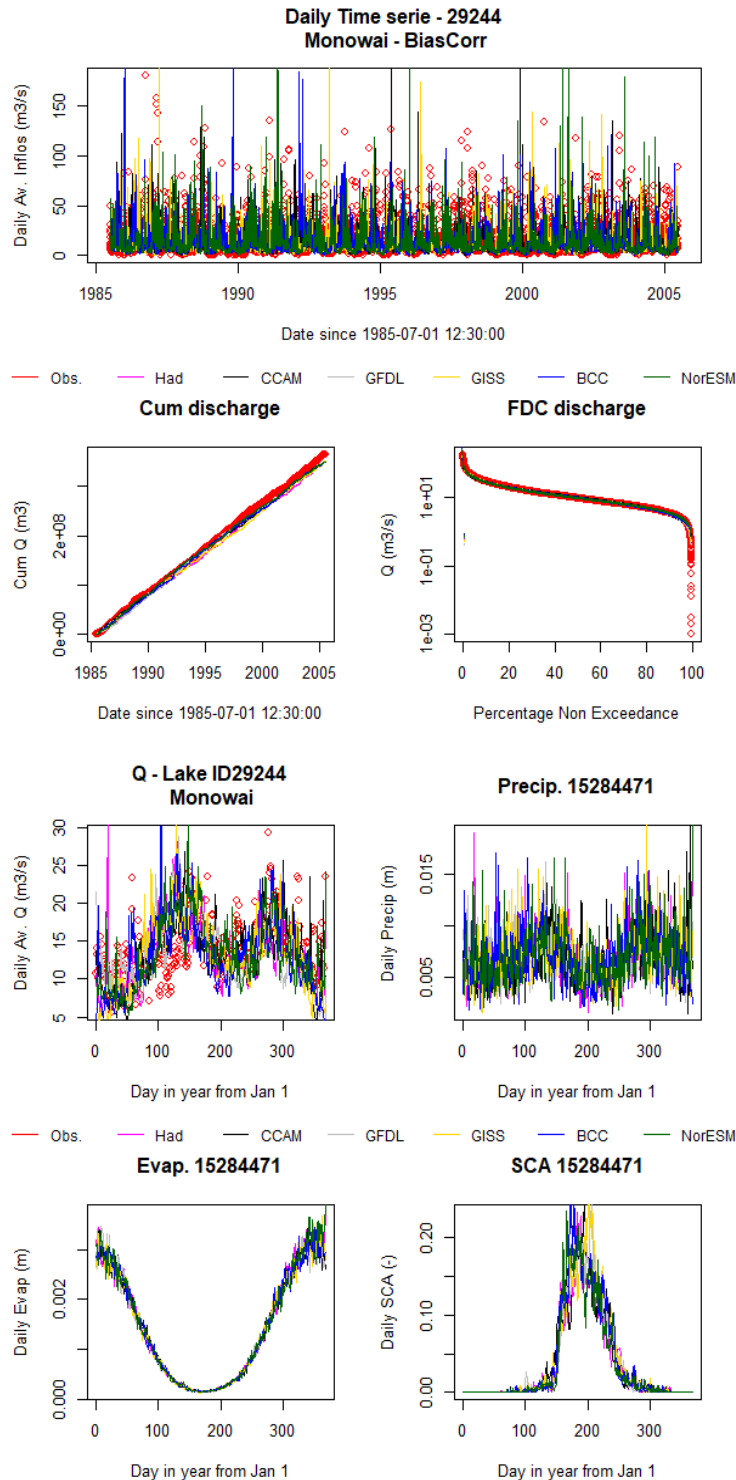


Figure B-8: Daily hydrograph, cumulated hydrograph and flow duration curves (top) daily average inflows, precipitation, evapotranspiration and snow area (bottom) for Lake Monowai inflows over the period 1985–2006. Observations (black) are compared with TopNet flows driven by GCMs; HadGEM-ES (light blue), CESM1-CAM5 (blue), GFDL-CM3 (yellow), GISS-E2-R (orange), BCC-CSM1.1 (red), and NorESM1-M (dark-green).

Bias corrected Lake Te Anau mean inflows error calculated to be around -1 % [-1%, -1%] across the 6 GCMs.

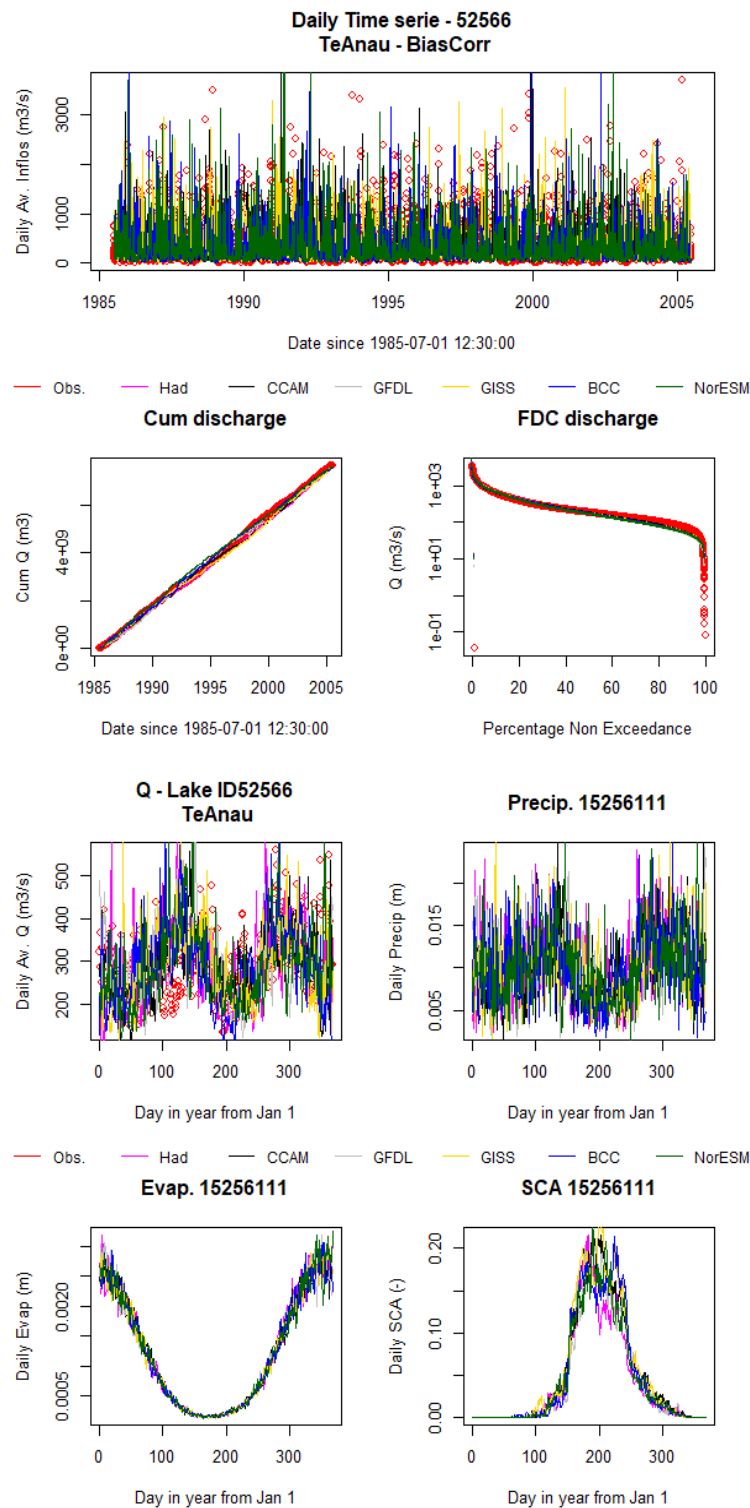


Figure B-9: Daily hydrograph, cumulated hydrograph and flow duration curves (top) daily average inflows, precipitation, evapotranspiration and snow area (bottom) for Lake Te Anau inflows over the period 1985–2006. Observations (black) are compared with TopNet flows driven by GCMs; HadGEM-ES (light blue), CESM1-CAM5 (blue), GFDL-CM3 (yellow), GISS-E2-R (orange), BCC-CSM1.1 (red), and NorESM1-M (dark-green).

Bias corrected Lake Manapouri mean inflows error calculated to be around -14 % [-16%, -11%] across the 6 GCMs.

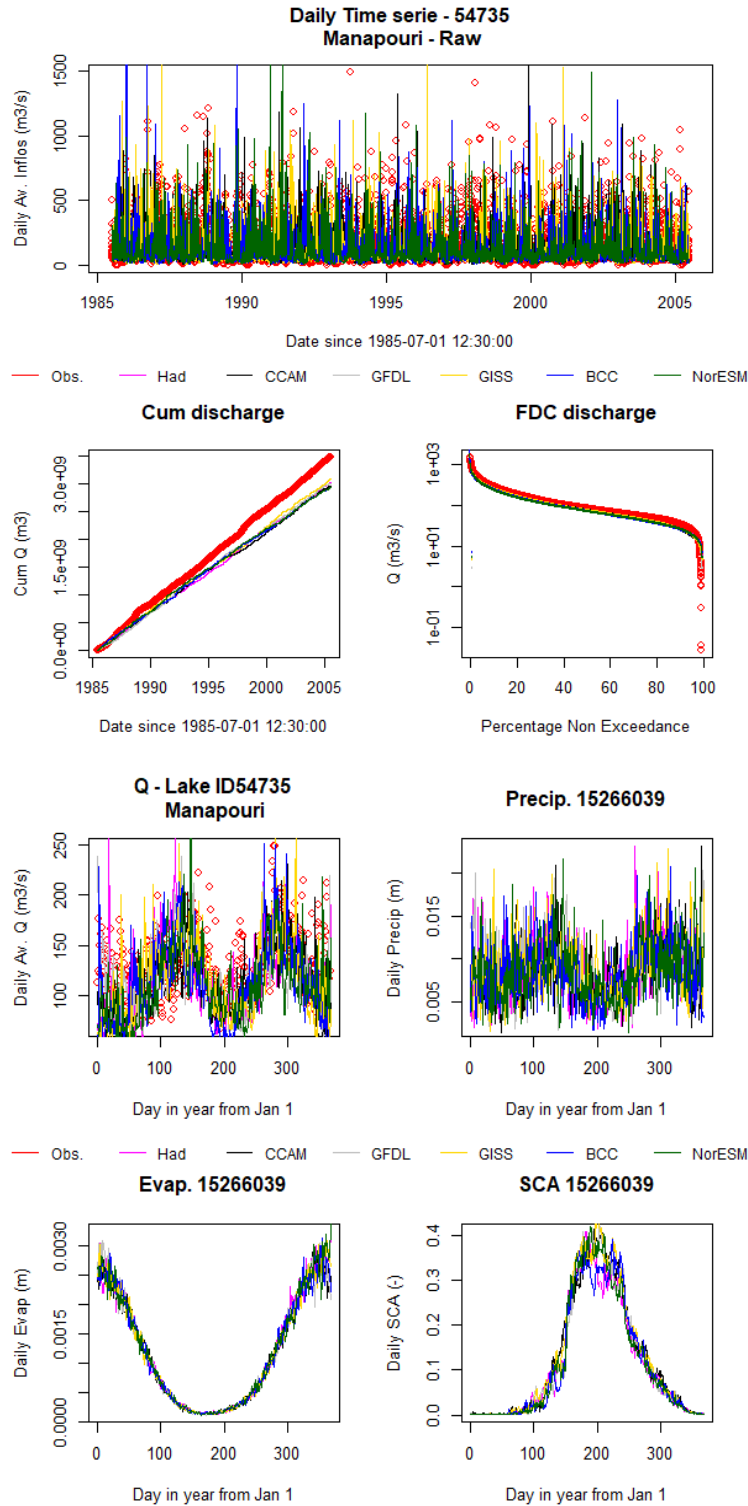


Figure B-10: Daily hydrograph, cumulated hydrograph and flow duration curves (top) daily average inflows, precipitation, evapotranspiration and snow area (bottom) for Lake Manapouri inflows over the period 1985–2006. Observations (black) are compared with TopNet flows driven by GCMs; HadGEM-ES (light blue), CESM1-CAM5 (blue), GFDL-CM3 (yellow), GISS-E2-R (orange), BCC-CSM1.1 (red), and NorESM1-M (dark-green).

Appendix C Monthly correlations for each period and RCP

For completeness, we show the plots and tables of monthly correlations for both the 2031–2050 and 2051–2070 periods for each of the four RCPs.

2031–2050 RCP 2.6

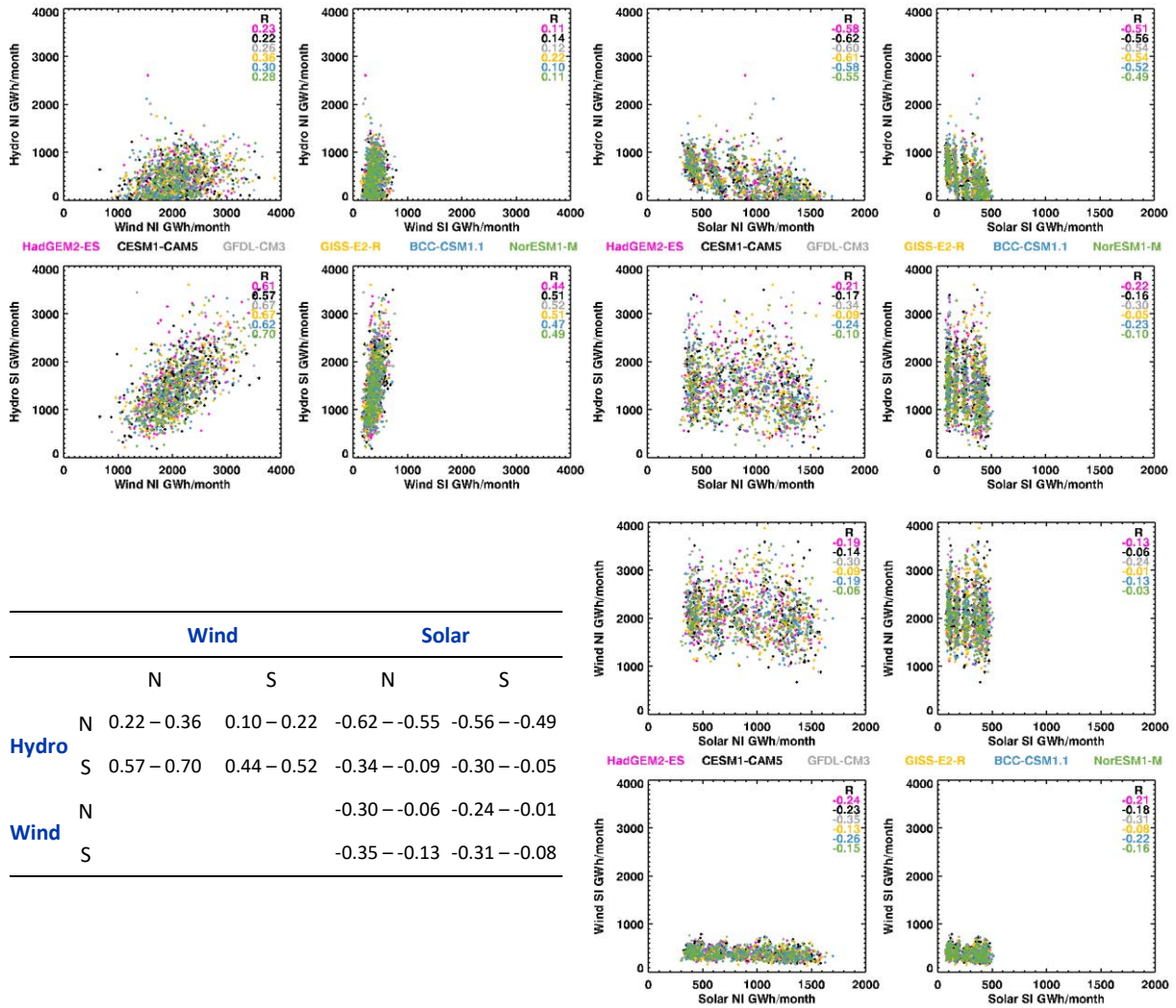


Figure C-1: Correlation of projected 2031–2050 monthly North and South Island hydro, wind, and solar generation for RCP 2.6 in the six CMIP5 models. Linear correlation coefficients for each GCM are shown within plots, and the ranges summarised in the table.

2031–2050 RCP 4.5

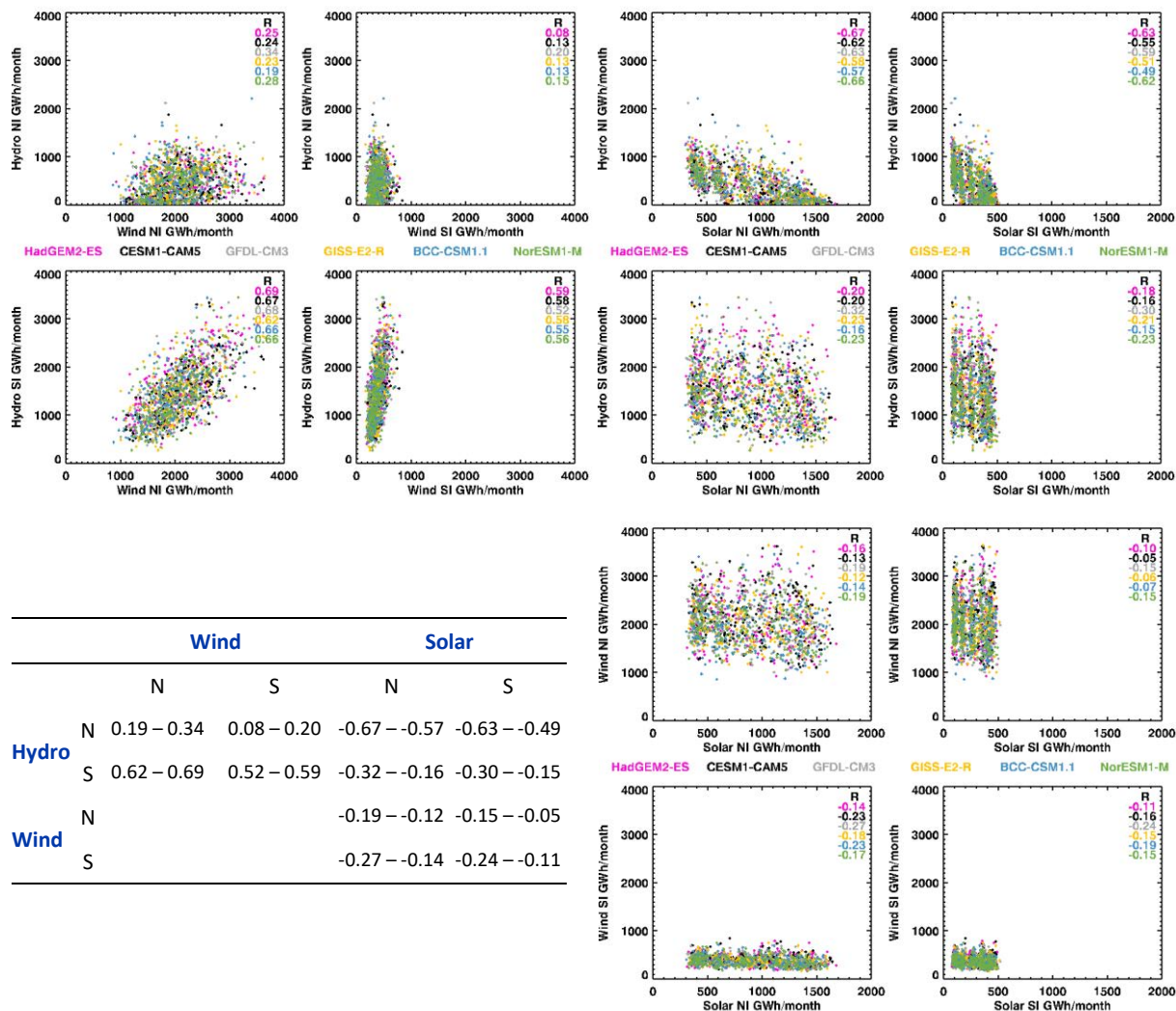


Figure C-2: Correlation of projected 2031–2050 monthly North and South Island hydro, wind, and solar generation for RCP 4.5 in the six CMIP5 models. Linear correlation coefficients for each GCM are shown within plots, and the ranges summarised in the table.

2031–2050 RCP 6.0

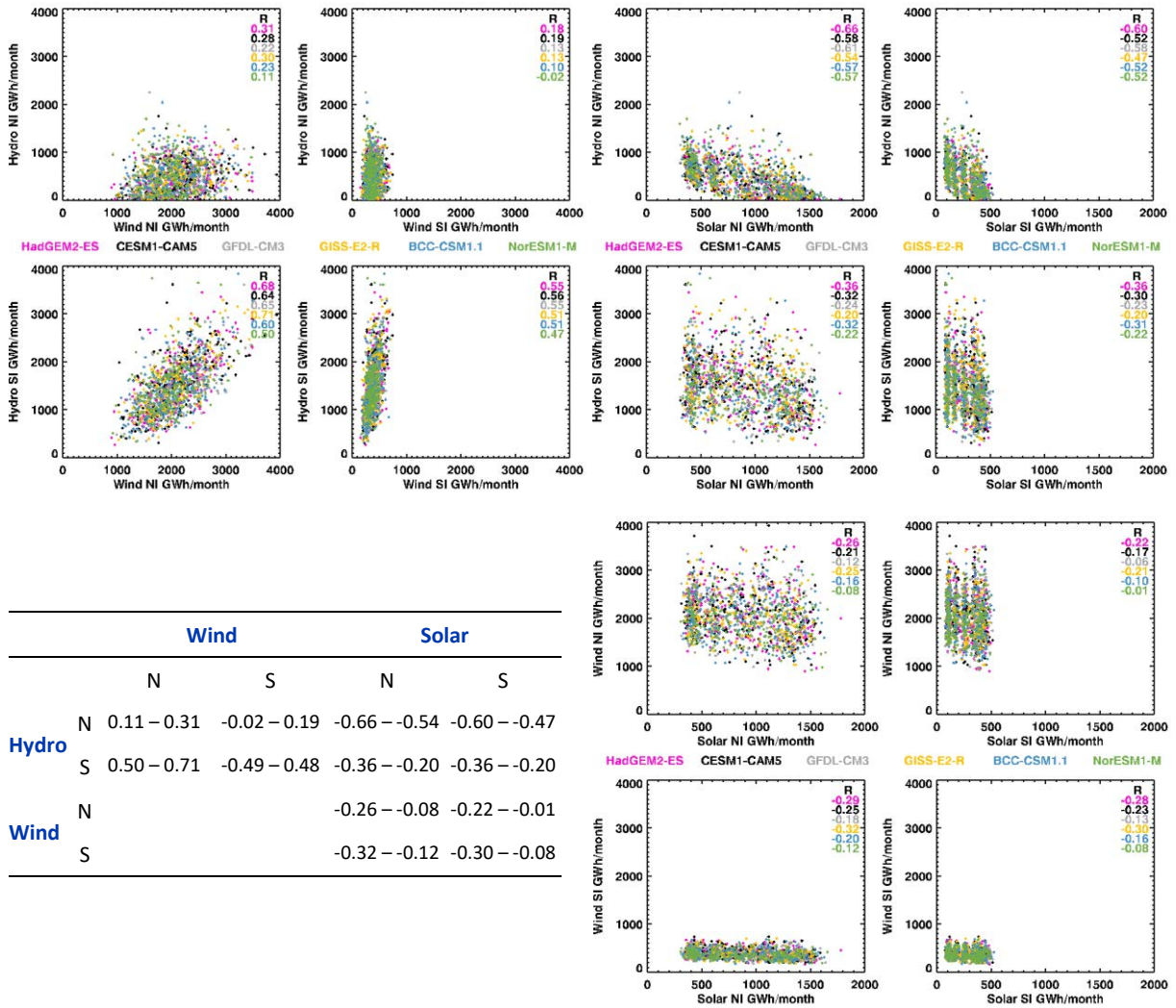


Figure C-3: Correlation of projected 2031–2050 monthly North and South Island hydro, wind, and solar generation for RCP 6.0 in the six CMIP5 models. Linear correlation coefficients for each GCM are shown within plots, and the ranges summarised in the table.

2031–2050 RCP 8.5

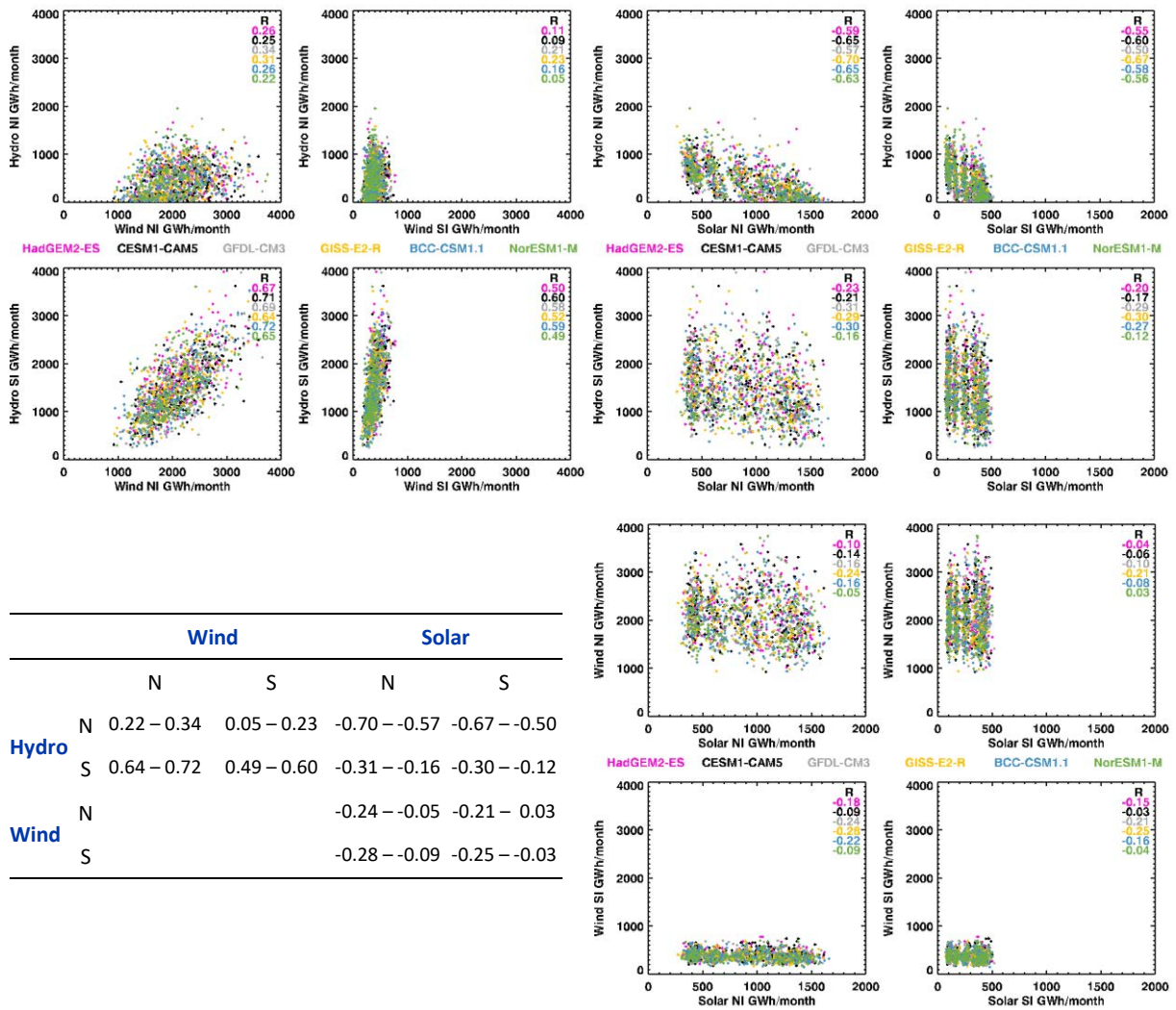


Figure C-4: Correlation of projected 2031–2050 monthly North and South Island hydro, wind, and solar generation for RCP 8.5 in the six CMIP5 models. Linear correlation coefficients for each GCM are shown within plots, and the ranges summarised in the table.

2051–2070 RCP 2.6

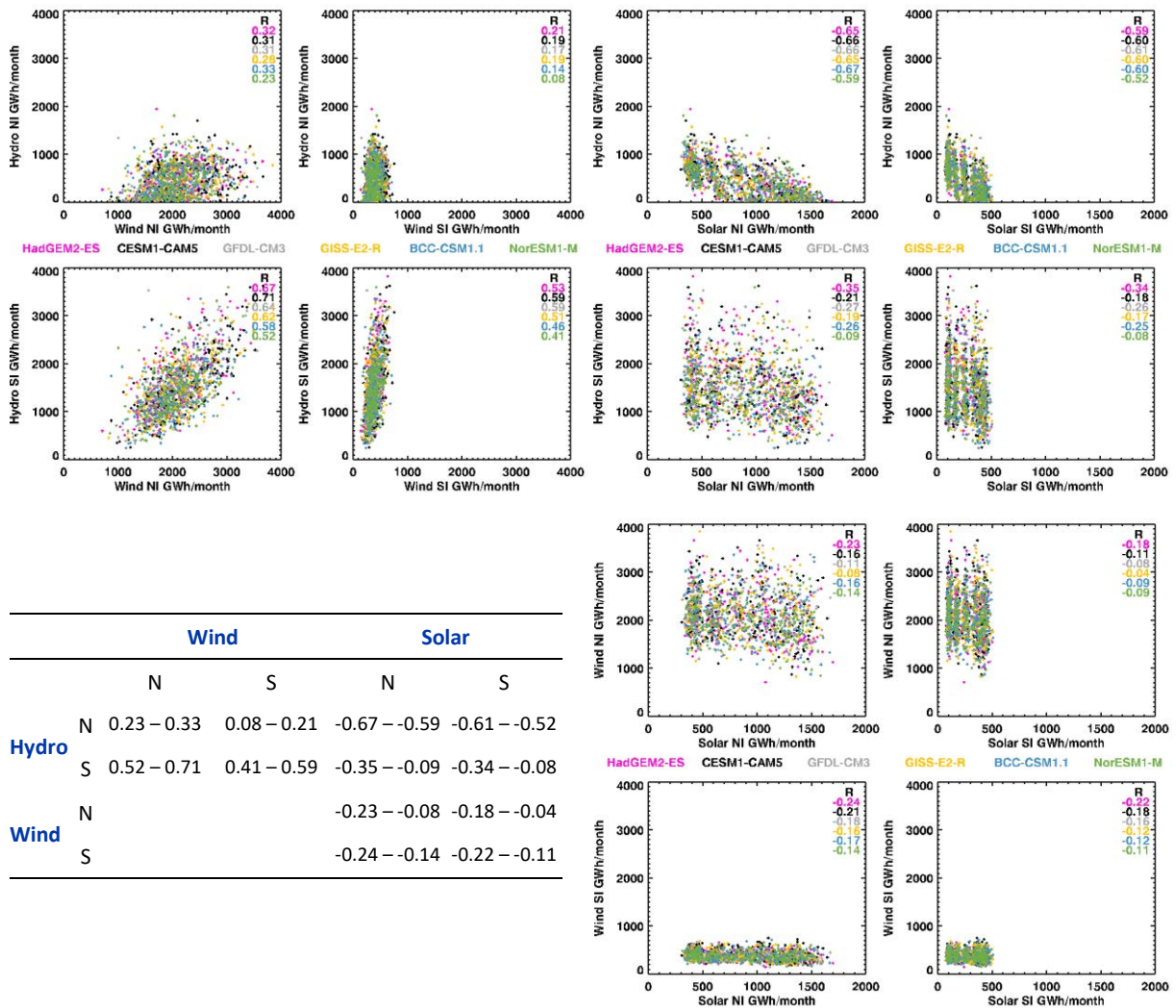


Figure C-5: Correlation of projected 2051–2070 monthly North and South Island hydro, wind, and solar generation for RCP 2.6 in the six CMIP5 models. Linear correlation coefficients for each GCM are shown within plots, and the ranges summarised in the table.

2051–2070 RCP 4.5

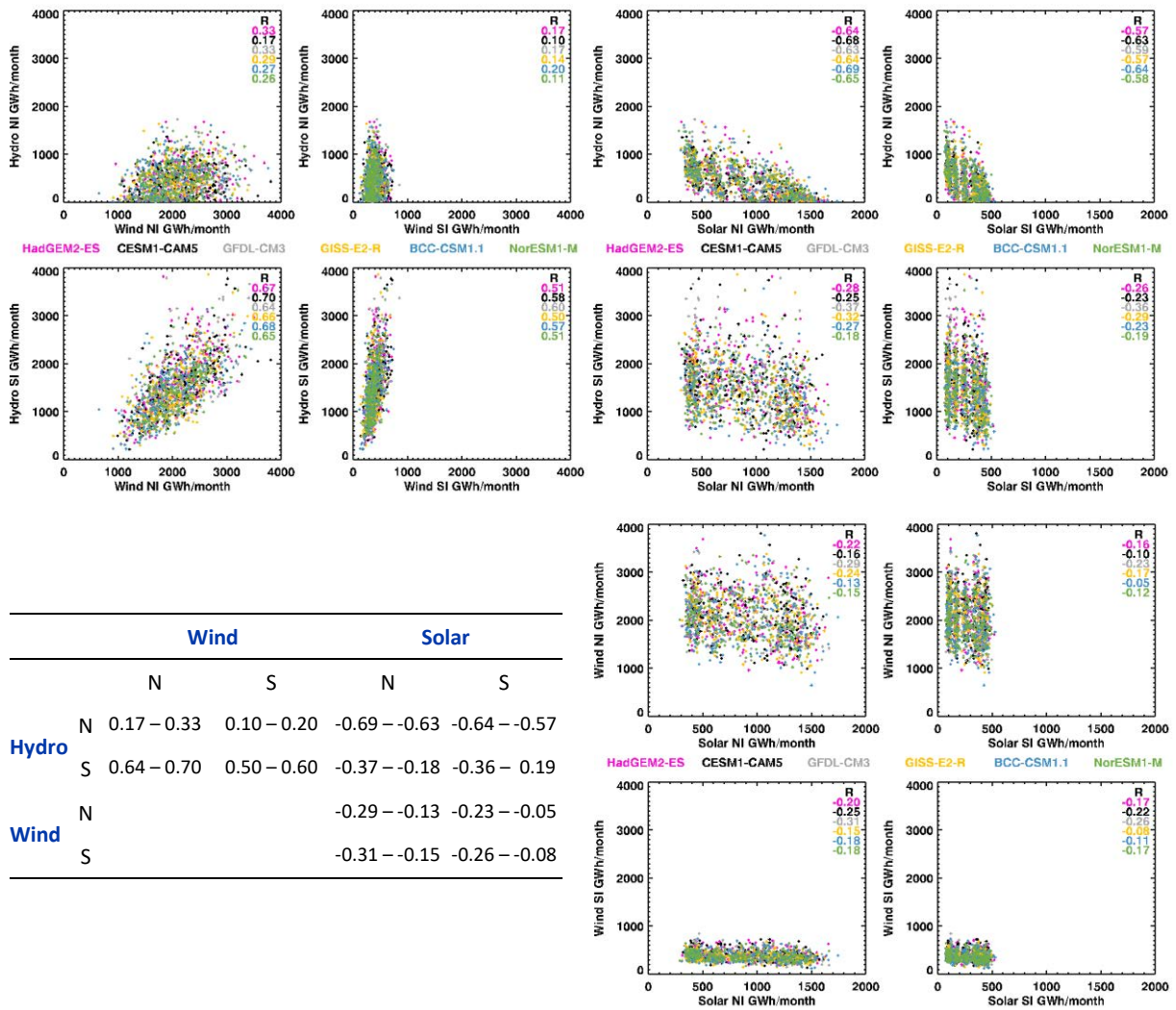


Figure C-6: Correlation of projected 2051–2070 monthly North and South Island hydro, wind, and solar generation for RCP 4.5 in the six CMIP5 models. Linear correlation coefficients for each GCM are shown within plots, and the ranges summarised in the table.

2051–2070 RCP 6.0

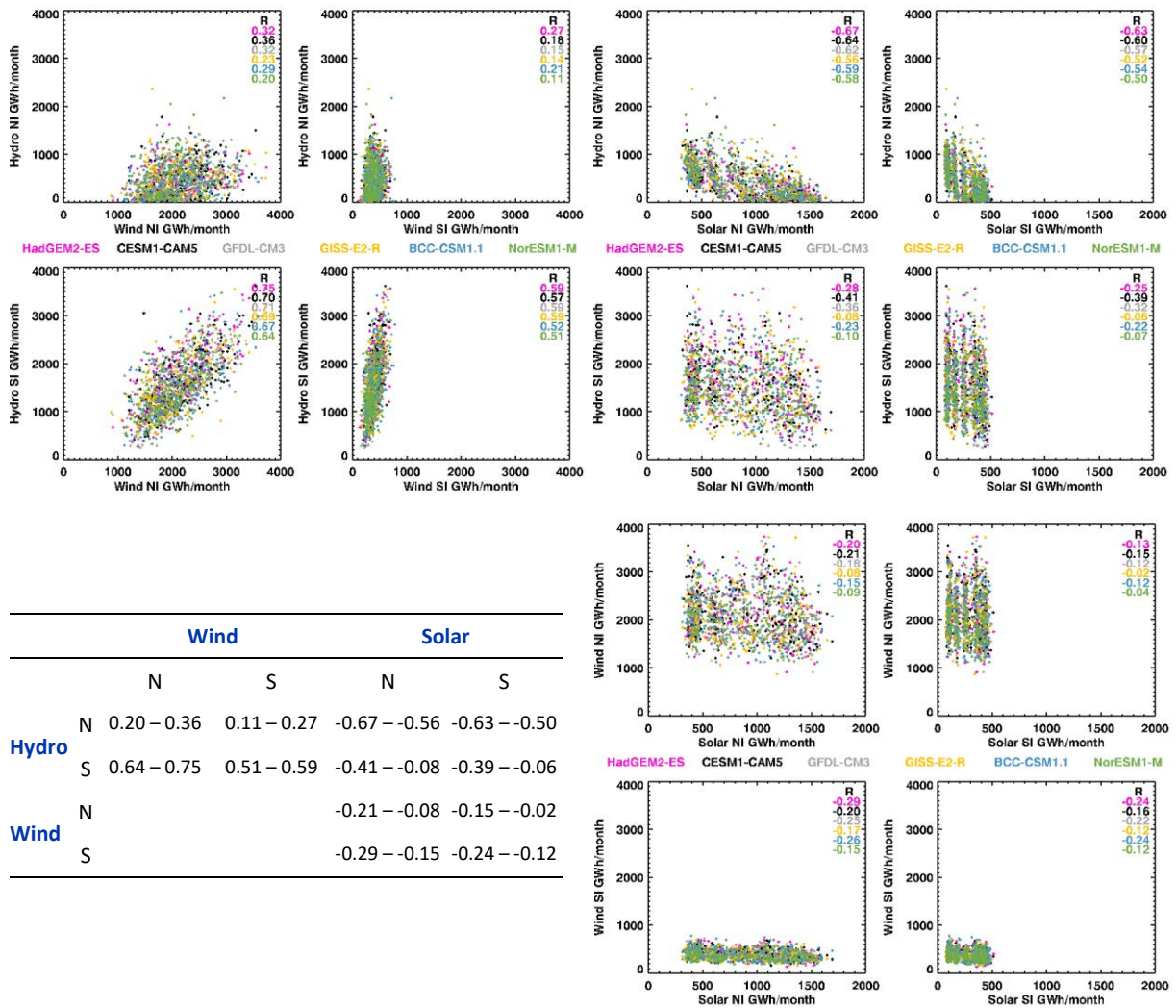


Figure C-7: Correlation of projected 2051–2070 monthly North and South Island hydro, wind, and solar generation for RCP 6.0 in the six CMIP5 models. Linear correlation coefficients for each GCM are shown within plots, and the ranges summarised in the table (same as Figure 7-3).

2051–2070 RCP 8.5

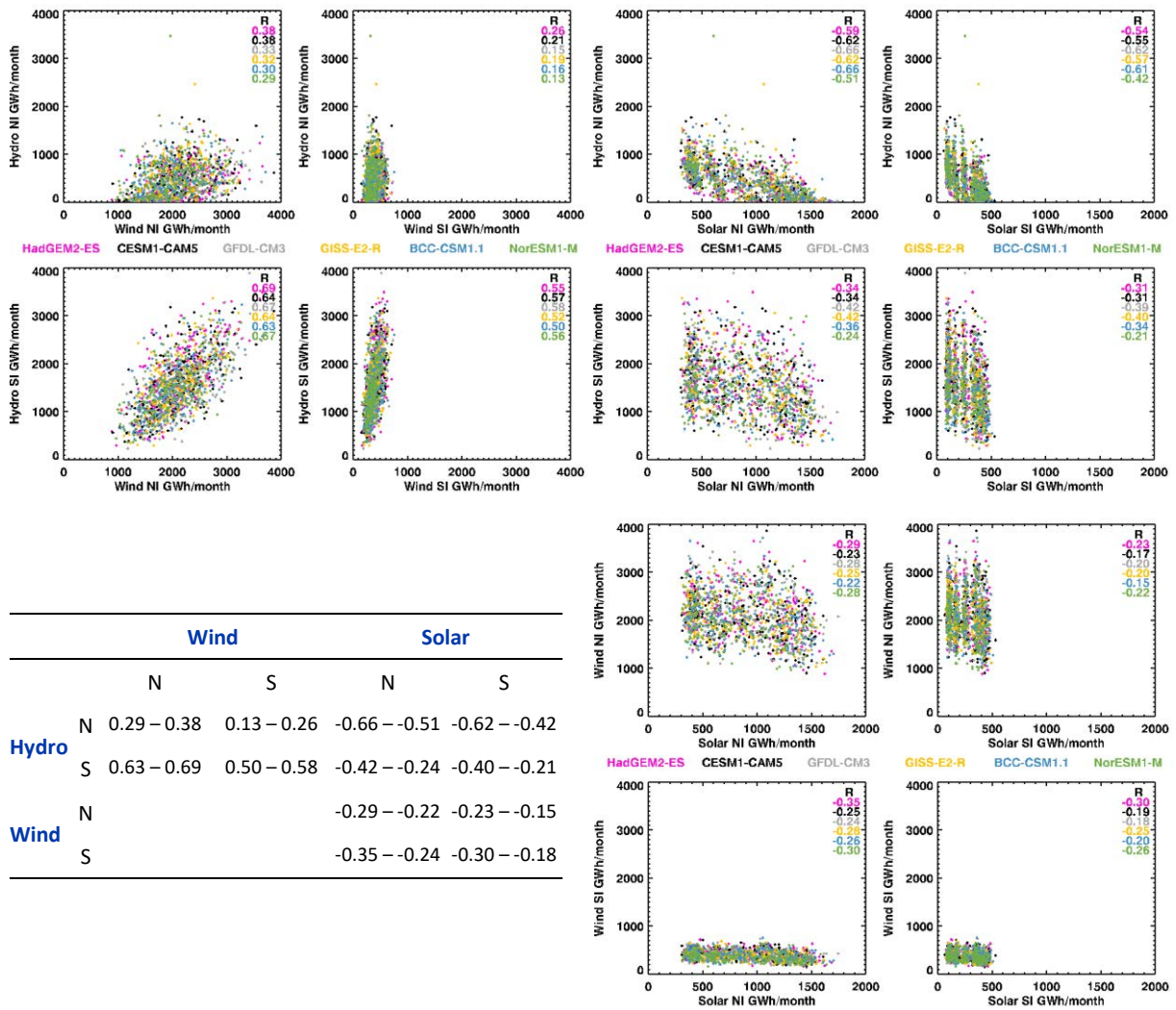


Figure C-8: Correlation of projected 2051–2070 monthly North and South Island hydro, wind, and solar generation for RCP 8.5 in the six CMIP5 models. Linear correlation coefficients for each GCM are shown within plots, and the ranges summarised in the table.